NATIONAL TECHNICAL UNIVERSITY OF ATHENS
SCHOOL OF NAVAL ARCHITECTURE & MARINE ENGINEERING
DIVISION OF MARINE ENGINEERING

DIPLOMA THESIS

ELASTIC SHAFT ALIGNMENT

ORESTIS VLACHOS

THESIS COMMITTEE:

SUPERVISOR:	CH. PAPADOPOULOS,	ASSISTANT PROF. N.T.U.A.
MEMBERS:	CH. FRANGOPOULOS,	PROFESSOR N.T.U.A.
	L. KAIKTSIS,	ASSOCIATE PROF. N.T.U.A.

ATHENS, APRIL 2015

ΕΘΝΙΚΟ ΜΕΤΣΟΒΙΟ ΠΟΛΥΤΕΧΝΕΙΟ
ΣΧΟΛΗ ΝΑΥΠΗΓΩΝ ΜΗΧΑΝΟΛΟΓΩΝ ΜΗΧΑΝΙΚΩΝ
ΤΟΜΕΑΣ ΝΑΥΤΙΚΗΣ ΜΗΧΑΝΟΛΟΓΙΑΣ

ΔΙΠΛΩΜΑΤΙΚΗ ΕΡΓΑΣΙΑ

Ελαστική Ευθυγράμμιση Αξονικού Συστήματος Πλοίου

Βλάχος Ορέστης

Εξεταστική Επιτροπή:

Επιβλέπων:	Χρ. Παπαδόπουλος,	Επ. Καθηγητής Ε.Μ.Π.
Μέλη:	Χρ. Φραγκόπουλος,	Καθηγητής Ε.Μ.Π.
	Λ. Καϊκτσής,	Αν. Καθηγητής Ε.Μ.Π.

ΑΘΗΝΑ, ΑΠΡΙΛΙΟΣ 2015

ACKNOWLEDGEMENTS

First and foremost, I would like to thank my supervisor, Christos I. Papadopoulos, for his support, counselling and above all, his patience.

Additionally, I would like to thank Minerva Marine and George Kloukiniotis, for providing detailed information on one of their vessels.

Special thanks goes out to *β*ETA CAE and George Korbetis in particular, for the wonderful cooperation we had over the course of almost two years. Without their contribution, the finite element analysis required for the completion of the present work would have neither been as extensive, nor as detailed.

I would also like to thank Kostas Stamatakis for his help with programming and for all the useful insight he provided, as well as Dimitris Fouflias, for his instruction and guidance on several issues.

Finally, I could not express how grateful I am towards my fellow classmates, Anastasis Charitopoulos, Pavlos Karadeloglou and Vagelis Fillipas for their friendship and encouragement throughout our studies in NTUA.

ABSTRACT

Proper alignment of ship shafting systems is of paramount importance for safe operations. In recent years, shaft alignment calculation and acceptance criteria have undergone several revisions. So far, a static analysis of propulsion systems, considering various hull deformation scenarios, has been common practice.

In the present work, the process and results of software development, aimed at providing a better approximation to the problem of shaft alignment, are discussed. The software solution proposed here, introduces bearing foundation stiffness and bearing hydrodynamic lubrication effects into alignment calculations. Four different types of vertical bearing offsets, including hull deformations, foundation elasticity and lubricant film thickness, are considered, as well as support position longitudinal shifts due to shaft-bearing misalignment.

As a case study, the shaft alignment of a typical VLCC vessel driven by a two-stroke low-speed Diesel engine is considered. The propulsion shaft of the ship is modelled as a statically indeterminate multi-supported beam. For a reference shaft alignment plan, the static equilibrium of the shaft is calculated using matrix analysis, taking elasticity of the bearing foundations into account. A detailed finite element model of the hull structure, complying with the meshing requirements set by Classification Societies, with focus on the aft end region of the vessel, is generated; the model is appropriate for accurate calculation of hull deformations, taking into account the contribution of shaft rigidity and the foundation of the main propulsion engine. Hull deformations are calculated for a set of typical loading conditions of the vessel.

Those deformations are used for calculation of the additional bearing offsets due to hull bending, and the corresponding effect on shaft equilibrium and bearing reactions. The process is carried out for two different operating conditions of the vessel, namely (a) for stationary loading of the propulsion shaft (zero rotational speed), and (b) for quasi- static loading of the propulsion shaft, taking into account oil-film characteristics of the bearings. In the latter case, pressure distribution at each bearing is calculated by the solution of the Reynolds equation in the lubricant domain.

Based on the above solution process, conclusions are drawn concerning the effects of hull deformations on shaft alignment plans, bearing hydrodynamic lubrication and friction power loss. Additionally, a set of comparisons between propulsion system modelling methods is carried out and, finally, a parametric analysis focused on the effects of viscosity on bearing hydrodynamic lubrication, shaft alignment and friction power loss is conducted.

ΣΥΝΟΨΗ

Η ευθυγράμμιση του αξονικού συστήματος ενός πλοίου έχει άμεση επίδραση στην ασφάλεια και τη δυνατότητά του να επιχειρεί. Τα τελευταία χρόνια, τόσο οι μέθοδοι υπολογισμού, όσο και τα κριτήρια αξιολόγησης καλής ευθυγράμμισης, αναθεωρούνται διαρκώς. Μέχρι στιγμής, ο υπολογισμός του πλάνου ευθυγράμμισης μέσω απλά εδρασμένων, στατικών μοντέλων του αξονικού συστήματος, σε συνδυασμό με ενσωμάτωση των παραμορφώσεων της γάστρας υπό διαφορετικές συνθήκες φόρτωσης, αποτελεί τον κανόνα.

Η παρούσα εργασία πραγματεύεται, την ανάπτυξη λογισμικού που σκοπό έχει να προσεγγίσει, με μεγαλύτερη ακρίβεια, το πρόβλημα της ευθυγράμμισης αξονικού συστήματος πλοίου. Το λογισμικό αυτό, πέρα από όσα αναφέρονται ήδη στην βιβλιογραφία, λαμβάνει υπόψιν την ελαστική παραμόρφωση των εδράσεων των σημείων στήριξης του αξονικού, καθώς και τις συνθήκες υδροδυναμικής λίπανσης του εδράνου, για τον υπολογισμό της ευθυγράμμισης. Υπό την προτεινόμενη θεώρηση, η κατακόρυφη θέση των εδράνων του συστήματος πρόωσης, πέραν του αρχικού πλάνου ευθυγράμμισης, επηρεάζεται από τις παραμορφώσεις της γάστρας του σκάφους, την ελαστική παραμόρφωση των εδράσεων και το πάχος του στρώματος υδροδυναμικής λίπανσης εντός των εδράνων.

Σην εργασία αυτή, έγινε μελέτη ενός τυπικού δεξαμενόπλοιου μεγάλης χωρητικότητας (VLCC) με κύρια διάταξη πρόωσης αποτελούμενη από βαδύστροφο δίχρονο κινητήρα Diesel. Το αξονικό σύστημα του σκάφους αναπαρίσταται ως υπερστατική δοκός πολλαπλών στηρίξεων. Μέσα από τη μέθοδο της μητρωικής ανάλυσης, με πρόβλεψη για την ελαστική έδραση, έγινε υπολογισμός των στοιχείων ενός πλάνου ευθυγράμμισης το οποίο ορίστηκε ως κατάσταση αναφοράς. Στη συνέχεια, δημιουργήθηκε ένα λεπτομερές μοντέλο πεπερασμένων στοιχείων για τη γάστρα του σκάφους, συμβατό με τις απαιτήσεις των νηογνωμόνων, προκειμένου να υπολογισθούν με ακρίβεια οι κατακόρυφες μετατοπίσεις των σημείων έδρασης του άξονα, λόγω παραμορφώσεων της γάστρας, για ένα εύρος καταστάσεων φόρτωσης.

Οι κατακόρυφες αυτές μετατοπίσεις ενσωματώθηκαν στους υπολογισμούς ευθυγράμμισης της εκάστοτε κατάστασης φόρτωσης/λειτουργίας. Επιπρόσθετα, στους υπολογισμούς ευθυγράμμισης συνυπολογίσθηκε και η επίδραση του στρώματος υδροδυναμικής λίπανσης των εδράνων για όσες καταστάσεις φόρτωσης αντιστοιχούν σε κατάσταση λειτουργίας της κύριας μηχανής. Η κατανομή της πίεσης σε κάθε έδρανο υπολογίσθηκε μέσω της εξίσωσης Reynolds.

Τα συμπεράσματα που αντλήθηκαν από τις λύσεις που προέκυψαν, μέσα από την παραπάνω θεώρηση, αφορούν την επίδραση των παραμορφώσεων της γάστρας στην ευθυγράμμιση του αξονικού συστήματος, τα χαρακτηριστικά της λίπανσης των εδράνων και τις σχετικές απώλειες ισχύος λόγω τριβής. Επιπρόσθετα, έγινε σύγκριση μεταξύ των μεθόδων υπολογισμού ευθυγράμμισης και τέλος, διερευνήθηκε η επίδραση του ιξώδους του λιπαντικού των εδράνων στο πλάνο ευθυγράμμισης και στις απώλειες ισχύος λόγω τριβής.

NOMENCLATURE

A	Beam cross-sectional area [m^2]
c	Bearing radial clearance [m]
D	Inner bearing diameter [m]
d	Outer shaft diameter [m]
e	Bearing eccentricity [m]
E	Young's modulus of elasticity [Pa]
f	Generalised load [N, N m]
f^*	Bearing friction coefficient
F	Friction force [N]
h	Lubricant film thickness [m]
h_{max}	Maximum lubricant film thickness [m]
h_{min}	Minimum lubricant film thickness [m]
K	Global stiffness matrix
k	Local stiffness matrix
L	Bearing length [m]
LoD	Bearing Length over Diameter ratio L / D
p	Pressure [Pa]
P_{loss}	Friction power loss [W]
R	Bearing inner radius [m]
S	Sommerfeld number
u	Generalised displacement [m, rad]
U	Tangential Velocity [m/s]
W	Bearing external load [N]
θ	Hydrodynamic film angle [degrees]
μ	Dynamic Viscosity [Pa s]
σ	Influence factor
ϕ, *phi*	Attitude angle [degrees]
ω	Angular velocity [s^{-1}]

LIST OF FIGURES AND TABLES

FIGURES

TABLES

1. INTRODUCTION

The propulsion system of conventional cargo ships typically consists of a two-stroke, or a four-stroke Diesel engine, and a shafting system with the option of a reduction gearbox, which transmits the engine power to the propeller (**Figure 1.1**). In ships propelled by four-stroke Diesel engines, a reduction gearbox is required. Due to the demand for high power output, the shafting system is usually subjected to a large amount of torque, whereas significant bending moments are also present, as a result of propellers getting larger in order to efficiently convert engine power into thrust. Proper design, therefore, demands that a shaft with large diameter is installed, which in turn increases the overall weight of the system. Radial shaft loads (propeller/shaft/engine weights) need to be supported by journal bearings (stern tube bearings, line bearings, crankshaft bearings).

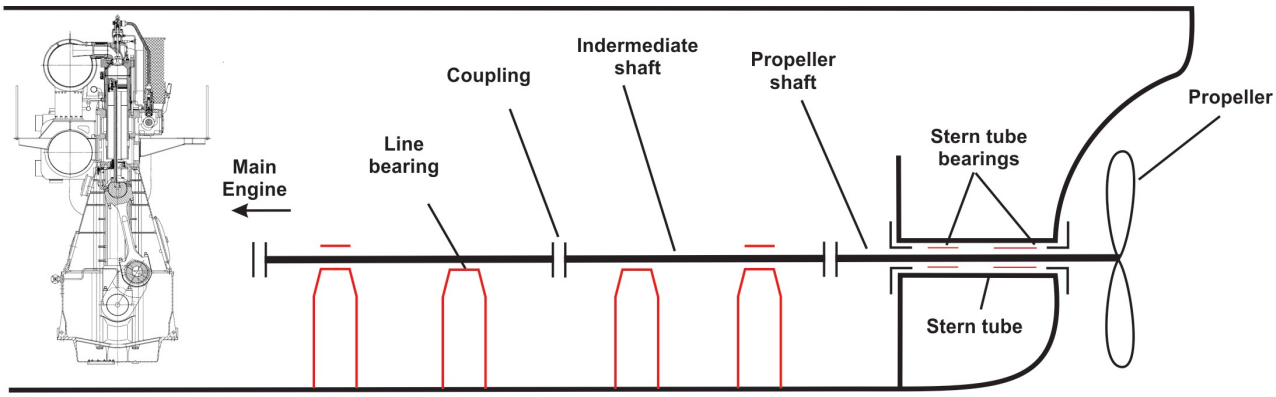

FIGURE 1.1: TYPICAL ARRANGEMENT OF THE PROPULSION SYSTEM OF A CARGO VESSEL

Proper design, installation and alignment of the shafting system of a ship is crucial for stable, efficient and reliable operation. Primarily, shaft alignment is concerned with the determination of proper longitudinal location and vertical bearing offset, aiming at an optimal distribution of bearing loads. The successful application of a shaft alignment plan is essential for trouble-free dynamic operation of the propulsion system, aiding in decreasing bearing wear, increasing bearing expected lifetime and decreasing maintenance and replacement costs.

Up until recently, a shafting system would be modelled as a rigidly supported assembly of beam elements. In reality, though, all support points correspond to all the non-rigid constructions that make up the bearings' foundation. Under the weight of the shaft, the bearings' foundation, being very stiff but not completely rigid, is expected to deform elastically, even at the scale of a few tenths of micrometres. This would result in small, unexpected alterations to the initially designed shafting plan that did not account for bearing foundation stiffness. As such, a more accurate approximation of the shafting system would require the inclusion of foundation stiffness into all relevant calculations.

In operation, shaft alignment may be considerably influenced by hull deflections, due to different loading and environmental conditions. The effect of hull deflections on shaft alignment is more pronounced in very long ships, with relatively flexible hulls and stiff shafts. In such cases, the robustness of shaft alignment at different loading conditions of the ship, taking hull deflections into account, should be carefully assessed. In this respect, the use of detailed Finite Element Analyses for the calculation of hull deflections becomes imperative.

1.1. Literature Review

Numerous concerns about the capability of a shafting system to operate at a satisfactory level, under different vessel loading conditions, have been raised, in related literature. D.G. Redpath (1983) in particular mentions that although no problems concerning intermediate shaft bearings should arise during launch or sea trials, it has been often reported that these bearings would overheat under some of the ship's other operating conditions. He goes on to attribute these occurrences to something as common as a change in the ship's trim, which in turn affects the longitudinal distribution of bending moments.

On the same note, G.C. Volcy (1983) [11] observed that, as power output per shaft increased in newbuildings of the time, a number of problems concerning the function of propulsion systems arose. His investigation led him to the conclusion that hull deformations may have had an adverse effect on the alignment of propulsion systems and he went as far as to propose a stiffening of ships' hull through reinforcement of the double bottom. Additionally, he documented a series of failures of the shafting system, mostly extreme tail-shaft bearing wear, caused mainly by insufficient stern tube slope boring and implementation of a problematic alignment plan as a result of errors in the initial calculations.

In the recent literature, the subject of shaft alignment has gained increasing attention. In their work, Devanney and Kennedy (2003)[5] have underlined the drastic deterioration of tanker new-building standards in the decade preceding their publication, and the corresponding effect on the reliability of the shafting system. Specifically, emphasis has been put on the severity of stern tube bearing failures in modern VLCCs and ULCCs, which may lead to loss of propulsion and vessel immobilisation. The authors claimed that the main reason of this failure is the design of propulsion shafts with decreased diameters, followed by improper shafting alignment. They suggested that (a) hull deflections should be thoroughly taken into account for a range of loading conditions of the ship, (b) the engine room structure should be reinforced, to minimise additional offset of the bearings, and (c) time varying loads on the stern tube bearing and heat dissipation in the lubricant domain should be considered.

In his work, Šverko (2003)[9] has highlighted several design concerns in propulsion shafting, especially for VLCC and large bulk carrier vessels. It was suggested that, in such vessels, shaft alignment is very sensitive to hull deflections; this behaviour was attributed to the increased hull flexibility of such ships (due to scantling optimisation and increased ship lengths) and to the increased stiffness of the propulsion shaft (due to the demand for higher propulsion power and, consequently, larger shaft diameters). It was concluded that if the actual hull deformations can be predicted accurately, an optimal set of bearing offsets for the vessel on even keel may exhibit a reasonably good performance at other loading conditions of the vessel; however, since hull deflections cannot be easily calculated with such accuracy, a practical solution could be to complete the alignment at dry dock conditions, and make provisions to correct (if needed) bearing vertical offsets when the reactions are verified afloat. Of key importance, are the remarks he made

about the stern tube bearing, based on calculation examples computed with the shaft alignment software developed by American Bureau of Shipping (ABS)[2]. He supports that the maximum absolute bearing-shaft misalignment allowed is 0.3 mrad, beyond which point, slope boring should be applied at the stern tube bearing. Additionally, due to some misalignment being inevitable, the single support point equivalent of a stern tube bearing should be longitudinally positioned closer to the aft end of the bearing at about a third of the bearing's diameter away. Finally, this was probably the first time that bearing film characteristics were studied, as the author used shaft alignment reaction forces as input to externally calculate bearing behaviour. In a subsequent work, Šverko (2006)[10] addressed the problem of predicting hull deflections through analysis of series of collected real life data. Hull deflections were estimated by measurement of shaft deflections using bending gauges. The goal of this study was to find appropriate dry dock bearing offsets that will result in acceptable alignment performance over a wide range of vessel loading conditions.

Murawski (2005)[7] also utilised a FEM model of a large container-ship, and introduced a new parameter to be considered: the stiffness characteristics of the bearing foundations. He performed a series of computations introducing bearing foundation stiffness to some support points while keeping others rigidly supported.What he found out was that this approach yielded results that were significantly different. In an effort to gauge bearing loading he also suggested calculating each bearing's Sommerfeld number as an estimate. Additionally, he hinted that the Sommerfeld number of the intermediate shaft bearing(s) should be 30~50% greater that the rest, to accommodate for loading scenarios where these bearings will have to support more load, due to a change in hull deflections. Elaborating on the importance of good oil film characteristics, he supported that proper oil film distribution should be checked during shaft alignment analysis, introducing a new design parameter. He concluded that, in a holistic approach to the shaft alignment problem, bearing stiffness and oil film characteristics of each bearing should be taken into account in the design stage.

In their study, Dahler et.al. (2004)[4] reported the results of an industrial project between DNV, MAN B&W and DAEWOO concerned with the numerical and experimental study of shaft deflections and bearing loads in large ships propelled by two-stroke Diesel engines. They utilised a complete FE model of the ship, which exhibited a fine mesh at the aft end of the ship hull (engine room). Focus was given on engine and crankshaft deflections and on the corresponding bearing loads. To this end, FEM analyses were performed taking into account the real crankshaft geometry, and the results were compared with simulations using simplified crankshaft models. Simulation results were also compared to experimental measurements. They concluded that FE-hull analyses can capture the general trend of hull deflections reasonably well, but fail to account for local variations in the curvature of the shaft, leading to inaccurate predictions of bearing loads. Finally, they suggested that by applying the final shafting plan after vessel launch, possible errors due to wrong estimation of hull deflections could be avoided.

Recently, BV (2013)[3] released Rule Note NR 592, concerned with Elastic Shaft Alignment (ESA) of ships. The proposed methodology of shafting alignment calculations takes into account hull deformations, oil film characteristics and stiffness of the bearings' foundation. The rule is mainly

applicable to ships characterised by a propeller shaft diameter greater than 750 mm, or between 600 mm and 750 mm, but with propeller weight greater than 30 tones or a prime mover with power output greater than 20 MW. The release of ESA makes the importance of shaft alignment in modern ships and detailed calculations at the stage of vessel design, evident.

1.2. Goal - Outline

1.2.1. Calculation method

As discussed in the introduction and literature review sections, a good approximation of the shaft alignment characteristics can be achieved through a static structural model of the shaft. So far, modelling bearings as simple supports (e.g. hinged points), fixed along the vertical axis of the coordinate system, has been the norm.

Many researchers have suggested that the model described above should also take into account the elasticity of support point foundation, as well as the overall behaviour of the lubricant film created between the shaft and the support bearings.

In the present work, the shaft alignment calculation procedures are revisited. Here, the aim is to introduce a more accurate method of calculating the variables involved in the design and implementation of a shaft alignment plan. Furthermore, through the proposed method, it is hoped that a deeper understanding of the design parameters that govern the problem of proper shaft alignment can be reached.

The proposed calculation method in question can be broken down to its primary components which comprise:

- A **structural model** of the shaft that models bearings as single point elastic supports (support point **foundation stiffness** is accounted for),
- A journal bearing model that provides detailed calculations of **lubricant film** characteristics for all support points,
- The **coupling** of the above in an iterative sequence that converges to the system's final state of equilibrium.

Utilising the proposed method, more detailed information on the following issues concerning shaft alignment can be obtained:

- The effect of bearing foundation stiffness on any alignment plan,
- The effect of bearing lubricant film thickness on any alignment plan,
- Bearing-shaft misalignment and its influence on bearing wear and actual support location,
- Pressure distribution at the lubricant film of each bearing,
- Power loss due to friction.

1.2.2. Software Development

In order to investigate the above, a large amount of calculations need to be made. To this end a dedicated piece of software was developed combining and expanding upon two existing programs:

- **ShaftAlign**, written by Christos I. Papadopoulos, Assistant Professor, School of Naval Architecture & Marine Engineering, National Technical University of Athens,
- **CranckShaftBearing,** written by Leonidas Raptis ,in the course of his diploma thesis, entitled "Software development for the solution of hydrodynamic lubrication problems in main bearings of marine Diesel engines" (2014).

The resulting software incorporates, among others, an overhaul of the existing code, a large expansion of the abilities of ShaftAlign, a new input file format for the end product, as well as all the interface necessary for ShaftAlign and CrankShaftBearing to cooperate efficiently.

An overview of the new program function is given in section 4 “Numerical Modelling”. To summarise, the user needs to input a detailed information on the geometry of a shafting system, hull deformations, support point vertical offsets (i.e. the initial alignment plan), as well as information on the bearings used to support the shaft, such as bearing radial clearance, length, diameter, lubricant viscosity, rotational speed and mean applied slope boring. The program offers the user four solution options depending on whether he or she wants to activate certain features. A solution is obtained through an iterative process; each iteration includes calculations of the structural equilibrium of the shaft and one set of bearing calculations, providing oil film characteristics such as film thickness. Once this coupled problem converges to a final set of values, the solution is presented to the user through a graphical user interface (GUI) and a series of output files. Finally, the user has the option to use the GUI to alter his initial input and re-run all calculations.

1.2.3. Case Study

In order to investigate the potential of the method proposed in this section, and to compare the results obtained through it against results produced by regular static analyses, a case study was carried out.

In the present work, a typical VLCC vessel, driven by a two-stroke Diesel engine is considered. The vessel has a propeller shaft diameter of 815 mm, therefore it is within the scope of the ESA Rule of BV.

First a 3D representation of the ships hull and compartmentation was created by manually digitising the ship construction plans, section by section. Afterwards, a detailed finite element model of the hull structure of the ship, complying with the meshing requirements set by Classification Societies, was generated with the use of the ANSA meshing software. This model was used to calculate hull deflections for each different loading condition.

For the study of the shaft alignment plan, the propulsion shaft of the ship was modelled as a statically indeterminate multi-supported beam; bearing stiffness and clearance were taken into account, and static equilibrium of the shaft was calculated using matrix analysis. Considering the undeformed hull of the vessel, a reference shaft alignment plan was assumed, and static equilibrium of the shaft was calculated. Next, a series of different ship loading conditions (laden/ ballast) are incorporated to the reference shaft alignment plan, as vertical offsets, and static shaft equilibrium is evaluated.

For each loading condition:

I. The hydrostatic equilibrium of the ship is computed,

II. The corresponding hull deformations are calculated,

III. The relative vertical displacements at the bearing locations are determined and,

IV. The quasi-static shaft equilibrium is evaluated. The computed bearing loads (reaction forces) are compared to those of the reference case.

2. Shaft Alignment

2.1. Definition

The propulsion system of conventional cargo ships typically consists of a large 2-stroke diesel engine directly coupled to the propeller, or an assortment of smaller 4-stroke diesel engines which drive the propeller through a gearbox. The shafting system consists of several components that help transmit the power generated by the ship's main engine (M/E) to the propeller. Typically , it comprises three parts: the crankshaft, an intermediate shaft and the propeller shaft, with the option of a gearbox in between the crankshaft and the intermediate shaft.

Along the length of each shaft, it is necessary to position support points that help support the acting radial weight of each piece. The propeller shaft is usually supported in the stern tube by two stern tube bearings. Typically, the aft stern tube bearing is quite long, with a length over diameter ratio well above unity, which allows for increased load capacity. The intermediate shaft is usually supported by one or two intermediate shaft bearings. Finally the crankshaft is supported by many crankshaft bearings whose number corresponds to the number of cylinders contained in the main engine.

Shaft alignment is the process through which the following can be determined :

- The **number** of all support points along the shaft,
- The **longitudinal position** of every support point along the shaft,
- The **vertical position** of each support point in relation to a pre-established reference line,
- The **angle** at which support bearings will be positioned in relation to a pre-established reference line, in order to minimise shaft/bearing misalignment,
- The proper **bearing dimensions** that would ensure the shaft weight is supported adequately,
- The **reaction forces** at the support the points, both in cold and hot M/E conditions, for a given set of all the above.

2.1.1. Importance of Proper Alignment

Failure to design a robust shaft alignment plan may lead to a series or unwanted results such as:

- Support bearings not contributing to supporting the load of the system and being practically useless,
- Supports bearings being loaded over their capacity which leads to damages and wear both for the bearing and the shaft and shortens the lifespan of the system and, most importantly, puts ship safety and operability into risk,
- Increased power loss, due to extreme friction at the shafting system,
- Bad coupling of gears in the gearbox, if applicable, that may lead to extensive gear teeth damage and could cause gearbox failure,

- Shaft bending moments could be greater than the allowed limit, which may lead to shaft failure due to fatigue.

On the other hand, a proper shafting plan may present us with the following benefits:

- Reduced shaft stresses,
- Evenly distributed bearing loads/bearings operating within nominal loading capacity limits,
- Longer system life span,
- Maintenance and repair cost reduction.

2.1.2. “Static” versus “Running” condition

Proper shaft alignment should be guaranteed for all conditions that a ship may encounter during operation. Most conditions can be divided into two broad categories: static and dynamic. In **static** conditions :

- The main engine (M/E) is not running — i.e., it is in cold condition,
- The eccentric thrust produced by the propeller is not considered and, likewise, any resulting bending moments (e.g., that generated in the thrust bearing) are also not taken into account. The propeller contributes to static loading of the shaft only by its gravitational force,
- At the bearing locations, the shaft can move freely in the vertical direction, within a span of twice the radial clearance of each bearing,
- The shaft is stationary, therefore hydrodynamic lubrication is not active, i.e., no fluid film can be sustained between the shaft and the bearing.

In **dynamic** (sea-going) conditions the following should be considered:

- The M/E, being in hot condition, is subject to thermal expansion, which should affect the vertical offset of all crankshaft bearings,
- Support bearings develop a fluid film that supports and lifts the shaft off of the lower half of the bushing,
- The eccentric thrust induced by the propeller can be applied as a bending moment,
- Any misalignment between the bearing and the shaft will result in a slight shift of the conceived single-point support position of the shaft along the bearings’ length.

In the present study, the following assumptions have been made, regarding dynamic (sea-going) conditions of the vessel: **(a)** a uniform vertical offset of the crankshaft bearings due to thermal expansion has been considered, **(b)** shaft vertical motion within bearing clearance is governed by the principles of hydrodynamic lubrication, and **(c)** shaft bending moments due to propeller eccentric thrust has not been considered.

2.1.3. Influence Factors

For a given number of support points in a shafting system and a given set of longitudinal positions of those support points, a change in the vertical offset of a single bearing will affect the distribution of reaction forces amongst all bearings. In this respect, if the number of bearings and their longitudinal position are held constant, it is appropriate to say that any one bearing exerts an influence on all other bearing reaction forces by means of its vertical position.

The influence factor of bearing i on bearing j is a measure of the change in reaction force of bearing j, caused by a unit vertical offset of bearing i.

As such, it can be calculated as:

$$\sigma_{ij} = \frac{W_{ij} - W_j^o}{y_i} \qquad \text{EQ. 2-1}$$

Where:

- σ_{ij} is the influence factor of bearing i on bearing j,
- W_{ij} is the reaction force of bearing j when bearing i has moved vertically by an amount of y_i,
- W^o_j is the reaction force of bearing j, while all bearings have zero vertical offsets (i.e., flat-line).

Using the above formulation, predicting every bearing reaction force for a set of vertical offsets, is made much easier, once all influence factors have been calculated:

$$W_{ij} = W_j^o + \sigma_{ij} \cdot y_j \qquad \text{EQ. 2-2}$$

The underlying concept of superposition that allows us to make such a claim is valid here because the vertical offsets imposed on the bearings are much smaller than the distance between each bearing.

Influence factors can also be a good measure of the sensitivity of the shafting plan to external disturbances. Vertical bearing offsets may change as a ship changes its loading condition due to hull bending, e.t.c. If the influence factor values of a system are small, the system is less sensitive to such changes. On the contrary if the system's influence factors are large, then the risk of bad alignment caused by the slightest change in vertical bearing offsets is greater.

2.1.1. SAG and GAP values

In the process of implementing a shaft alignment plan, all segments that make up the shafting system, are placed onto their respective support bearings. In this uncoupled state, the flanges of each shaft hang freely. In order to bring all flanges together and couple the shafts a significant amount of force needs to be exerted and if the flanges are too far apart this is often impossible. Additionally, the position of shaft segment flanges relative to each other, strictly dictates the bending and reaction forces of the coupled shafting system. The inverse is also, valid: for a given shaft alignment plan, decoupling its segments would result in specific flange-to-flange distances. Being able to predict these distances for a specific alignment plan is thus important. A way of

measuring flange distance employs two variables: SAG and GAP. SAG is the vertical distance between the top edges of each flange. Respectively GAP is the minimum horizontal distance between facing flange edges, or sometimes the horizontal distance between a flange's upper and lower edge.

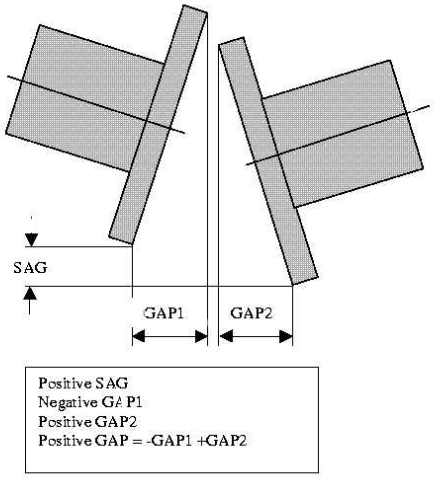

FIGURE 2.1: SAG AND GAP VALUE MEASUREMENT [8]

The figure above (**Figure 2.1**) illustrates some possible arrangements of shaft flanges and how SAG and GAP values are measured. SAG and GAP calculations can be carried out using simple beam theory.

2.2. Regulations

Class regulations regarding shaft alignment of rotating machinery, such as the prime mover of a ship, are more or less homogeneous between all major classes. The main body of regulations outlines the following minimum requirements:

- A detailed shaft alignment plan, illustrating all considerations taken and all assumptions made must be submitted for approval,
- The results of the analysis carried out prior to plan implementation must be shared with the class,
- Analyses must be carried out for various ship operating (hot/cold) and loading (Ballast Arrival, Full Load Departure, e.t.c.) conditions, taking the corresponding hull deformations and main engine thermal expansion into account,
- Stern tube slope must be thoroughly investigated under any alignment plan, and single, or even multi-slope, boring must be applied whenever necessary, to prevent excessive shaft misalignment,
- Bearing reactions should be within allowed limits,
- The details and procedures followed during the implementation of the plan must be available to the class reviewer,
- All the above must be checked and verified through testing by the class.

Getting into the the specifics of the above requirements, the following details are explicitly prescribed.

2.2.1. Bearing Reactions

Allowed bearing reaction forces are defined by a series of requirements. First and foremost all bearings must be in contact with the shaft at the bottom half of their geometry, and “positive” reaction forces are defined in such a way that the above statement is true.

Secondly, reaction force values must be within a range of acceptable limits. Most major classes set a hard upper limit for mean pressure at 0.8 MPa for white metal bearings and 0.6 MPa for composite anti-friction materials. Maximum pressure is allowed to go as high as 40 MPa by NK standards, whereas Bureau Veritas [3] links reactions to lubricant film thickness, setting a minimum limit at 30 μm. The American Bureau of Shipping (ABS) [2] does not set an explicit lower limit, but instructs the following:

> “ ***Bearing Reactions***
>
> *[…]Any positive static load is therefore acceptable. However, for practical reasons, at least 10% of the allowable load would be desired on the bearing in order to prevent unloading due to unaccounted-for disturbances.[…]*

Strangely enough, the verification of reaction forces through testing contains a significant amount of uncertainty as some classes allow for deviations between prescribed calculations and measured reactions as high as ±20%. In any case classes decree that measured reactions take precedence over calculations. As ABS decrees:

> *“[…]Analytical models do not always represent the propulsion systems accurately and may not always provide sufficient information to ensure an “error free” alignment procedure.[…]”*

2.2.2. Bearing Misalignment

Misalignment between the shaft and the bearings is reported by most classes as an equally important parameter to check on. While the main focus is on the aft stern tube bearing the condition of the rest should not be overlooked.

As for the stern tube bearing, the limitations set for the maximum angle of misalignment between the shaft and the bearing bushing are relative to its dimensions. Relative misalignment angles must not exceed the ratio of the bearing radial clearance over the bearing length under any circumstances. If initial calculations prove otherwise slope boring must be applied to the inner bearing surface, or the bearing should be inclined.

Some classes [3][12] suggest that multiple slope boring should be applied to the tailshaft’s inner surface. This is justified by the fact that stern tube bearings are usually quite long, and shaft bending can be significant within that length. A two-step boring arrangement may prevent the shaft from contacting the bearing bottom shell more effectively, as portrayed in **Figure 2.2**.

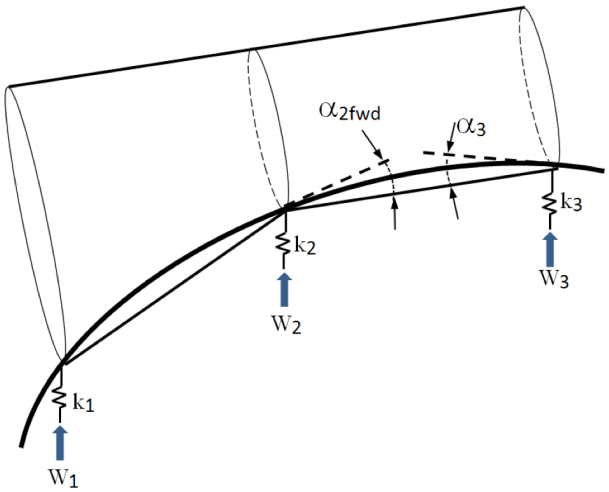

FIGURE 2.2: TAIL SHAFT BEARING WITH MULTI-SLOPE BORING [12]

2.2.3. Class Review Shortlist

The sum of parameters all major class requirements demand to be investigated and verified in a review are the following:

- Shaft Strength,
- Bearing reactions,
- Thermal expansion of M/E,
- Hull deformations of the aft part of the ship for a series of loading conditions,
- Influence factors matrix,
- Shaft elastic curve,
- Bearing misalignment, and adequacy of stern tube bearing slope boring or inclination,
- Reduction gear contact conditions (if applicable),
- Crankshaft and M/E bedplate deflections.

2.3. Shaft alignment plan implementation

2.3.1. Preliminary calculations

The first step taken in order to achieve proper alignment is choosing the number and longitudinal position of support bearings. Once that is decided, a very basic, “flat-line”, calculation of bearing reaction forces and shaft deformations is carried out for this arrangement of support points with all vertical bearing offsets set to zero. At this point, the system’s influence factors are also calculated. In the next step, appropriate vertical offsets of all support points need to be determined aiming at a distribution of reaction forces such that the loading capacity of each bearing is not exceeded, as well as minimising the slope of the shaft at each support point, which translates into minimal shaft/bushing misalignment. At this point the slope boring that needs to be applied to the aft stern tube bearing is calculated, as it is often unavoidable to take such measures due to propeller weight resulting in significant shafts slope values. Finally deflections and SAG-GAP values are being calculated for all shafts in decoupled state. It should be noted, at this point, that in order to obtain appropriate SAG and GAP values, the use of temporary support points during shaft coupling is commonly employed in practice.

2.3.2. Application

After all calculations have been carried out, all individual shaft segments are placed upon the support bearings, and if need be, upon additional temporary support aids. At this stage all parts are not coupled and their edges are free to hang. SAG-GAP and deflection values are verified using filler gauges. If the pre-calculated SAG and GAP values are not closely obtained, all necessary height adjustment are made and the forces needed to couple all flanges are calculated and applied. The working crew usually starts by laying down the propeller shaft first and letting it hang freely. With the flange of the propeller shaft as a reference point, all temporary supports are placed and forces are applied to ensure that correct SAG and GAP values between that and the next segment, which is the intermediate shaft, are achieved. The same process is repeated between the I/M shaft and the crankshaft.

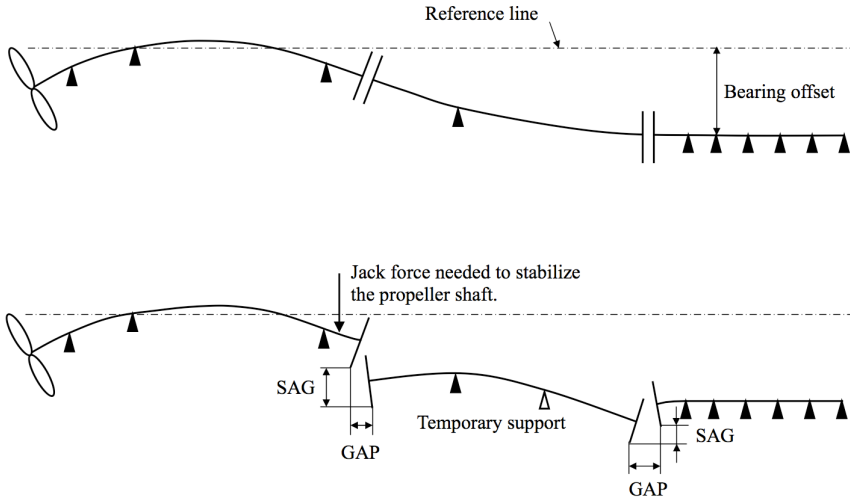

FIGURE 2.3: SAG AND GAP ALIGNMENT PROCESS [8]

With all shafts coupled, extensive testing and measurement of shafting plan parameters is performed. The main focus is on the actual bearing reactions being equal to the ones calculated prior to shafting plan application. Should they be found to differ from the calculated values, corrective action is taken to rectify any inequalities.

2.4. Measurements

2.4.1. Reference Line

A shafting plan is mainly defined as a set of support point offsets (vertical or angular) from a pre-defined reference line. In order to accurately apply any shafting plan a clear definition of this reference line needs to be established in the physical world along with a credible method of measuring distances from it. Practical solutions to this problem have been put to practice and evaluated throughout the years and the industry has settled on the following methods:

The Piano wire method

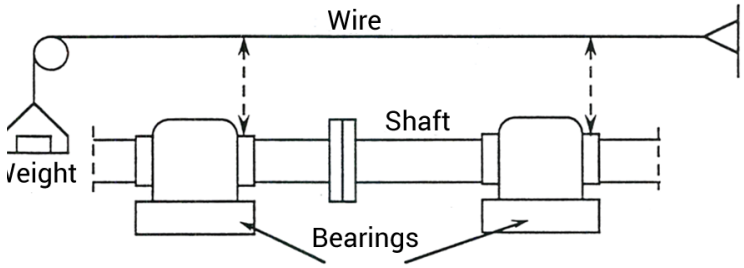

FIGURE 2.4: THE PIANO WIRE METHOD [14]

In this method a thin metal string/wire is bound to the main engine's aft part above the shaft on one end, and on the other end a weight is suspended through a pulley in order to keep the wire tense and as straight as possible. Of course it is only possible to achieve a near-straight form of the wire with this technique and consequently deflection values along its length need to be calculated. All distances are measured from this reference point and corresponding wire deflections are added according to the longitudinal position. This method is not very accurate due to the following apparent reasons:

- The wire can never rest perfectly and almost always vibrates at small amplitudes.
- It is hard to measure anything without touching the wire and thus altering its vertical position and the measurement.

Optical Methods

Another method of verifying the implementation of a shafting plan, is one that relies on optical means to measure distances from a reference line. In this method, precision optics in the form of a telescope and an arrangement of sighting targets are being employed.

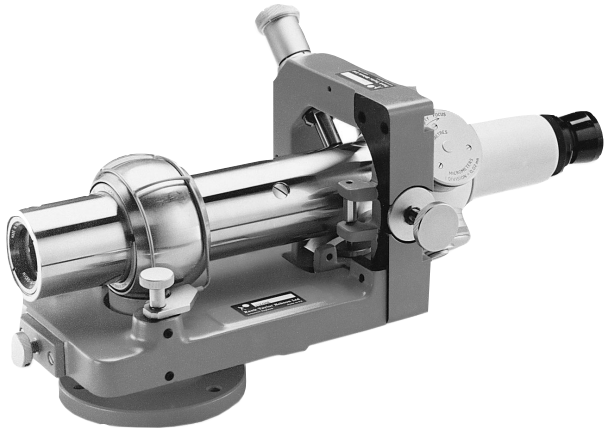

FIGURE 2.5: A TELESCOPE USED FOR SHAFT ALIGNMENT [14]

First, in order to establish the reference line the telescope is positioned on one end of the shafting system, usually right outside of the stern tube. A reference target is positioned on the other end and the rest of the targets are positioned in the exact vertical and longitudinal positions that the shafting plan dictates support bearings should be.

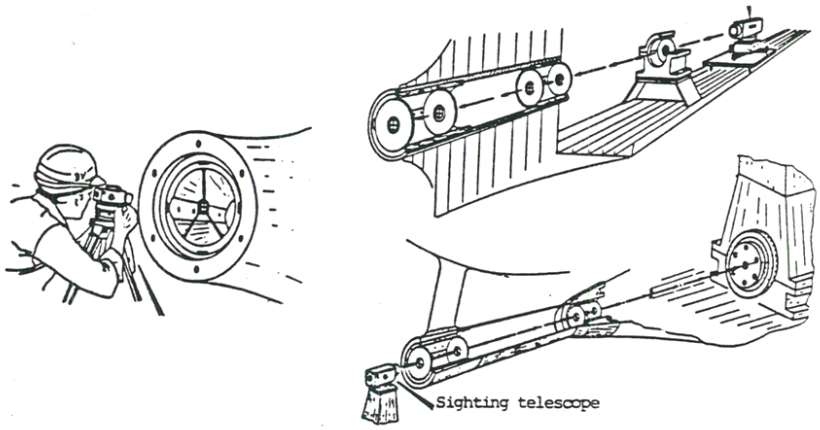

FIGURE 2.6: SIGHTING MEASUREMENT PROCESS [14]

The telescope can be adjusted through a set of three graded dials. One is used to focus at a specific distance (a reading of which can be obtained simply by looking at the values inscribed on the dial). The other two are used to adjust the telescope's vertical and lateral offset.

The first step of this method is to establish the reference line by perfectly aligning the telescope with the centre of the reference target. Once the reference line has been established, the offsets of all support points can be measured by simply adjusting the telescopes dials to achieve perfect focus and alignment with any of the targets positioned there. The read-out from the dials combined with the reference values produces the actual offset of each target. In case the resolution of scale on the graded dials is not sufficient, the targets themselves are inscribed with

concentric circles of various diameters that supplement the scale of the dials, providing improved resolution.

Through this method there is the added benefit of being able to place objects at any pre-defined position.This is done by simply setting the telescope at a specific focus distance and offset, and then moving the object around until it is perfectly in focus and aligned with the telescope.

2.4.2. Bearing Reaction Forces

Once the shafting system has been assembled, all shafts have been coupled and all temporary support points have been removed, it is time to measure the reaction forces of the support points. This is a way to verify that all preliminary calculations of the designed shafting plan were accurate.

Hydraulic Jack Testing

The method most commonly used employs hydraulic jacks to measure support reactions. To measure the reaction force of a single bearing in static, cold condition, a jack is positioned as close to the bearing as possible while still being beneath the shaft along its centreline. A micrometer is placed right on top of the shaft and a load cell is placed between the jack and the shaft. At first the shaft is jacked-up for at least 0.5 mm before any other measurement is taken, in order to ensure that there is at least a 0.5 mm tolerance for the testing to effectively take place. Then the shaft is jacked up all the way until it comes in contact with the upper shell of the bearing and then down again for a few times. This process helps eliminate systematic measurement errors. Finally simultaneous measurements of shaft vertical displacement and the jack reaction force are taken.

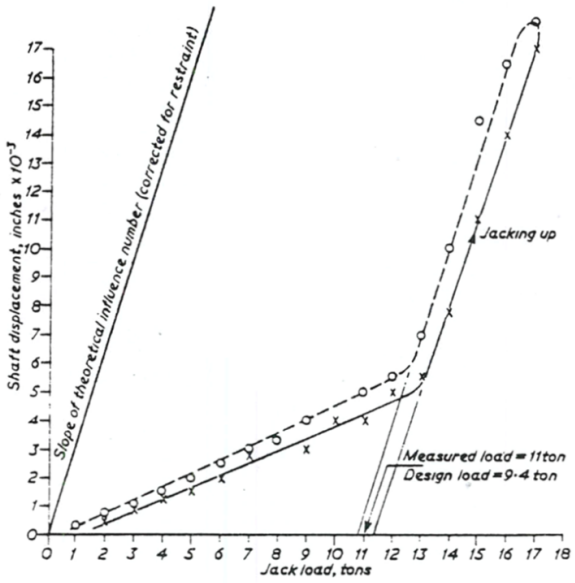

FIGURE 2.7: JACK-UP TESTING MEASUREMENT CURVES [2]

Figure 2.7 illustrates what a curve, obtained from such measurements, typically looks like. The first part of the curve features a milder slope, which represents the fact that the load of the shaft is still partially supported by the bearing. This is possible if we consider that the bearing and its foundation are elastically deformed under the weight of the shaft and thus need to fully

decompress before they completely lose contact with the shaft. The next part of the diagram depicts a steeper slope which corresponds to the influence factor of a support point placed at the exact location of the jack upon itself. The closer the jack is to the bearing, the closer this influence factor's value is to the bearing's actual influence factor. In this fashion, it becomes clear that the jack needs to be as close to the bearing as possible. Finally, it is clear that the measurements differ depending on whether they were taken while the shaft was being lifted upwards by the jack or on the way down. This difference can be attributed to friction.

To obtain a value from the above curve we need to extend the steeper part of the curve all the way until it intersects with the horizontal axis. The force value at the intersection is the desired support load value (e.g. 11kN in the Figure above).

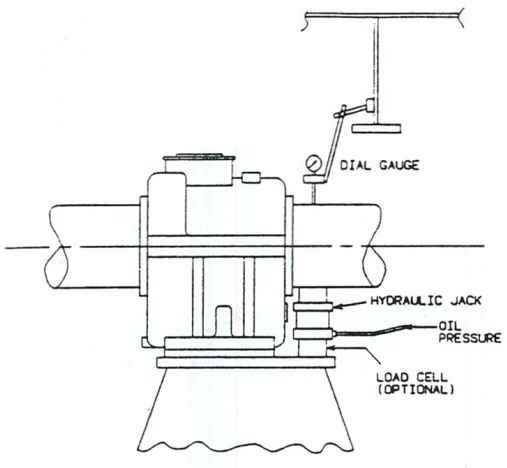

FIGURE 2.8: HYDRAULIC JACK AND MICROMETER GAUGE PLACEMENT [2]

This method can also be used to investigate whether the shaft has suffered permanent deformations in the form of bending. By taking four measurements while rotating the shaft by 90° after each measurement (for a full circle), we can compare the reactions obtained and if they do not much within some tolerance, we can conclude that the shaft is skewed.

Strain Gauge Testing

Another method of validating a shafting plan and the accuracy it was applied with is through the use of strain gauges. Bending stress at any point of the shaft can be measured with the application of a strain gauge during alignment. This method allows for the measurement of strain on the shaft surface and thus, implicitly, the calculation of reaction forces.

The advantages of using this method can be summarised bellow:

- The measurement method is quick, and well-established,
- It can be used to measure reaction forces in place where it is difficult to place a hydraulic jack,
- It provides a way to also measure lateral deformations.

On the downside, the calculations needed to produce reaction forces from deformations, demand a very detailed and careful modelling of the shafting system.

3. Journal Bearings

3.1.1. Introduction

Journal bearings are the most simple type of radial bearings. In this type of bearing, the stator is a plain hollow cylinder. The shaft (rotor) sits on the inner bearing surface and in-between them is a gap that is usually filled with lubricant. The basic geometry of a bearing can be viewed in **Figure 3.1.** As the shaft begins to rotate within the bearing, the lubricant is dragged along the periphery of the rotor and is forced to enter the converging (wedge-like) geometry generated between the shaft and the bearing. The incompressible lubricant develops pressure which separates the shaft from the bearing, preventing them from contacting one another directly in a situation often called “dry friction”. The dry friction scenario needs to be avoided, because when two metal surfaces grind against each other, they can cause severe damage to one another, that can render one of the two parts useless very fast.

The main advantages of using such bearings are:

- They can be used in projects with high precision demand as they can be constructed with small tolerances,
- The have a high capacity when it comes to absorbing and damping vibrations and sudden force impulses,
- Hydrodynamic lubrication minimises wear, thus increasing lifespan,
- Their construction is simple.

The lubricants role in this setup is to prevent these surfaces from coming in contact and support the weight of the shaft as it rotates within the bearing. This is achieved by means of hydrodynamic lubrication, and a basic prerequisite for this is that the shaft and the bearing have a relative rotational velocity greater than zero.

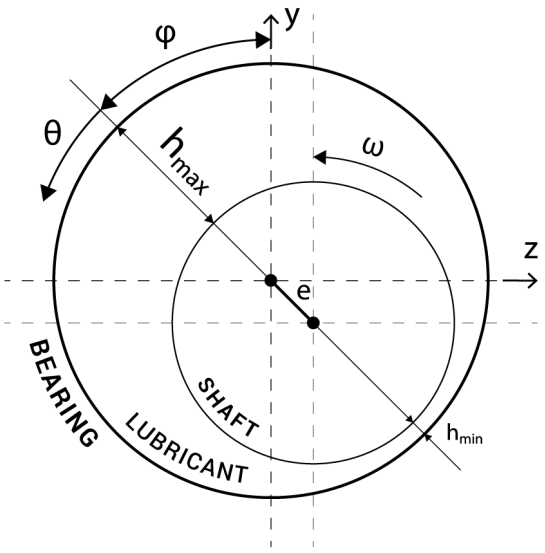

FIGURE 3.1: BEARING GEOMETRY

3.1.2. Hydrodynamic Lubrication Principles

Let us define a problem of similar geometry and physical properties to that of a shaft within a journal bearing. To start off, let there be a shaft of diameter **d** that rotates inside the inner surface of a hollow cylinder of diameter **D > d**, with D - d being equal to the bearing **clearance**. In between the two surfaces there is an ample amount of a lubricant fluid. During steady state operation at a constant rotational speed, the shaft rests slightly off centre, relative to the bearing as pictured in **Figure 3.1.** This way it is obvious that there is a spot along the circumference where the distance between the two surfaces is minimal. This offset can be described using two variables:

- Attitude angle **φ** : The angle at which minimal distance between shaft and bearing is observed,
- Eccentricity **e** : The off-centre distance along the radius at angle **φ**. If the shaft was resting right at bearing centre, **e** would be equal to zero and shaft-bearing distance would be constant along the circumference and equal to the bearing radial clearance. In any other case the minimum shaft-bearing distance is equal to the radial clearance minus eccentricity. The greater the load the bearing has to support, the bigger the eccentricity it will exhibit.

The geometry of the problem can be further simplified if we picture the inner bearing surface as if it had been cut lengthwise and rolled open on a flat surface. We can make the same mental abstraction for the shaft, retaining shaft to bearing distance, and now we have two surfaces facing each other (**Figure 3.2**). The outer shaft surface and the inner bearing surface form a converging region, where the distance between the two grows smaller along the circumferential coordinate until it reaches a minimum at angle φ, and a diverging region where the exact opposite takes place. Since the gap between the two surfaces is filled with lubricant, the minimum distance spot coincides with the minimum film thickness location of the lubricant.

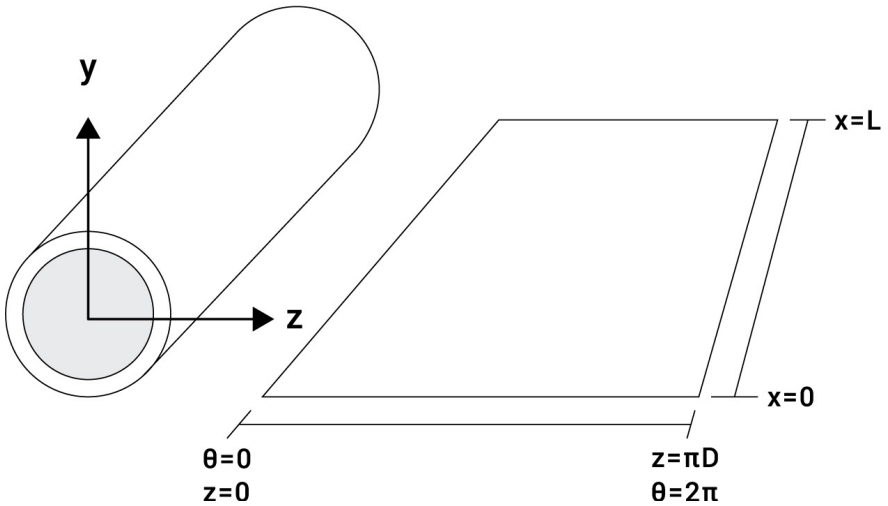

FIGURE 3.2: UNWRAPPED BEARING GEOMETRY

As mentioned above, the purpose of this type of lubrication is to prevent the two metal parts form contacting one another and to support the weight of the shaft. The latter demands that lubricant pressure is high enough to carry that load. To that end, pressure buildup in the lubricant domain should be achieved somehow. In journal bearings, pressure is developed by means of

hydrodynamic lubrication. For the following analysis to be valid, the basic assumptions that need to be true are:

- The lubricant is a Newtonian, viscous fluid,
- Lubricant inertia induced forces are negligible compared to viscous forces,
- Gravitational forces can be neglected,
- The lubricant is an incompressible fluid,
- Lubricant viscosity remains spatially constant (iso-viscous condition),
- Lubricant flow is steady (temporal effects are neglected, steady-state condition is assumed),
- Bearing inner diameter to bearing clearance ratio is close to infinity,

The mathematic expression governing hydrodynamic lubrication is called the Reynolds Equation:

$$\frac{U}{2}\cdot\frac{\partial h}{\partial z}=\frac{1}{\mu}\left[\frac{\partial}{\partial z}\left(\frac{h^3}{12}\cdot\frac{\partial p}{\partial z}\right)+\frac{\partial}{\partial x}\left(\frac{h^3}{12}\cdot\frac{\partial p}{\partial x}\right)\right] \quad \text{EQ. 3-1}$$

Where:

- U is the tangential velocity of the shaft,
- μ, is the lubricant dynamic viscosity,
- h is a function that describes lubricant film thickness in 3D space and,
- p is the pressure distribution in 3D space.

The above equation can be derived in many ways, such as from the Navier-Stokes equations with the application of the assumptions listed previously. It becomes clear that there needs to be a non-zero relative angular velocity term for hydrodynamic lubrication to come into effect. Part of what the Reynolds equation describes is also the geometry's influence on the spatial rate of pressure change. The specific part of the geometry that induces pressure buildup is the bearing-shaft convergence section. Thus, there are two requirements for hydrodynamic lubrication:

- Relative velocity between the two surfaces,
- A convergent geometry that resembles a wedge.

This way, due to shaft motion, the lubricant is dragged into the wedge volume, and for mass to be conserved along the flow direction, a gradient of pressure is generated as the wedge converges. Pressure increases at the beginning of the wedge, restricting inflow, while it decreases near the end of the wedge boosting outflow. The existence of a pressure gradient causes the fluid velocity profile to bend inwards at the entrance and to bend outwards at the exit.

Boundary Conditions

To solve the Reynolds equation, appropriate boundary conditions must be set. Of all the boundary conditions proposed, the most notable are:

- The Full-Sommerfeld condition which dictates that pressure is equal to zero at the edges of the unwrapped bearing geometry. A direct consequence of this boundary condition is that negative bearing pressure of similar distribution and magnitude is developed at the diverging section of the geometry, which makes total pressure equal to zero and effectively cancels out lubricant capacity to support any weight. Thus this condition is unrealistic as it yields unrealistic results,
- The Half Sommerfeld condition, which assumes that the pressure distribution at the converging section is identical to the one given by the full Sommerfeld condition, whereas negative pressure values at the diverging region are taken equal to zero. the results obtained with the use os half-Sommerfeld condition are not vey accurate, since this condition leads to violation of mass conservation in the diverging part of the bearing,
- The Reynolds condition. This boundary condition suggests that no negative pressure values should be observed and that at the boundary between zero and non-zero pressure the following condition should apply: $p = dp / dx = 0$. The Reynolds boundary condition gives more accurate results in comparison to the Full and Half Sommerfeld conditions, and it is used for the pressure calculations of the present work.

3.1.3. Operation and Performance Parameters

Load Capacity

Having obtained an expression for lubricant pressure we can now integrate it along the circumference and length of the outer shaft surface. This way, the total hydrodynamic load developed by the lubricant film can be obtained. We can further break down this load into a pair of perpendicular forces acting along the main coordinate system axess y-z (**Figure 3.1**), whose resultant force is that same total bearing load. These forces are easier to match up against the weight of the shaft and any other externally applied load. The following expressions relate the obtained pressure to the load the lubricant can support.

$$W_y = \int_0^{2\pi}\int_0^{L} p \cdot \sin(\varphi + \theta - \frac{\pi}{2}) \cdot R \cdot dx \cdot d\theta \qquad \text{EQ. 3-2}$$

$$W_z = \int_0^{2\pi}\int_0^{L} p \cdot \cos(\varphi + \theta - \frac{\pi}{2}) \cdot R \cdot dx \cdot d\theta \qquad \text{EQ. 3-3}$$

$$W = \sqrt{W_z^2 + W_y^2} \qquad \text{EQ. 3-4}$$

Sommerfeld Number

The Sommerfeld number is a non-dimensional characteristic bearing number. It comprises design (R, c, L, D) and operating (μ, ω, W) parameters. All bearings operating at the same Sommerfeld number have the same operational characteristics and have equal non-dimensional parameter values. It can be calculated using the following formula:

$$S = \left(\frac{R}{c}\right)^2 \cdot \frac{\mu \cdot \omega \cdot L \cdot D}{W} \qquad \text{EQ. 3-5}$$

Where:

- R is the shaft radius,
- c is the bearing clearance,
- μ is the dynamic viscosity of the lubricant,
- ω is the shaft angular frequency in rads per second,
- L is the bearing length,
- D is the bearing diameter and,
- W is the total, externally applied, load.

It can be seen from the above formula that it is a dimensionless quantity. The Sommerfeld number is an important parameter because it takes into account and combines all the variables involved in the design and operation of a bearing. For a given bearing, the larger the value of the Sommerfeld number, the less severe the loading of the bearing is, and vice versa.

Friction Force and Friction Coefficient

The assumptions made so far demand that the lubricant is a Newtonian fluid and the lubricant viscosity cannot be neglected, otherwise the shaft rotation would not be able to induce lubricant motion and there would be no flow. An implication of this assumption is that shear stresses are present at the shaft lubricant interface, the integral of which yields the total friction force.

$$F = \int_0^L \int_0^{\pi D} \left(\frac{2y - h}{2} \cdot \frac{\partial p}{\partial z} + \frac{U}{h} \right) \cdot dz \cdot dx \qquad \text{EQ. 3-6 [1]}$$

Friction coefficient, f*, can be defined as a ratio of friction force to bearing total load: f* = F / W.

Power Loss

Power loss in journal bearings comes from friction alone. If power loss was equal to zero then the shaft would be able to transmit the full amount of power available to its final destination (e.g. the propeller). Some of it, though, is taken away by friction in each support bearing. Friction power loss of a bearing can be calculated as:

$$P_{loss} = F \cdot U = W \cdot f^* \cdot \omega \cdot R \qquad \text{EQ. 3-7 [1]}$$

Where:

- f* is the friction coefficient of the bearing,
- W is the total bearing load,
- F is the total friction force of the bearing,
- ω is the angular frequency of the shaft,
- R is the inner bearing radius.

Bearing Misalignment

Under ideal conditions, the shaft and bearing centrelines are parallel. In this case bearing-shaft misalignment is zero and this way bearing misalignment can be defined as the angle between the centrelines of these two parts. Usually, misalignment values are not zero. As with external load, misalignment angle can be similarly resolved into two angles, one about each axis of the coordinate system of **Figure 3.1**. Thus, lateral misalignment angles describe shaft rotations about the vertical y axis, and vertical misalignment angles describe rotations about the horizontal z axis.

Bearing-shaft misalignment has a negative impact on the lubrication characteristics of a bearing. For any given pair of eccentricity and attitude angle values, the misaligned shaft is brought closer to the bearing surface, minimum film thickness decreases and the lubricant becomes much less able to support the weight of the shaft. In some situations the shaft will start grinding against the inner bearing surface until portion of the bearing's lower part has been removed by the shaft. This kind of adaptation is expected to happen during the first years of a system's operation and is considered to improve bearing performance as it reduces the effect of misalignment.

Another consequence of bearing-shaft misalignment is that it changes the pressure distribution of the lubricant. In a zero-misalignment situation lubricant pressure is lengthwise symmetrical, with a maximum value located at the centre of bearing surface. On the contrary, under some misalignment, pressure will form a more discreet peak, with maximum pressure being located closer to the edge of the bearing and closer to the longitudinal point of minimum film thickness.

4. Numerical Modelling

4.1. Matrix Analysis

4.1.1. 3D Beam Element

In its simplest form, the shafting system is a long circular multi-supported beam. Being a multi-supported beam means that solving for bearing reaction forces and other system information, is a statically indeterminate problem. To work around this limitation, in a way that is sensible for computer based programming, Matrix Analysis is employed as the main solution method of the shaft alignment problem. In the present work, the propulsion shaft is represented by an assembly of three dimensional multi-supported beam elements. These elements are defined by their geometry and physical properties. Every such element interacts with other elements and its environment through a pair of connection points positioned at each one of the beam's edges (**Figure 4.1**). These points are called "nodes".

FIGURE 4.1: BEAM ELEMENTS AND NODES ABSTRACTION

All external forces (e.g. propeller weight) and internal loads (e.g. beam distributed weight) are applied as generalised loads. Similarly all translations and rotations are only expressed as generalised nodal displacements. An element of such properties in 3D space has six degrees of freedom (DOFs) per node: 3 rotations about each axis per node and 3 translations along each axis per node, for a total of twelve DOFs per beam. In the same fashion a beam's loading condition can be described by 3 moments about each axis per node and 3 forces parallel to each axis per node.

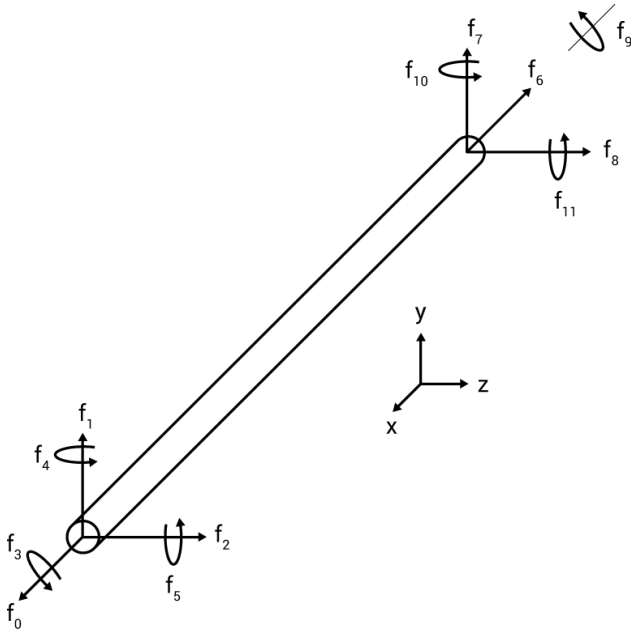

FIGURE 4.2: NODAL DEGREES OF FREEDOM

This type of element is capable of describing accurately a beam that is being subjected to all kinds of generalised loads and deformations. **Figure 4.2** illustrates all of the above:

- f_0 and f_6 describe axial loads, and the corresponding axial compression or expansion is described by u_1 and u_6,
- f_3 and f_9 correspond to twisting moments and the corresponding twist angle is described by u_3 and u_9,
- f_2 and f_8 correspond to shear forces, and the corresponding lateral translation is described by u_2 and u_8,
- f_1 and f_6 correspond to vertical shear forces, and the corresponding vertical translation is described by u_1 and u_6,
- f_4 and f_{10} correspond to lateral bending moments about the y axis, and the corresponding rotation angle is described by u_4 and u_{10},
- f_5 and f_{11} correspond to vertical bending moments about the z axis, and the corresponding rotation angle is described by u_5 and u_{11},

	Forces	Moments	Translations	Rotations
Axial, Twisting	f_0, f_6	f_3, f_9	u_0, u_6	u_3, u_9
Horizontal, Lateral	f_2, f_8	f_4, f_{10}	u_2, u_8	u_4, u_{10}
Vertical	f_1, f_7,	f_5, f_{11},	u_1, u_7,	u_5, u_{11},

TABLE 4-1: FORCE AND DISPLACEMENT VECTOR BREAKDOWN

The above sets of generalised loads and displacements can be written in vector form for each node:

$$\begin{bmatrix} u_0 \\ u_1 \\ u_2 \\ u_3 \\ u_4 \\ u_5 \end{bmatrix} \qquad \begin{bmatrix} f_0 \\ f_1 \\ f_2 \\ f_3 \\ f_4 \\ f_5 \end{bmatrix}$$

The load vector can be related to the displacement vector, through the application of basic principles of mechanics (Hughes and Paik (2010)). Each individual displacement described by a degree of freedom can be related to the generalised loads that cause that displacement. This relation is a function of beam geometric and mechanical properties. For example load $\mathbf{f_0}$ causes axial compression or expansion and the corresponding nodal displacement $\mathbf{u_0}$ are related to each other with a factor that is a function of cross sectional area A, Young's modulus E and beam length L : (AE)/L which is commonly known as a beam's **resistance, or stiffness** to axial compression, or tension. These factors can be assembled into a matrix which is called the element's stiffness matrix k.

$$\begin{bmatrix} f_0 \\ f_1 \\ f_2 \\ f_3 \\ f_4 \\ f_5 \end{bmatrix} = \begin{pmatrix} k_{11} & \cdots & k_{16} \\ \vdots & \ddots & \vdots \\ k_{61} & \cdots & k_{66} \end{pmatrix} \begin{bmatrix} u_0 \\ u_1 \\ u_2 \\ u_3 \\ u_4 \\ u_5 \end{bmatrix} \qquad \text{EQ. 4-1}$$

Matrix **k** is composed of 6x6 elements each representing how the elements of load vector **f** interact and relate to the elements of displacements vector **u**. The elements of matrix **k** are a function of the geometric and material properties of the beam (length, second moment of cross sectional area, Young's modulus of elasticity, cross sectional area, e.t.c.). This simple linear relation indicates that loading a beam with load vector **f** will produce a set of displacements **u**. Similarly it means that a beam develops a set of reaction forces **f**, should its nodes be constrained at specific positions described by a non-zero vector **u**.

Matrix **k** is a square **symmetric** and **singular** in every case. The matrix's **symmetry** represents the simple fact: that each of the elements node affects its counterpart in such a way that produces forces and displacements of equal magnitude, but opposite direction. The fact that the matrix is **singular** represents mathematically that the inverse for that matrix does not exist and thus, we cannot solve for vector $\mathbf{u = f^{-1}k}$. Such a system is called indeterminate.

At this point it is important to note that a set of initial constraints is necessary for the above system of simultaneous equations to have a solution that makes physical sense. If no such constrain exists then the beam is free to move in 3D space. Under these conditions, the beam will be accelerated by the force vector, performing rigid body motion and making the number of possible displacements infinite, which is what makes our system indeterminate.

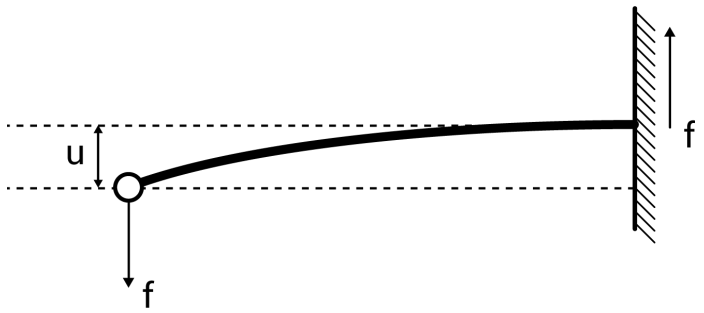

FIGURE 4.3: A BEAM FIXED AT ONE END

An example of such a set of constraints would be given if one of the beam's ends were fixed in space (e.g. clamped on a wall as in **Figure 4.3**). In this case, all six DOFs describing the displacements of the fixed node would be equal to zero should we choose to place our reference point onto that node. This would mean that the elements of matrix **k** that relate load vector elements with these DOFs would be of no importance. It would also mean that the square sub-matrix of **k** that does not contain these elements is the only part of the system that could be used to solve for **u**. Fortunately this sub matrix is not singular. In this fashion, we have obtained a new set of simultaneous equations that can be solved for both **f**, for those **u** elements that are fixed,

and **u**, for those **f** elements that are imposed on the beam. In this example a force of magnitude f would be needed to cause the non-constrained node to be displaced by u to a new position and to be held there. The corresponding DOF of the constrained node would be subjected to a force of equal magnitude, but opposite direction and equilibrium of forces would be achieved.

4.1.2. Assembly of 3D Beam Elements

A combination of more than one 3D beam elements can produce objects of more complex geometry. In the present work the simple geometry of three shafts (i.e. the propeller shaft the I/M shaft and the crankshaft) connected through flanges, can be represented by an assembly of beams, of various length and diameters, in a collinear arrangement.

Local element vectors **f** and **u** can also be combined into global vectors **F** and **U** if the DOFs of each node are arranged in sequence starting with one node and moving on to the next one. For example the DOFs of node *No.1* would take up **U** vector elements *0* to *5* and node *No.2* would continue from element *6* and go on until element *11*. Obviously beams that share a node at their common end make use of the same DOFs. In the previous example, node *No.2* lies at the right-hand end of the first beam and, at the same time, at the left-hand end of the second beam. An arrangement of three beams would thus need only four nodes to be perfectly defined. This, effectively, links beam displacements at their common end, producing a system of beams that retains compatibility of deformations. Similarly the local stiffness matrices **k** can be used to synthesise a global stiffness matrix **K** that describes the whole model. In this case, each beam contributes its stiffness elements to form the terms that affect common node DOFs.

In **Figure 4.4**, a shaft consisting of four beam elements, with hinge support points, is presented. This model is the simplest approximation of a shafting system, as it utilises only simple supports for the constrained nodes (i.e., bearing positions) where the shaft is considered to be hinged in this regard. This type of constrain allows for rotations about the Z axis, but means that nodes are constrained for all other DOFs.

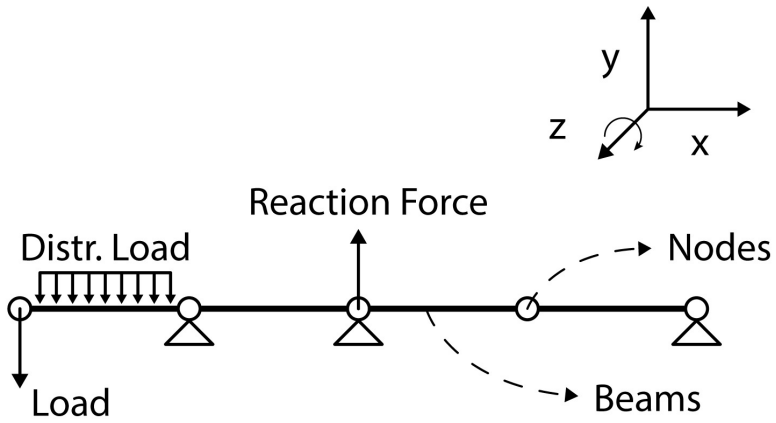

FIGURE 4.4: MODELLING OF THE SHAFTING SYSTEM: SIMPLE MULTI-SUPPORTED BEAM APPROACH

External loads and deformations are applied to the beam nodes. All internal loads (e.g. the distributed weight of a beam) can be expressed in terms of equivalent nodal generalised loads, through the application of basic principles of mechanics (Hughes and Paik (2010)). The degrees of

freedom allowed for each node are three rotations about, and three displacements along the principal axes of the 3D Cartesian coordinate system. Vertical loads, such as propeller weight, or the shaft's own weight, are parallel to the **y** axis, while axial loads are parallel to the **x** axis and shaft bending moments are applied about the **z** axis.

When modelling a shafting system, boundary conditions are known for both the force vector and the displacement vector. Additionally the designer of such a system needs to know the displacements at all system nodes including those where external forces have been applied. Similarly all nodal forces need to be calculated, even at nodes where displacements have been externally imposed. Solving this problem by hand amounts to simply dividing global matrix **K** to its two sub matrices. One would be used to solve for **F** and the other to solve for **U**. This is not the best solution method for a computer program, as it involves lots of matrix manipulation operations, which are resource costly and time consuming.

A more suitable method involves creating a second, dummy global stiffness matrix **K'** and a second, dummy load vector **F'**. The dummy stiffness matrix diagonal term values that correspond to constrained DOFs, with fixed displacement positions, are set equal to unity and the rest of the terms in the same rows are replaced with zeros. The values of dummy load vector **F'** that correspond to constrained DOFs are replaced with the corresponding fixed displacement values, while the rest of the vector remains identical to the initial load vector **F**. When solving for global displacements vector $\mathbf{U = K'^{-1} F'}$, all fixed displacement values will be simply passed over to the displacements vector, while the rest of the vector's elements will be computed correctly. In a subsequent step the actual loading vector **F** is computed as **F = K U**. This time, vector **U** contains all information regarding constrained DOF displacement values, and the multiplication with **K** will provide us with the forces required to keep the constrained nodes firmly held at their positions. In similar fashion, the load vector's elements that correspond to externally applied loads, will be equal to the ones initially applied, because corresponding vector **U** displacements were computed correctly using the dummy vector and matrix.

4.1.3. Elastic Support

In order to incorporate the effects of bearing foundation elasticity directly into our calculations a slightly more complex model is needed. In **Figure 4.5**, a shaft consisting of regular beams supported by beam-like elements that can only be subjected to axial stress is displayed. In this model, the geometric (cross section area A, length L) and material (Young's modulus, E) properties of each support beam are such that the desired axial stiffness of bearing foundation is accurately simulated. It is worth noting that the horizontal shaft retains the ability to freely rotate about the z axis as pictured in the Figure, while on the lower end all support beams are clamped to the ship foundation. The fixed nodes will be henceforth called support nodes.

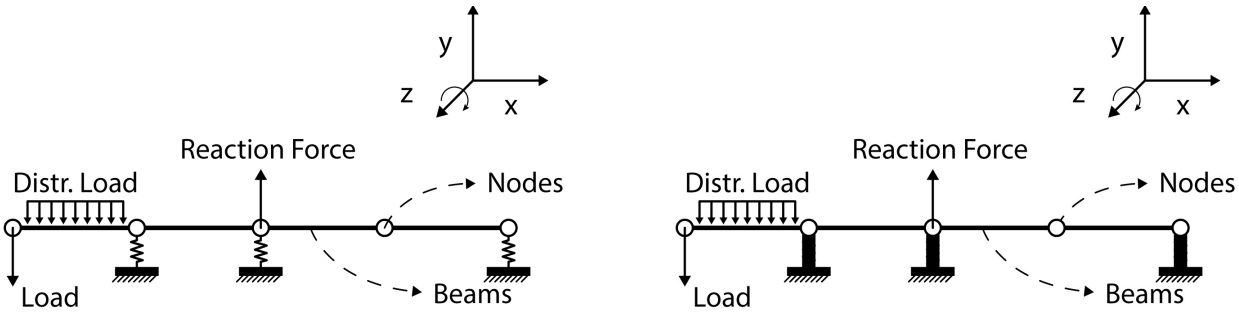

FIGURE 4.5: MODELLING OF THE SHAFTING SYSTEM: INTRODUCTION OF BEARING FOUNDATION ELASTICITY

In this type of modelling the total number of beams and nodes is expanded by a number equal to the number of supports. The nodes that lie right above the support nodes can freely move vertically, as support beams deform elastically. All nodes shall now be called shaft nodes, save for support nodes. The designer of such a system would want to specify vertical bearing offsets for the support nodes which in turn will drug along the shaft nodes connected to them through support beams. All forces are applied onto shaft nodes alone and cause all beams to deform freely.

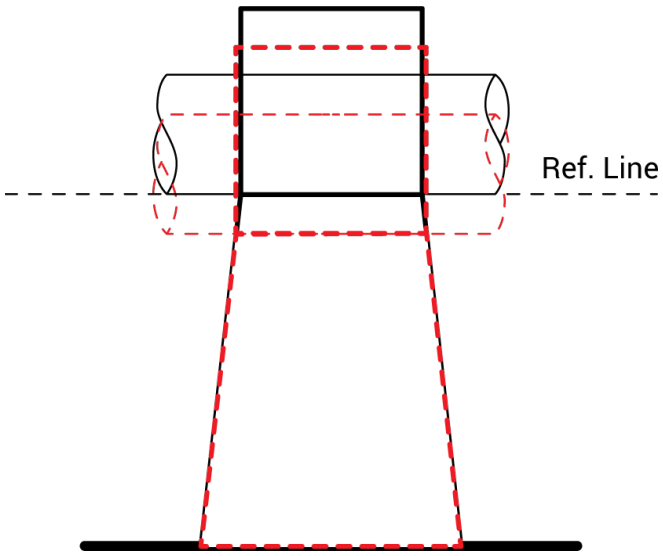

FIGURE 4.6: THE EFFECTS OF BEARING FOUNDATION ELASTIC DEFORMATION

The effects of elastic deformation are displayed in **Figure 4.6**. Every bearing supports its part of the shaft's weight as determined by the matrix analysis conducted on the model. This weight is applied as a point load to the shaft node that lays right above each support node. Shaft nodes are free to move vertically and compress bearing foundations to a significant amount, in proportion to the forces applied to them. Equilibrium is achieved because reaction forces of equal magnitude and opposite direction develop at every support node. These forces correspond to the actual bearing reaction forces and constitute the main output of the above process.

4.2. Shaft Support and Journal Bearings

The propulsion shaft of a ship can be modelled as a multi supported beam. In practice, the shaft is supported by hydrodynamically lubricated journal bearings. Geometrically, a journal bearing is a hollow cylinder of length L, which encloses a solid shaft that rotates about its axis at a revolution rate of N RPM. The inner diameter D of the bearing is slightly larger than that of the shaft; the difference between the bearing and the shaft radius is called “clearance” c. Therefore, the shaft may undergo a small displacement before contact with the bearing surface. In normal bearing operation, this gap is filled with a thin layer of lubricant, of dynamic viscosity μ, which supports the weight of the shaft by means of hydrodynamic lubrication [1]. This lubricant film has a thickness h that varies along the circumference of the bearing bushing from a minimum value of h_{min}, to a maximum value of h_{max}. To achieve equilibrium between the shaft weight and the load supported by the lubricant film, the shaft will not come to rest at the lowest part of the bushing, but at an angle φ relative to the y-axis on the y-z plane, also known as the attitude angle. In particular, φ is the angle between the (vertical) load line and the line passing through the centres of the shaft and the bearing (**Figure 3.1**). At this angle, the lubricant film thickness attains its minimum value, whereas the shaft centre does not coincide with the bearing centre. The length of the straight line that connects the two, is known as “eccentricity” e, and is usually made non-dimensional using the following formula: $\varepsilon = e / c$, where c is the bearing radial clearance as noted above.

All bearings, including the M/E crankshaft bearings, are assumed to be in a steady-state “running” condition; that is the propulsion shaft is assumed to be rotating at a constant speed, whereas the shaft loads are assumed constant (not time dependent). With these assumptions, lubricant flow between the bushing and the shaft can be thought of as steady flow. Additionally, the flow is assumed **incompressible** and **isothermal** (lubricant viscosity is assumed constant). As discussed in section 3.1.2, the flow characteristics in the lubricant domain (pressure, shear stress and velocity fields) can be computed by solution of the well-known Reynolds equation (EQ. 3-1).

Here, ambient pressure is assumed at the sides of the bearings, whereas a **Reynolds boundary condition** (dp/dx=0) is applied at the film rapture region. Simulations of fluid flow and pressure development of the bearings have been performed utilising a custom in-house code, which solves the Reynolds equation, with considerations for misalignment effects (details may be found in Raptis, 2014).

Having computed the pressure and shear stress distributions, expressions for calculation of load capacity, W, and friction force, F, can be formulated by simple integration over the inner surface of the bearing. This becomes an easier concept to grasp if we consider the cylindrical geometry of the bearing, as if it had been cut lengthwise and rolled open on a flat surface (**Figure 3.2**). On this rectangular plane, the length runs from zero to L along the x-axis, whereas the breadth runs from zero to πD along the z-axis, or from 0 to 2π if we visualise this side in a circular shape. Expressions EQ. 3-2 to 3-7 can be used for calculation of W and F.

Since the propulsion shaft exhibits an elastic line, the part of the shaft inside the bearing is not (generally) parallel to bearing surface, causing effects of misalignment (**Figure 4.7**). As presented

in section 3.1.3, misalignment leads to non-symmetric pressure distribution along the bearing length, therefore, the resultant bearing support force is acting at a point lying at a distance from bearing mid position. The actual position of the bearing support force influences the behaviour of the shaft overall, since it changes the longitudinal position of the single-point supports utilised in the model of **Figure 4.5**. In the present work the effect of misalignment is taken into account by calculations of bearing pressure distribution, which allows for a precise calculation of the location of single point shaft supports (**Figure 4.7**). The new locations of shaft support points (being a function of misalignment angle) is then fed into shaft alignment calculations.

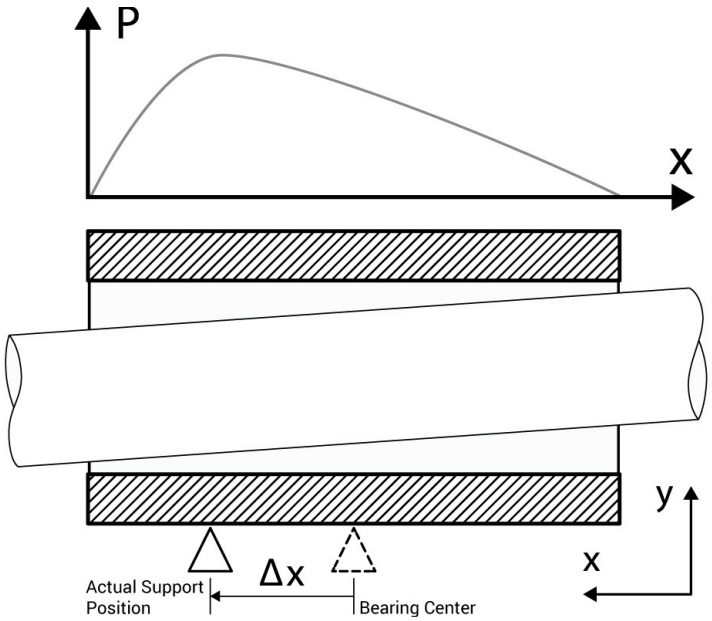

FIGURE 4.7: PRESSURE BUILD-UP IN THE LUBRICANT DOMAIN AND RESULTING SHIFT OF SINGLE-POINT SUPPORT POSITION

The approach described above allows us to model the interactions between support bearings and the shaft. For a given set of y-axis bearing offsets, we can obtain a set of reaction forces and misalignment angles, through matrix analysis. The above can be fed into the bearing solution process and output a set of vertical displacements that correspond to the oil film thickness and a new support point position along the length of each bearing, which in turn is fed back into the matrix analysis calculations. A new system is created based on the new longitudinal and vertical positions and the process is repeated until the reaction forces converge to a set of values. The above coupled problem outlines an iterative process that comes to an equilibrium providing a better approximation of the shafting system behaviour under realistic operating conditions.

4.3. Solution Algorithm

4.3.1. Overview

The aim of software development, in the present study, is to provide an analysis tool for whoever needs to design a shafting system's alignment plan, oversee its implementation and carry out its long-term maintenance. The numerical modelling and tools employed to this end, where theoretically described in the previous sections. In this section the specifics of the solution process are discussed and all considerations made during that process are listed. All programming was conducted using object-oriented C++ programming language. In this section, any references made to "objects" reflect the structure of the code and the C++ objects created therein.

The problem being solved here is a **coupled** problem consisting of two parts: **Matrix Analysis** and **Bearing Hydrodynamic lubrication**. Both parts deal with some parameters of the shaft alignment problem that are unique to them alone and, at the same time, both parts have an exchange of variables that are common between the two. This way an active connection and an **interaction** between the input and output parameters of both parts is established.

Support Point Modelling

The common ground between these two main parts is the modelling of the shaft **support points**. It is important to outline here how these support points are modelled, and how does this choice of modelling affects and interacts with the solution process of each part.

In the present study:

- The shaft is mounted on single point supports. This means that the contact area between a bearing and the shaft is a **single point**,
- During the solution process, support point foundations can elastically deform, along the **vertical** axis, under the influence of the reaction forces they need to develop to support the shaft,
- At the beginning of the solution process, support points may be offset **vertically** by constant values corresponding to the designer's initial alignment plan, and/or to ship hull deformations under different loading conditions,
- A constant **angle** of slope boring may be imposed on certain support points in accordance with the designer's initial alignment plan,
- In case of bearing misalignment, the **longitudinal** position of support points will shift, during the solution process, in order to better model the single point support equivalent of the pressure distribution support area within each bearing,
- During the solution process, the **vertical** position of support points will change by a value that corresponds to the film thickness that each bearing developed, under the influence of a specific reaction force,

The above description specifies that a support point's vertical position, relative to a reference line, can change in four different ways:

- Two offsets that remain constant throughout the solution process:
  - Offsets due to hull Deformations and,
  - Initial alignment plan offsets.
- Two offsets that change during the solution process:
  - Offsets due to elastic compression of support point foundations and,
  - Offsets due to bearing lubricant film thickness.

The final offset of any given support point is in fact the sum of the above. It should be noted here, that the values of the four parts that make up this final offset might be of opposite sign. **Figures 4.8 A** and **B** illustrate an example of how these four offsets may work towards the same or opposite direction.

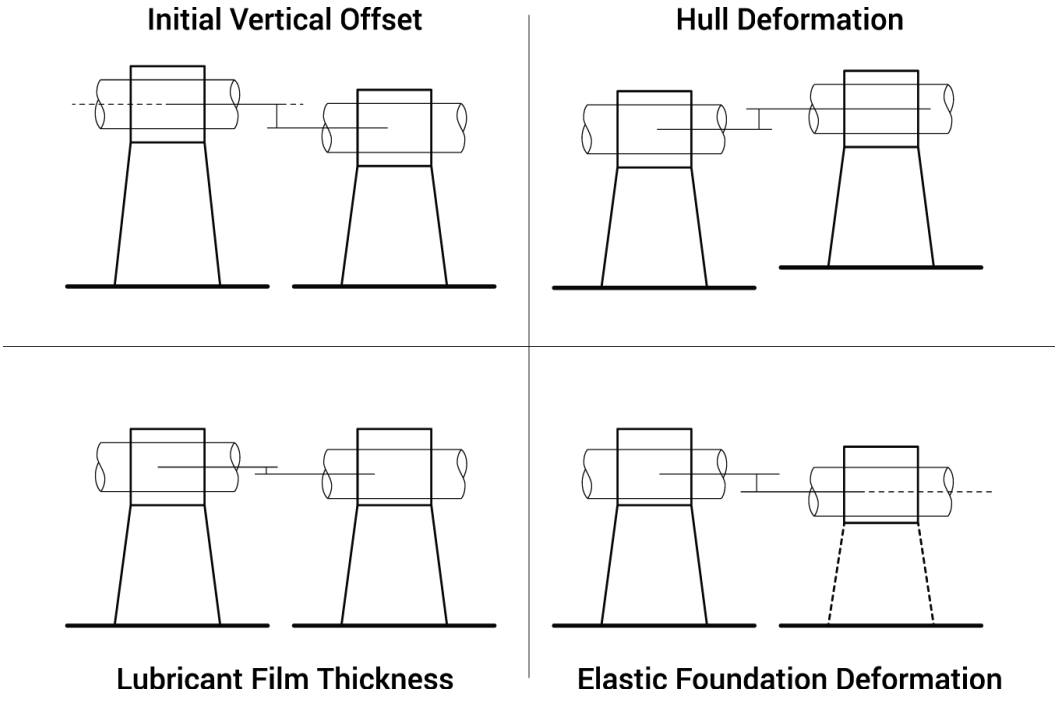

FIGURE 4.8 A: SEQUENTIAL APPLICATION OF OFFSETS

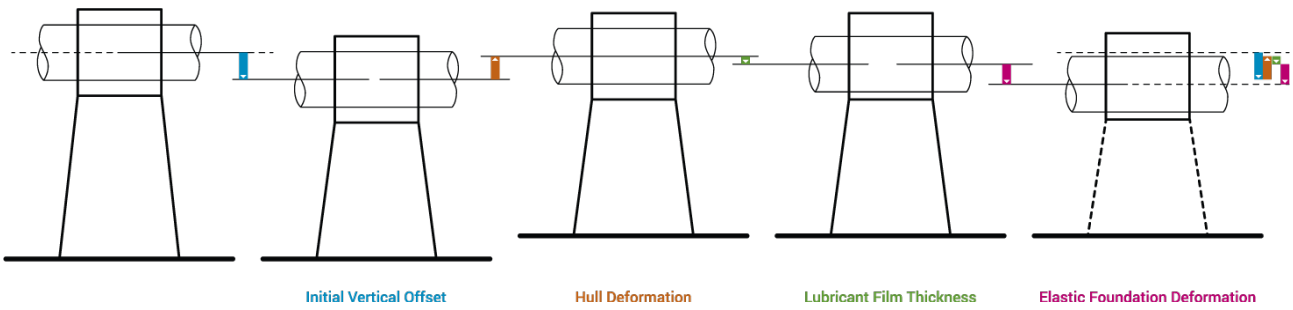

FIGURE 4.8 B: ALL OFFSETS RELATIVE TO THE REFERENCE LINE

4.3.2. Model Creation

All calculations described in this chapter demand a significant amount of input from the user. Modelling a shafting system, under the assumptions presented in this work, requires information on geometric and material properties, as well as operating condition parameters. All the above is supplied by the user through an input file. The input file that the user needs to submit should contain the following:

- The number N of shaft segments, i.e. the number of beam elements of the system,
- A list of all N segment lengths in meters,
- A list of all N segment weights per unit length,
- A list of all N segment second cross sectional area moments,
- A list of all N segment values of Young's Modulus,
- A list of all (N+1) initial, externally applied, vertical, nodal forces,
- The number M of constrained nodes, which is equal to the number of bearings in the system,
- A list of the constrained nodes ID number (e.g. 6 for the sixth node in line from the left-most end of the shaft),
- A list of all M initial vertical bearing offsets,
- A list of all M bearing foundation stiffness values,
- A list of all M hull deformation induced vertical offsets foreach bearing,
- A list of all M lubricant dynamic viscosity values in Pa s,
- A list of all M bearing Length over Diameter ratios,
- A list of all M bearing Diameter values,
- A list of all M bearing Radial Clearance values,
- A list of all M shaft rotational speed values in RPM,
- A list of all M bearing applied slope boring values in rads,
- A list of values that toggle bearing calculations for a constrained node. Thus, all, or some constrained nodes may be modelled as journal bearings and have a bearing object instance created for them.

The above input helps create two different shaft models that can be used for rigid or elastic support calculations.

The shaft model usually comprises many segments of various geometric properties. For each segment a beam element object instance is created with specific geometric and mechanical properties. At the moment of construction, the beam object's local element stiffness matrix is also created.

Prior to beam element object creation, a set of shaft nodes in 3D space is created. Each node is positioned at the intersection of two, or in some cases three, beams. Node objects contain all

displacement and force vector information associated with the beams they are attached to. They also contain the bearing objects. Bearing object instances are only created if:

a) A node is marked as constrained,
b) Every single piece of information that concerns a given bearing is input correctly, and
c) The bearing toggle is set accordingly.

4.3.3. Matrix Analysis

In the following segment the focus is on the matrix analysis part of the solution algorithm. This means that the process described bellow completely disregards the modelling of bearing hydrodynamic lubrication and all relevant calculations.

Simple Support

Simple support modelling is the most straightforward of the two options offered by the program. It is by default the active option when an input file is opened for the first time.

Under this type of modelling, the beam segments described in the input files correspond to the shaft. All shaft nodes designated as “constrained” are hinged. This means that they remain rigidly in the exact coordinates initially dictated by the shafting plan (designer’s offsets) and can only perform rotations about the three cartesian coordinate system axes. This provides us with an adequately constrained model of a multi-supported statically indeterminate system that can be solved through matrix analysis.

During the solution process the following steps take place:

A. All forces and equivalent loads (external and internal) are applied to the nodes,
B. All constraints are recorded to a global DOFs vector and applied to the corresponding nodal DOFs,
C. All nodal forces are copied over to a global Force vector **F** and a dummy global force vector **F’** is created,
D. A global displacements vector **U** is created and initialised,
E. The global stiffness matrix **K** is assembled from all the local beam element stiffness matrices,
F. A dummy global stiffness matrix **K’** is created in the way described under section 4.1.2,
G. Global force vector **F** values are copied over to dummy global force vector **F’**,
H. For every constrained DOF, the generalised displacement’s constraint value is copied over to its corresponding spot on the dummy force vector **F’**,
I. The inverse of dummy global stiffness matrix **K’** is calculated,
J. Global displacements vector **U** is calculated as: $\mathbf{U = K'^{-1} \cdot F}$,
K. Global force vector **F** is calculated as: $\mathbf{F = K \cdot U}$,
L. All constrained node reaction forces are reported,
M. All nodal displacements and forces are reported.

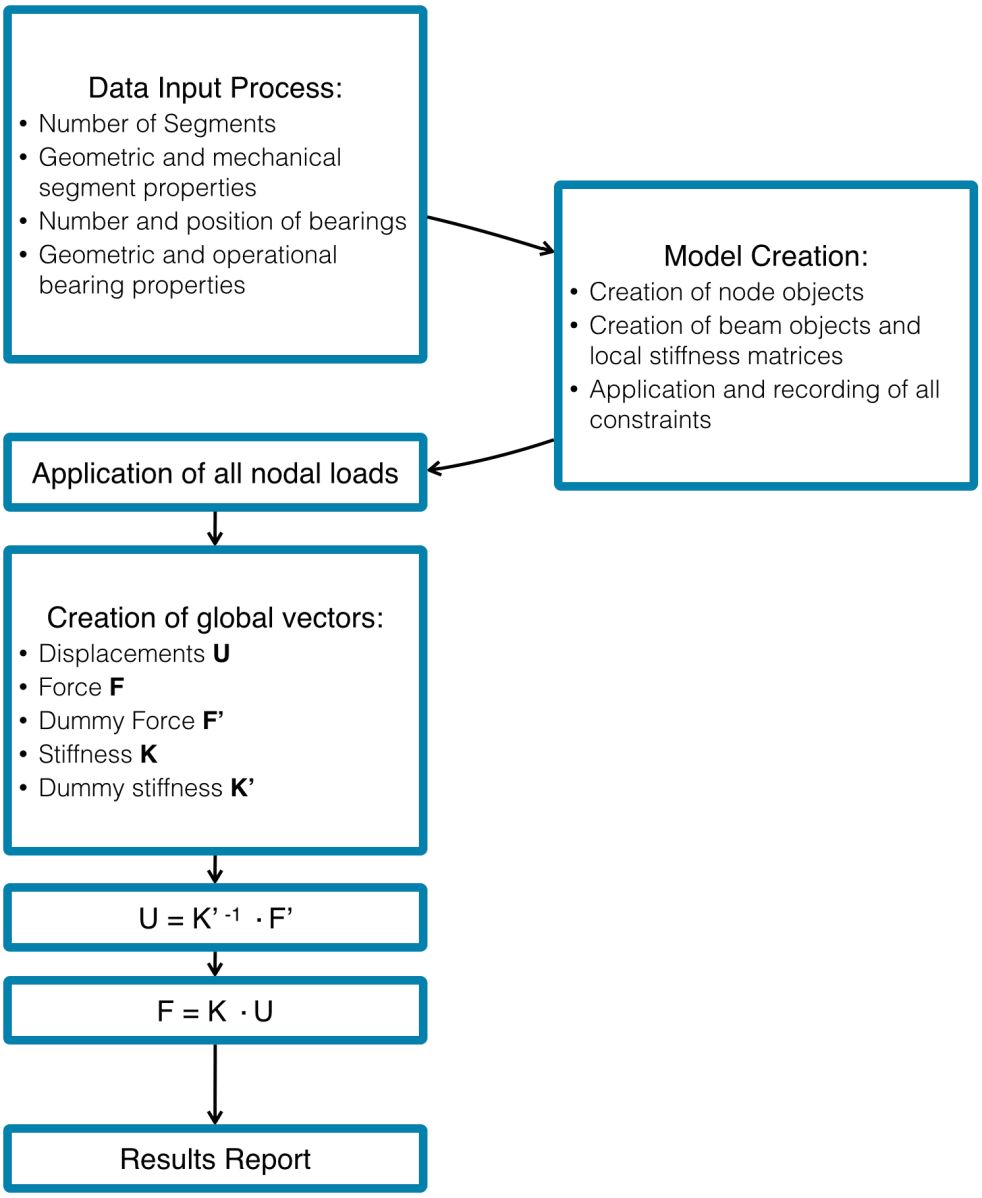

FIGURE 4.9: MATRIX ANALYSIS FLOWCHART - SIMPLE SUPPORT

Elastic Support

As discussed in section 4.1.3, elastic support modelling utilises an extra set of beam elements to act as bearing supports and approximate the compression, or expansion, that the actual supports would exhibit under the influence of the bearing reaction forces. This kind of modelling does not demand extra input data, as the only crucial piece of information required is the foundation stiffness value already found in the input file. The mechanical and geometric properties of the support beams are adjusted in order for them to behave as linear springs with axial stiffness equal to the stiffness value prescribed in the input file.

In this case, a few extra objects need to be created:

- A set of support nodes and,
- A set of support beams that connect pairs of support and shaft nodes.

The creation of the above objects and the differences in the overall management of the shafting system demand that a few more processes take place before the actual matrix analysis tis conducted. In this type of model, the support nodes are fixed while the shaft nodes are free. Additionally, all constant vertical offsets and bearing properties, are copied from the shaft nodes where they were initially stored at input, over to the support nodes. These offsets are then applied to the fixed support nodes and all bearing objects are created within each support node object.

Apart from the steps required to create support nodes and beams and copy over some of the simple model properties to the support nodes, the rest of the solution process remains the same. The main difference is that this time, the process is applied to a larger and more complex model.

A noteworthy point, is that the formerly constrained shaft nodes are now allowed to move as the system deforms, and that their displacements will be **directly calculated** through the matrix analysis process, since the new model accounts for their interaction with their corresponding support beams. As all support beams were created with the aim of approximating springs of a certain stiffness, the vertical deformations of all support beams can be predicted if the reaction forces are known.

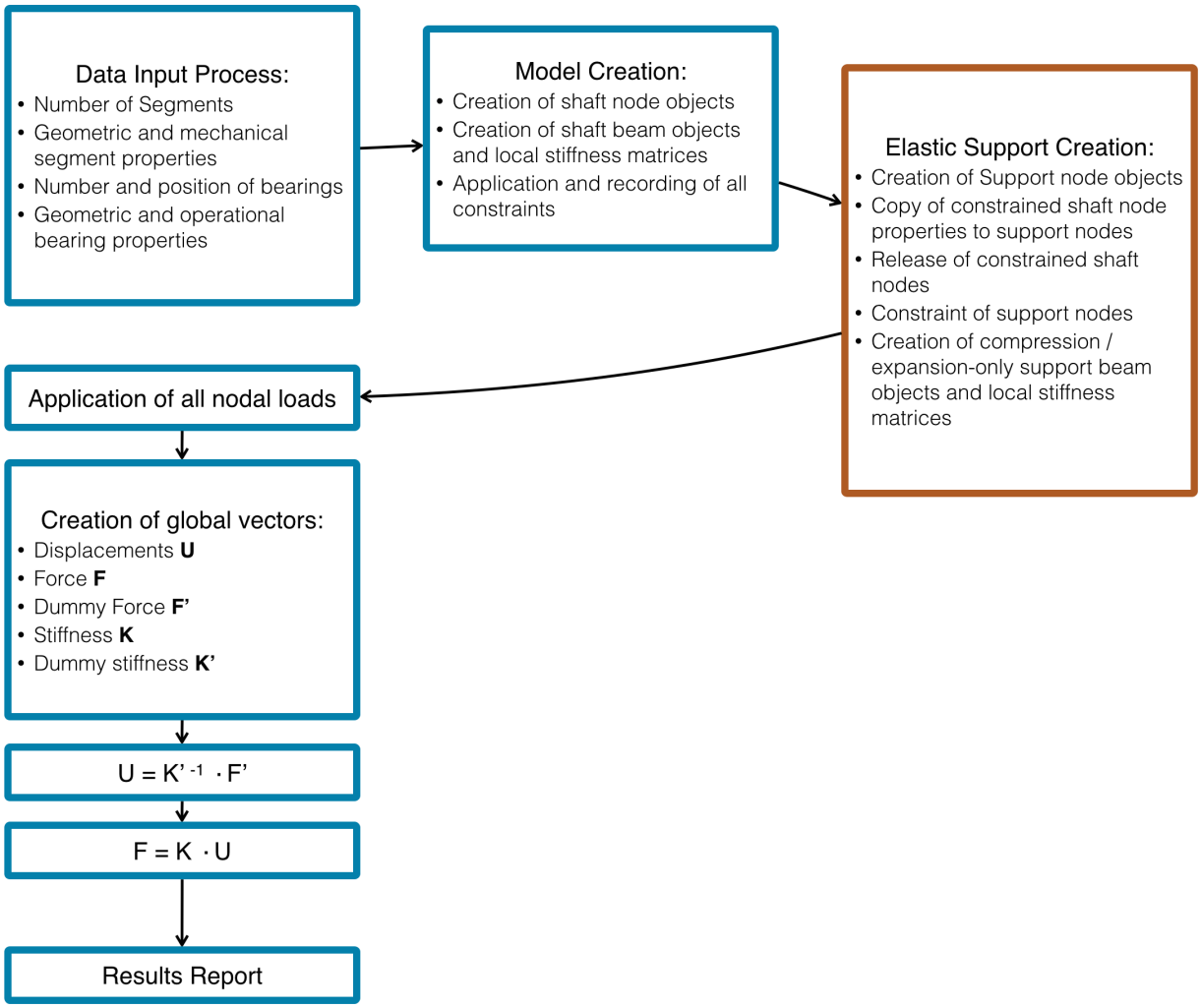

FIGURE 4.10: MATRIX ANALYSIS FLOWCHART - ELASTIC SUPPORT

4.3.4. Bearing Hydrodynamic Lubrication

This part is presented here as described in "*L. RAPTIS, Software development for the solution of hydrodynamic lubrication problems in main bearings of marine Diesel engines, Diploma Thesis, National Technical University of Athens, School of Naval Architecture & Marine Engineering, Athens (March 2014)*".

The problem of Journal bearing hydrodynamic lubrication is handled by a C++ library, external to the main body of the program, based on the work of L. Raptis. Although some refinements and modifications have been made to the original code, the core functionalities remain, largely, the same and follow the same algorithm as the original. It should be noted that, for the scope of this study, a steady state problem is solved, which means that journal rotational speed is considered constant.

If the user chooses to model a support point of the shaft as a journal bearing in his input file, an instance of a bearing object is created within the node object that represents that point. The main input required in order to create and meaningfully initialise a bearing object instance contains the following:

- Inner bearing diameter D,
- bearing Length over Diameter ratio,
- bearing lubricant dynamic viscosity values in Pa s,
- bearing Radial Clearance,
- shaft revolution rate values in RPM,
- bearing applied slope boring values in rads,
- misalignment angles about the horizontal and vertical axes,
- the external horizontal and vertical loads applied to the bearing.

Most of the above data is stored in the user input file, with the exception of misalignment values and external loads. The values of the latter are unknown until the program has started solving the matrix part of the problem. In effect, these values are the output of the matrix analysis process.

The bearing code tackles the hydrodynamic lubrication problem by considering the unwrapped bearing problem. The inner surface of the beating is in effect a rectangular plane (**Figure 3.2**).

Bearing length L, is laid down parallel to the **x** axis, while the bearings circumference is parallel to the horizontal **z** axis and corresponds to the plane width. The plane is initially discretised along its length and width into a grid of points. The grid can be fine, or coarse, depending on the user input. Upon this two-dimensional plane, the code tries to find a film thickness geometry h(x,z) that is capable of supporting the externally applied loads.

Lubricant film thickness can be fully modelled as a function of four independent variables: eccentricity (*e*), attitude angle (*phi*), misalignment angle about the **z** axis and misalignment about the **y** axis. It is helpful to remember at this point, the link that exists between *e*, *phi* and minimum film thickness. While, the two misalignment angles are constant throughout the plane, eccentricity and attitude angle values depend on the longitudinal axis coordinate. Despite that, if eccentricity

and attitude angle values are known at a specific cross section, film thickness function values can be calculated for the whole plain. Similarly, if a representation of the whole plane's film thickness has been obtained, eccentricity and attitude angle values can be calculated at any longitudinal position. In this section any mention made to eccentricity and attitude angle, refers to the values of these variable in the middle section of the bearing length, unless specified otherwise.

For a given set of misalignment angles, film thickness calculations still require a set of two variables, *e* and *phi*. Initially an estimate for the values of these two variables is used and specific film thickness values are obtained at each grid point of the plane. For the next step, the Reynolds equation (EQ. 3-1) is solved for pressure, numerically by means of the Gauss-Seidel iterative method. That distribution is then integrated along both axes and the hydrodynamic load value is obtained. If this value is equal to the value of the resultant of all externally applied loads, then the code proceeds to calculate a set of output data, such as friction power loss and maximum pressure.

If the above condition is not met, the process is repeated from the point of film thickness calculation. The underlying concept here, is that, since the shaft rotational speed is steady, for each specific film thickness distribution, there is only one corresponding pressure distribution, which can either adequately support externally applied loads, or not. Misalignment angles, i.e. two out of the four independent variables that describe film thickness, are set externally and can be considered as constants to the solution process described in this section. The only variables left that can shape film thickness into a distribution capable of supporting the external loads are eccentricity and attitude angle. This chain of dependencies specifies that *e* and *phi* are linked to the hydrodynamic load that the bearing can develop.

At his point it becomes clear that, if the initially estimated pair of *e* and *phi* values do not correspond to a hydrodynamic load approximately equal to the external load, then a better pair needs to be found. This often involves a search process through all the available pairs of such values. The initial version of the code, as developed by L. Raptis, employed a combination of methods that helped retrieve more fitting sets of values for *e* and *phi*, with a two variable Newton-Rapshon method being dominant among them.

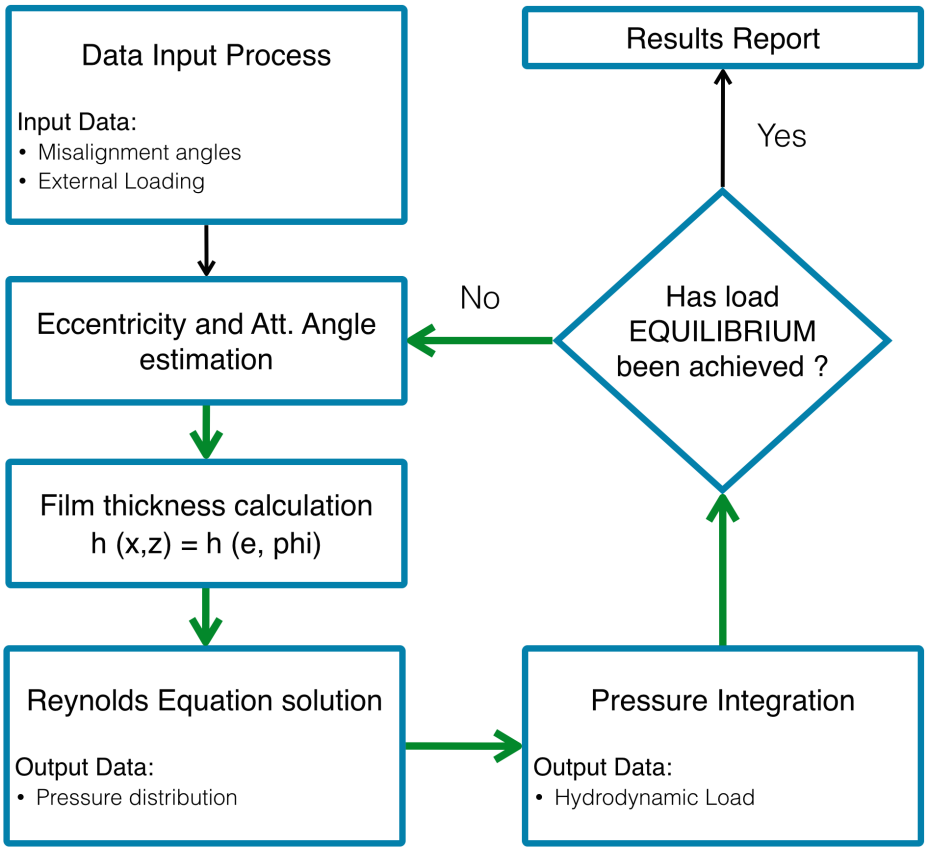

FIGURE 4.11: BEARING HYDRODYNAMIC LUBRICATION SOLUTION ALGORITHM

For each, possibly correct, pair of *e* and *phi* values, the end result can only be verified if the full calculation process is followed, up to pressure integration. This search can prove to be time consuming, should the number of incorrect pairs be greater than ten. Combined with the fact that more than one bearings need to be "solved" for any shafting plan, total processing time becomes quite long and needs to be shortened. To this end, a better way of acquiring estimates for *e* and *phi* has been devised and utilised within the frame of this study.

Eccentricity and Attitude angle estimates

In the previous part of this section, a clear relationship between the pair of eccentricity and attitude angle values and the total load the lubricant can support was established. In reality, any bearing loaded externally will develop the appropriate pressure distribution required to support that load. In this state *e* and *phi* have specific values. Additionally, the bearing's operating and loading condition can be adequately described by its Sommerfeld number. The relation that exists between a bearing's loading condition and *e,* dictates that the greater the load a bearing is required to support, the greater the eccentricity value and more importantly the smaller the Sommerfeld number value.

In an effort to take advantage of the link between *e* values, bearing condition and Sommerfeld number the above problem solving process was inverted and simplified: A specific eccentricity value at zero attitude angle was imposed on the bearing and all other variables such as total hydrodynamic load were calculated. In this situation, the actual non-zero attitude angle that would

yield the same results is equal to the angle between the resultant hydrodynamic force vector and the vertical **y** axis.

If this inverse solution process is followed for a series of eccentricity values ranging from nearly zero to maximum, then a similar series of hydrodynamic load and Sommerfeld number values can be obtained for all possible loading conditions that any specific bearing can support. These series of solution data can be browsed with the help of the Sommerfeld number that corresponds to each loading condition: For any external load imposed, the Sommerfeld number can be calculated and compared to the closest available Sommerfeld number of the pre-calculated solution data. This way, a pair of *e* and *phi* values can be matched to any Sommerfeld number and an accurate estimate can be retrieved, without the need to go through time consuming calculations. **Figure 4.12** describes the estimate retrieval method.

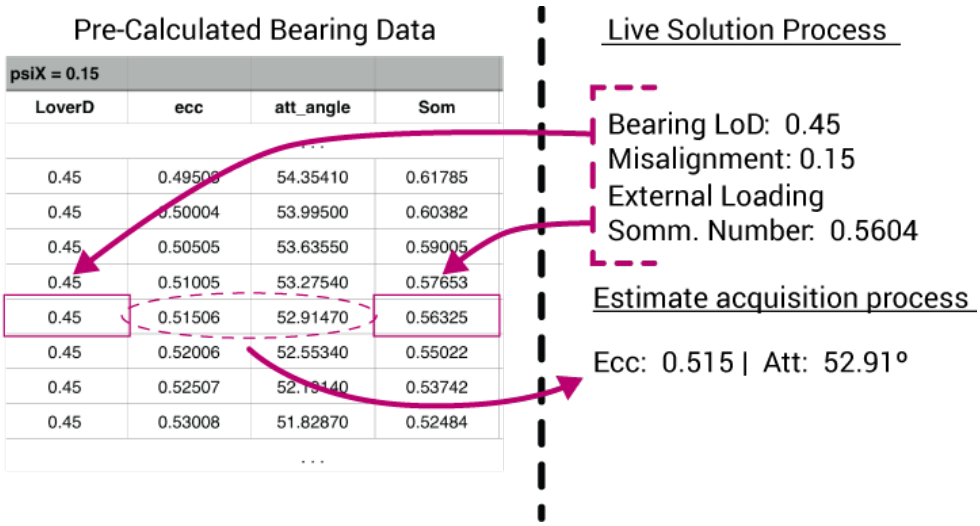

FIGURE 4.12: ESTIMATES ACQUISITION PROCESS

The limitations of the above method are mainly related to the bearing geometry and the misalignment angles. Any given bearing, depending on its Length over Diameter (LoD) ratio can support different maximum loads. To bypass this limitation, the process was repeated for many different LoD values, ranging from 0.1 to 3.5, and solution data was obtained for each one.

Similarly, different sets of misalignment angles result in different film thickness distribution for a given set of *e, phi* and LoD values. The same remedy was applied, in this situation, and the problem was solved for vertical, non-dimensional, misalignment values ranging from 0 to 0.35. In total, for each misalignment angle value the full set of all LoD values was solved with *e = [0.03,0.98]*, in small increments of 0.005.

Another benefit of this new approach is that, the user can choose to solve the whole bearing problem without having to go through the process of calculating film thickness, solving the Reynolds equation and integrating the pressure field. The program can determine the new support position as well as *e* and *phi* values at this support position, by simply going through the pre-calculated values with the problem's Sommerfeld number as the search key item. The "goodness of fit" for this type of "solution" is determined by how small the eccentricity increments of the pre-calculated data are.

4.3.5. Coupled Problem Solution Algorithm

As stated in section 4.3.5, matrix analysis and bearing hydrodynamic lubrication interact to form a coupled problem. The interaction is mainly found in the way both problems handle the points of the shafting system.

In any real world application, a shaft rests on a journal bearing surface, parallel to its principal axis or at a given misalignment angle. Either way, the bearing supports part of the shaft's weight. Once the shaft starts rotating, the lubricant that fills the space between the shaft and the bearing inner surface, forms a film layer, of a certain thickness, capable of developing high enough pressure to support the shaft. Depending on how acute the shaft-bushing misalignment is, the local pressure values are higher wherever the shaft-to-bearing distance is smaller, and thus wherever the lubricant film thickness is smaller as well. In these cases, the lubricant film may develop such a pressure distribution, that its main load bearing capacity is actuated around an area closer to the bearing surface edge, rather than its centre. If the lubricant pressure distribution were to be modelled as a single point force vector, its position would also be off centre.

The **interaction** in the problem described, lies in the fact that bearing lubrication characteristics depend on the externally applied load and shaft-to-bushing misalignment angle. At the same time shaft support points are shifted to a new position lengthwise and they are also vertically offset by an amount equal to the lubricant film thickness.

Matrix Analysis

The **first** step in the coupled problem solution process, is to establish a model for the shafting system. The model can be either simply supported, or elastically supported. Following that, the problem of matrix analysis is solved once and the global generalised load and displacement vectors are obtained. These vectors contain all support point reaction force and all bearing misalignment values.

During operation, bearing lubricant will develop a layer of certain thickness and if the misalignment angle of the shaft is large enough, its support point will shift by a fraction of the bearing's length. The lubricant film vertical offset and longitudinal support point shift will alter shaft alignment displacements and consequently, reaction forces. Thus, after this initial matrix analysis process, all bearing lubrication characteristics need to be evaluated.

Bearing Equilibrium

The first step of analysing the shafting system provides the program with information regarding the conditions under which the support bearings will operate. Every bearing object is then required to engage in its own solution process, until it reaches an equilibrium between external forces and lubricant pressure. When this stage is reached, at a cross section in the middle of the bearing's length, the shaft rests at a specific attitude angle and eccentricity combination. The lubricant film thickness can be fully described by these two parameters for a given set of misalignment angles.

Another important output variable, is the longitudinal position of support. Since the shaft's new support point for this bearing will be off centre, the elevation that will take place because of the

film thickness, is better described by the values of film thickness at this new position of support. The above process is the **second** step of the solution method.

Model re-arrangement

The **third** step in this coupled solution process, is to shift constrained shaft and/or support nodes according to their new support position and to add this new film thickness offset to the other vertical offsets already applied. In the case of a simply supported model, only the constrained shaft nodes need to be shifted, whereas if the model is elastically supported, both the support nodes and the free shaft nodes at the other end of support beams have to be moved.

This rearrangement of the model imposes the following changes:

- The lengths of the beams preceding and succeeding a support point node change mutually to accommodate this shift. One of them becomes shorter, while the other becomes longer.
- The change in beam length means their local stiffness matrices and the global stiffness matrix need to be re-evaluated.

After the new model has been created, a new round of matrix analysis is conducted and new load and displacement vectors are calculated. Steps two and three are repeated until the end of the process.

Iterative process

At this point in the solution process, it becomes evident that for every time the program goes through each of the steps two and three (matrix analysis and bearing equilibrium), one of the two parts of the method will always be one step behind. For example, if we were to stop the process right after bearing equilibrium, matrix analysis would not be up to date with the vertical and longitudinal support point offsets.

These two steps are thus interlocked in an iterative process that needs a termination condition. The aim of this iteration is to produce a series of sets of reaction forces and support point offsets that each converge to specific values. In this fashion, a convergence condition can be defined, for either the global force vector, or the global displacements vector.

The program is coded in such a way that it can evaluate convergence by using either of these vectors. Here, for the description of the solution algorithm, the use of the force vector is assumed. During the iterative process, a copy of the previous iteration force vector is kept, so that at any given moment, the current force vector values can be compared against its previous values. In order to determine if convergence has been achieved to a specific degree, at the end of step three, the program creates a “difference” vector by calculating the absolute difference between the force vector of the n^{th} and the force vector of the $(n-1)^{th}$ iteration. The program then examines the elements of the difference vector that correspond to the support reaction forces and determines if each reaction force has changed more than a certain limit. If the change is bellow the limit, this node is marked as having converged. For the program to terminate its iterative process, all nodes need to be marked as having converged **at the same time**. If not, calculations continue and it is perfectly possible for a node that was previously marked as having converged to

lose that status in the next iteration. This means that convergence for a single node does not imply that its condition is held stationary until all the other nodes catch up with it and converge.

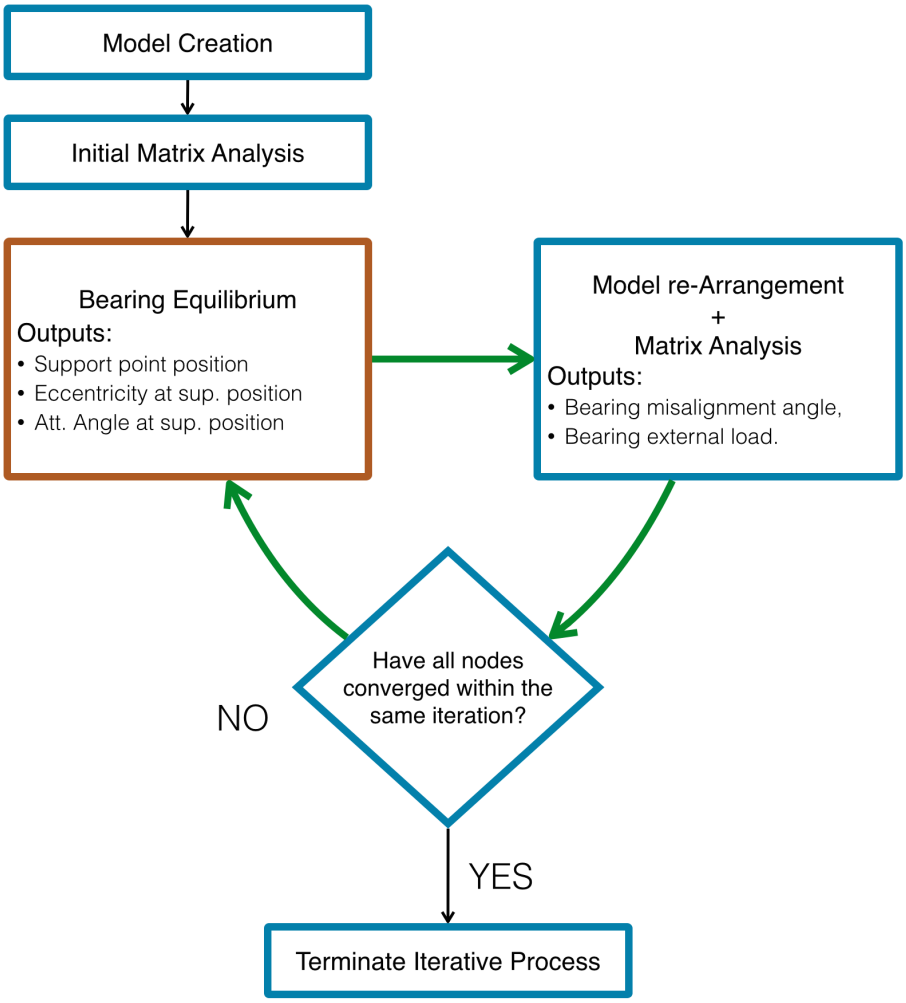

FIGURE 4.13: COUPLED SOLUTION PROCESS FLOWCHART

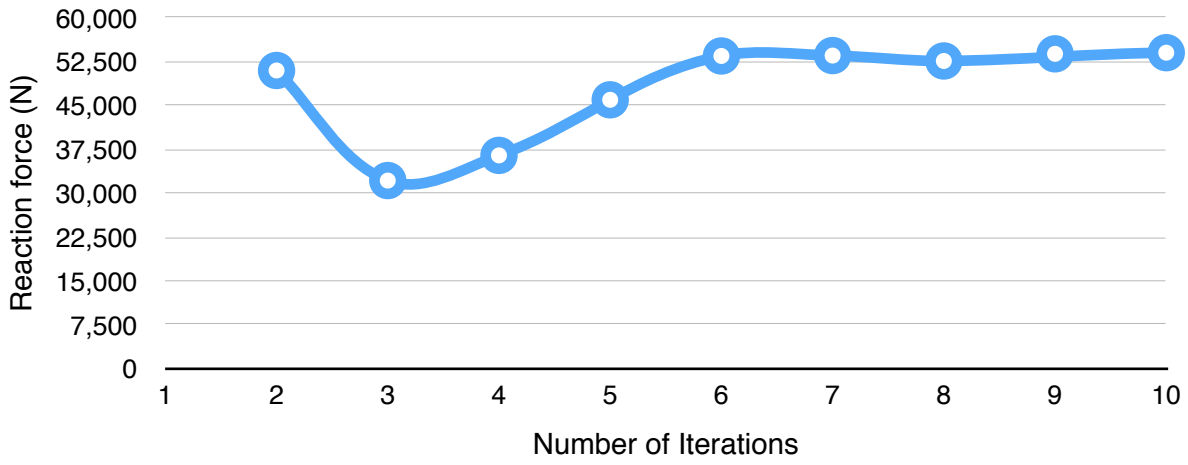

FIGURE 4.14: AN EXAMPLE OF THE ALGORITHM'S CONVERGENCE FOR A SINGLE BEARING

5. Case study

5.1. Ship FEM model

TYPE	CRUDE OIL TANKER
DEADWEIGHT	320000 T
LENGTH BETW. PERP. LPP	320.00 M
BREADTH B	60.00 M
DEPTH D	30.50 M
SCANTLING DRAFT T	22.50 M
SERVICE SPEED V_S	15.9 KN
MAIN ENGINE	WÄRTSILÄ 7RT-FLEX84T-D
KEEL LAID	APRIL 2010

TABLE 5-1: MAIN CHARACTERISTICS OF THE VLCC VESSEL OF THE PRESENT STUDY

Under normal operational conditions a vessel is subjected to hydrostatic loads that balance vessel displacement. The magnitude and longitudinal distribution loads depend on vessel loading condition. For each different loading condition, a state of static equilibrium is achieved, and in that state, the hull reacts to the imposition of external loads by means of deflections. Of course these deflections of the hull depend heavily upon the global and local strength of the construction, both of which are usually constant, but it is unquestionable that as the loads applied to the hull change, so will hull deflections.

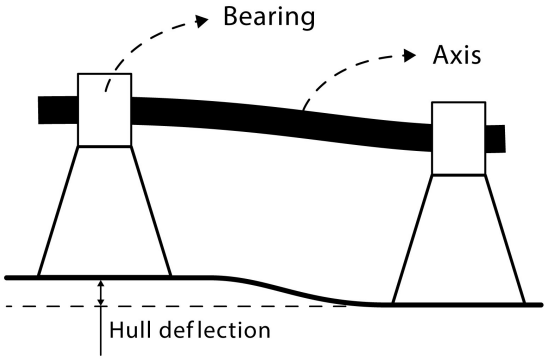

FIGURE 5.1: THE INFLUENCE OF HULL DEFLECTIONS ON THE SHAFTING SYSTEM

The aft part of the ship and more specifically the engine room, where the shafting system is housed, will also be affected by the overall deflections of the hull. The foundations of shafting system bearings will be subjected to a set vertical deflections for each different loading condition.

Shafting system alignment is usually conducted either before launch (i.e., in a dry-dock condition), or afloat in lightship condition. It is therefore important to study the alignment plan's behaviour, at these loading condition that a ship will, probably, spend the most of its service time. In a sense

the aim here is to investigate the effects of the hydrostatically induced loading on hull deflections, and in turn, the behaviour of the ship's alignment plan under these deflections.

In order to investigate these effects, we need to know how the hull of a given ship deforms under a series of common loading conditions. To this aim a finite elements method model of a contemporary VLCC (2010), currently in service, was created and its structural behaviour was studied under various common loading conditions.

I. Digitising hull construction drawings

At this point I would like to point out the significance of the help received from Minerva Marine Inc. who were so kind as to provide the particulars of one of their vessels in as much detail as they could.

It is common shipyard practice, that the most detailed drawings of a ship's hull, such as the lines plan, are generally not provided to the future ship owner after the completion of all construction work. As a result the closest available drawing was the construction sections of the aft and fore part, as well as the midship section. These drawings had to be digitised to a format that would be easy to input to most CAD software: a series of point coordinates on the Y-Z, transverse plane, along the periphery of each section present in the drawings.

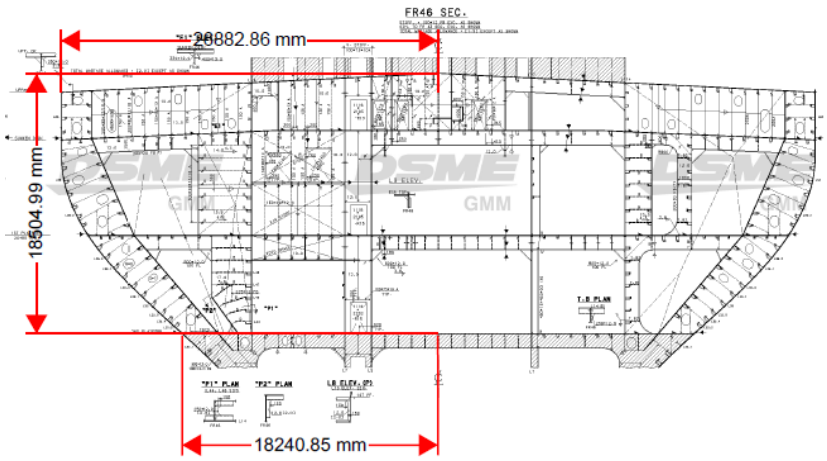

FIGURE 5.2: CONSTRUCTION DRAWING OF THE UPPER PART OF FRAME NO.46 WITH MEASUREMENTS

To achieve that goal, the Engauge Digitizer software tool was used. Because of the variability in drawing and filing standards throughout the range of the drawings, on every sheet of each of them, the effective scale had to be ascertained by measuring a locally depicted length and comparing that to the measured output. For each section measurements of their maximum height and breadth were conducted in order for their scale to be more easily accessible. Each section had to be isolated in a separate picture format file and then input to the digitiser. The first step of the process required the user to input three reference points so that the absolute scale of the drawing could be determined and output correctly in the set coordinates. The bottom of the centre line was chosen as the point of origin in all drawings Then, the user could input one-by-one the points whose coordinates he wished to obtain by clicking on points along the drawing of the section. The output was a comma delimited file (.csv) that could be easily imported into and

manipulated through the use of any spreadsheet editing software. Sometimes, the above process had to be applied more than once per section as the drawings divided the sections vertically into two parts (upper and lower), requiring the user to match these two parts by joining the output list of coordinates.

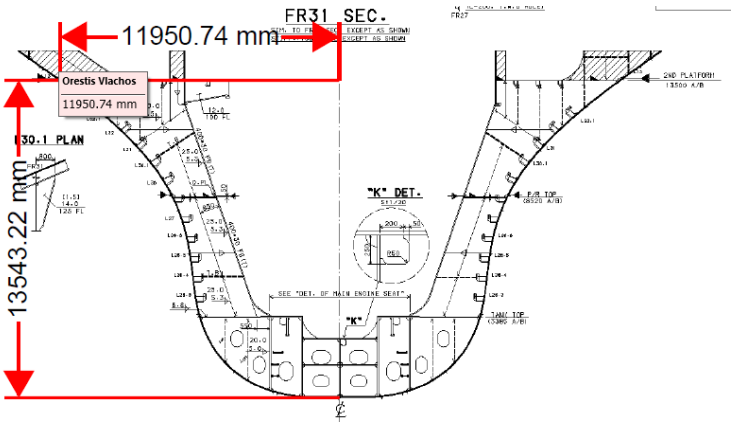

FIGURE 5.3: CONSTRUCTION DRAWING OF THE UPPER PART OF FRAME NO.31

A similar process was carried out in order to obtain the vessel's profile and match it with the coordinates of each frame digitised.

II. Creating and fitting ship sections and hull surfaces

All the above coordinates were combined to a single text file with care taken to position the points of each transverse section at their proper longitudinal distance from the point of origin, the aft perpendicular. The text file was then input into the Rhinoceros 3D CAD software package developed by McNeel Software Inc and yielded a cloud of points in 3D space.

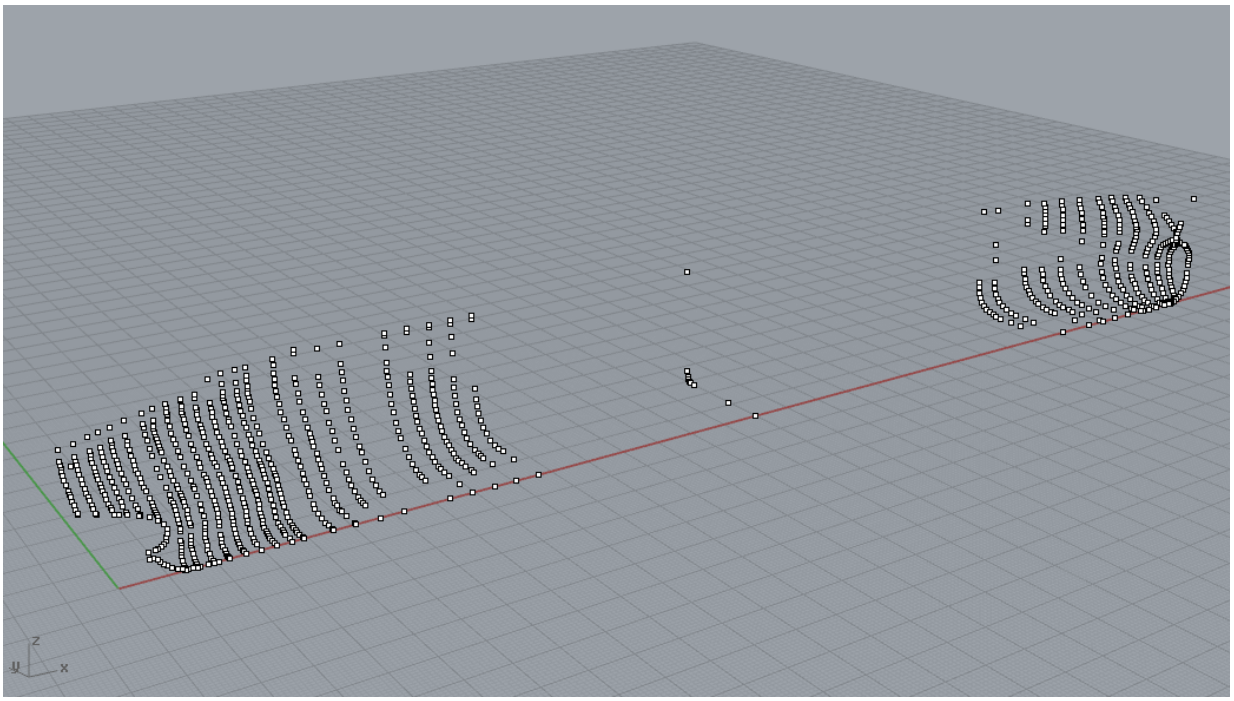

FIGURE 5.4: INPUT CLOUD OF POINTS

Following that input, the ship profile points were interpolated through a polyline (cubic b-spline). Each section's input points were then interpolated in a similar way, with special care taken in order to correctly impose the starting and ending tangency conditions for each frame polyline separately. The resulting frame lines obtained purely through raw input data interpolation required an extensive amount of fairing so as to resemble the original. The significant differences in the observed sections form can be attributed mainly to the digitisation process and more specifically to the fact that there was a limited accuracy in the way points were chosen (through mouse clicks) in combination with an equally limited drawing resolution for the sections. The process of fairing each section was conducted with a limiting tolerance of a few millimetres so as to avoid a great distortion of the actual design and any alterations in the overall representation of the actual ship particulars this distortion would invite.

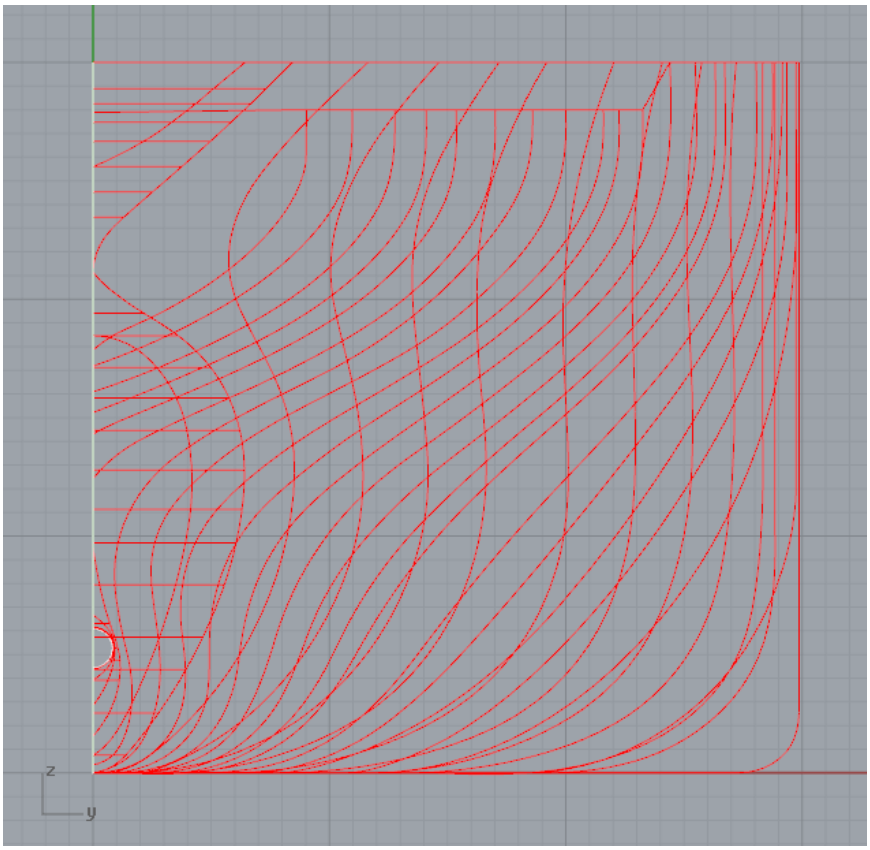

FIGURE 5.5: FORE AND AFT SECTIONS AFTER FAIRING

Once the full set of sections had been faired to an acceptable degree, it was time to fit surfaces spanning several sections at a time aiming to represent the outer skin of the hull. For the parallel body part of the ship, the information provided by the faired sections was sufficient for the creation of a single smooth surface. Creating a unified surface with at least G1 geometric continuity for the aft and fore parts of the ship required that these parts be broken down to smaller surfaces with the use of waterline-like cross section profiles created between two or more transverse sections. The surfaces created in this fashion were then joined to yield a single unified polysurface with no gaps or other defects.

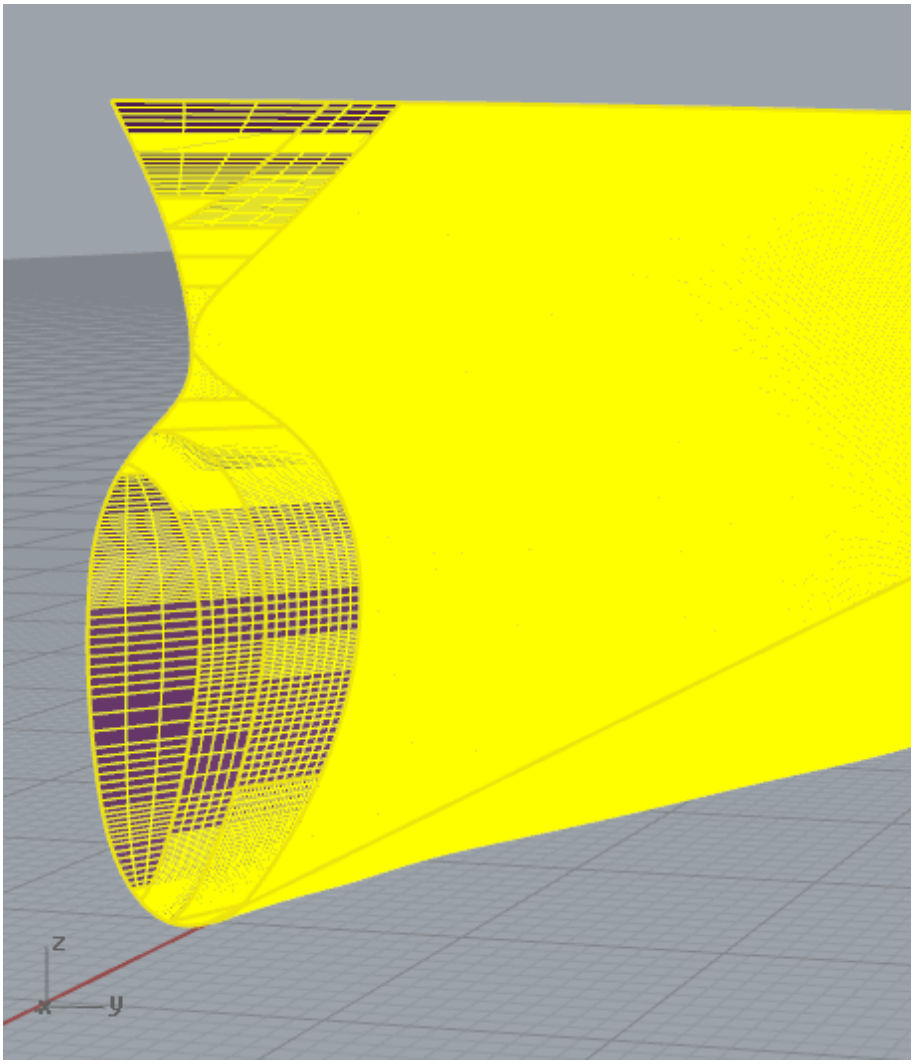

FIGURE 5.6: BOW PATCH SURFACE DETAIL

The final stage in the process of trying to create a faithful representation of the actual vessel's hull was the compartmentation of the cargo hold and ballast spaces. First, the ship was divided longitudinally into compartments comprising the cargo tanks, the fore peak and aft ballast tanks and the M/E room. This was done by creating a series of transverse surfaces intersecting with the hull's surface at various positions longitudinally and then using the hull as a cutting tool to isolate the parts internal to the ship's skin. The same method was applied in creating the ship's double bottom. As for the double skin, the goal was set to create closed volumes of equal or nearly equal capacity to the ones of the actual ship, the capacity plan and her trim and stability manual being the only guides available. The above goal was achieved within a tolerance margin of approximately 0.7% for most tanks.

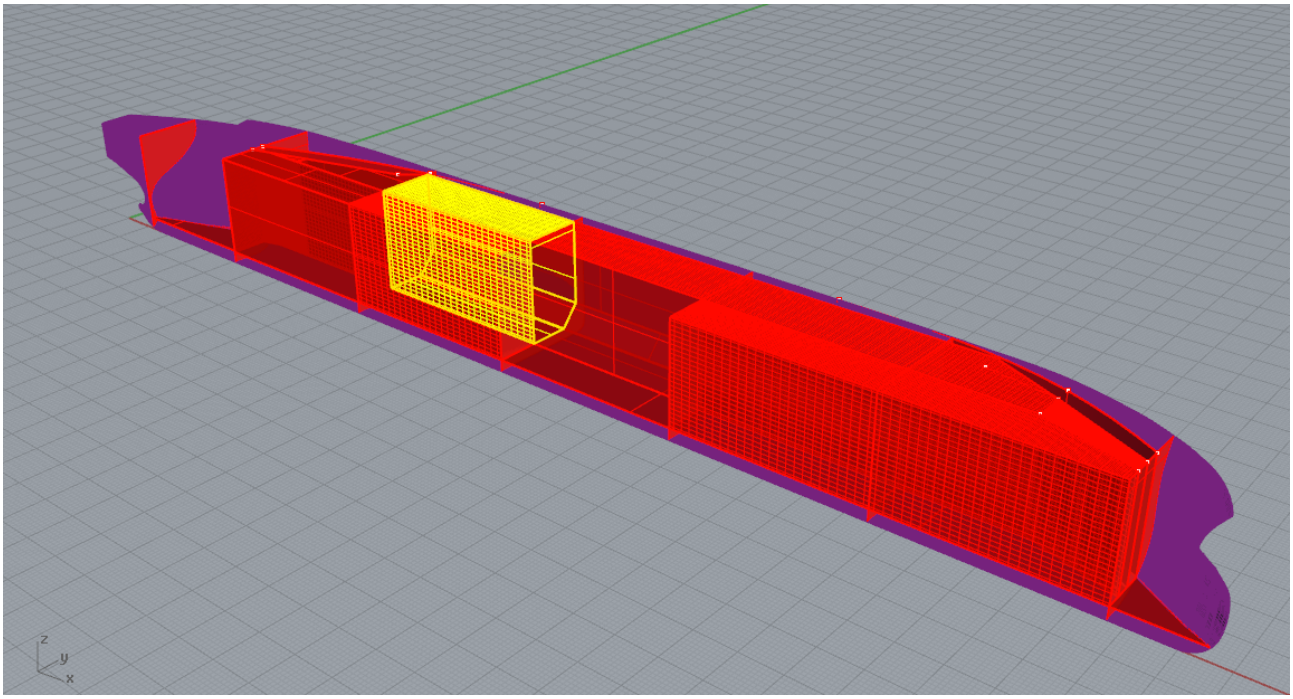

FIGURE 5.7: COMPLETED PROJECT WITH COMPARTMENTS HIGHLIGHTED

III. End result and comparison with the original

The ultimate goal of the above process was to create a faithful digital representation of an actual VLCC ship, currently in service, based on data obtained from an original shipyard design. The purpose of this effort was to provide a basis upon which further FEM analysis could be conducted, and all deflections along the line of the shafting system support points could be determined.

The most accurate way of comparing the overall resemblance of the model to the actual ship was the cross-examination of their hydrostatic properties. **Tables 5-2** and **5-3** contain data of the model, the actual ship and comparisons between the properties of Volume Displacement, Longitudinal centre of Buoyancy and Floatation as well as wetted surface area and Water plane area for a series of drafts in increasing order.

Draft (m)	Model Volume Displacement (t)	Actual	Dif.	Model Center of Buoyancy (m)	Actual	Dif.	Model Center of Floatation (m)	Actual	Dif.
3	40031.8	40060	-0.07%	177.054	176.95	0.06%	176.664	176.54	0.07%
4	54479.7	54656	-0.32%	176.914	176.79	0.07%	176.393	176.24	0.09%
5	69229.1	69529	-0.43%	176.771	176.65	0.07%	176.103	176	0.06%
6	84215.5	84621	-0.48%	176.629	176.5	0.07%	175.85	175.68	0.10%
7	99388.7	99884	-0.50%	176.489	176.36	0.07%	175.533	175.43	0.06%
8	114722	115291	-0.49%	176.331	176.21	0.07%	175.082	175.05	0.02%
9	130192	130833	-0.49%	176.15	176.05	0.06%	174.521	174.52	0.00%
10	145789	146504	-0.49%	175.941	175.85	0.05%	173.844	173.86	-0.01%
11	161507	162301	-0.49%	175.7	175.62	0.05%	173.059	173.08	-0.01%
12	177348	178226	-0.49%	175.424	175.35	0.04%	172.159	172.18	-0.01%
13	193311	194281	-0.50%	175.113	175.05	0.04%	171.131	171.14	-0.01%
14	209403	210471	-0.51%	174.762	174.7	0.04%	169.949	169.94	0.01%
15	225633	226807	-0.52%	174.367	174.31	0.03%	168.556	168.53	0.02%
16	242016	243300	-0.53%	173.921	173.87	0.03%	166.962	166.97	0.00%
17	258560	259950	-0.53%	173.422	173.38	0.02%	165.268	165.35	-0.05%
18	275266	276768	-0.54%	172.874	172.84	0.02%	163.538	163.6	-0.04%
19	292122	293742	-0.55%	172.288	172.26	0.02%	161.938	161.97	-0.02%
20	309114	310853	-0.56%	171.682	171.65	0.02%	160.663	160.67	0.00%
21	326227	328086	-0.57%	171.077	171.05	0.02%	159.664	159.68	-0.01%
22	343446	345425	-0.57%	170.485	170.46	0.01%	158.908	158.92	-0.01%
		ABS MAX	0.57%		**ABS MAX**	0.07%		**ABS MAX**	0.10%
		Average	-0.48%		**Average**	0.04%		**Average**	0.01%

TABLE 5-2: HYDROSTATICS COMPARISON BETWEEN MODEL AND SHIP FOR A SET OF DRAFTS (PART 1)

Draft (m)	Model Wetted Surface Area (m^2)	Actual	Dif.	Model Water Plane Area (m^2)	Actual	Dif.
3	15053.8	15276	-1.45%	14269.7	14443	-1.20%
4	15833.5	16071	-1.48%	14610.3	14765	-1.05%
5	16580.1	16810	-1.37%	14877.4	15004	-0.84%
6	17306.3	17543	-1.35%	15086.5	15201	-0.75%
7	18015.9	18244	-1.25%	15256.6	15352	-0.62%
8	18713.7	18933	-1.16%	15403.9	15490	-0.56%
9	19407	19616	-1.07%	15534.9	15621	-0.55%
10	20100.1	20301	-0.99%	15657.4	15749	-0.58%
11	20795.9	20988	-0.92%	15779.1	15876	-0.61%
12	21497.7	21682	-0.85%	15901.5	16004	-0.64%
13	22208.1	22384	-0.79%	16026.4	16136	-0.68%
14	22930.7	23099	-0.73%	16158.8	16276	-0.72%
15	23672.8	23835	-0.68%	16304.1	16429	-0.76%
16	24434.6	24585	-0.61%	16462.9	16590	-0.77%
17	25207.8	25347	-0.55%	16625.3	16750	-0.74%
18	25987.8	26108	-0.46%	16784.3	16915	-0.77%
19	26761.4	26859	-0.36%	16926.5	17062	-0.79%
20	27513.2	27583	-0.25%	17054.7	17189	-0.78%
21	28249.4	28282	-0.12%	17168.1	17304	-0.79%
22	28974.8	28966	0.03%	17267.8	17402	-0.77%
		ABS MAX	1.48%		**ABS MAX**	1.20%
		Average	-0.82%		**Average**	-0.75%

TABLE 5-3: HYDROSTATICS COMPARISON BETWEEN MODEL AND SHIP FOR A SET OF DRAFTS (PART 2)

The end result is most satisfying, especially if we consider the scarcity of detailed information on exact geometry of the hull. On average, most of the above hydrostatic properties are off the mark

by a maximum absolute value of less than 1%. The same maximum relative difference is observed throughout the range of different drafts examined, for all properties.

In summary, the correspondence between the model and the actual ship is satisfactory for the overall properties (volume displacement, wetted surface), the longitudinal properties that govern trim (LCF, LCB) and the ones that play a part in transverse stability (Water plane area).

IV. FEM analysis of the ship model

5.1.1. Finite element analysis of the ship hull

This part of the analysis is presented here as described in [13].

The main characteristics of the studied VLCC are presented in **Table 5-1**. Finite Element Analysis is performed to calculate the hull deformations of the vessel, under different loading conditions. Of particular importance are the deformations at the bearing locations of the propulsion shafting system. The static analyses are conducted with the aid of the ANSA pre-processor and the MSC/NASTRAN solver. Here, thermal loads from the engine or the environment are not taken into consideration.

First, a FEM model of the ship structure is generated. The whole structure of the ship is represented by first-order shell elements; at the stern tube region, solid tetrahedral elements are used. Stiffeners are represented by beam and truss 1-D elements. A coarse mesh is generated for the whole structure (element length of 0.95 m), except for the engine room floor, where finer meshing (element length of 0.2 m) ensures results of higher accuracy (**Figures 5.8** and **5.9**).

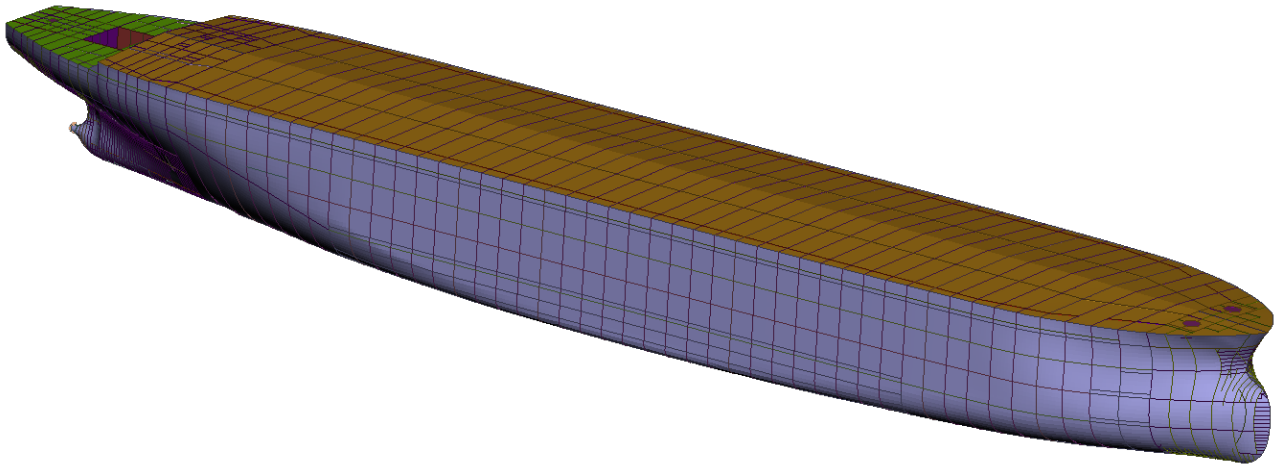

FIGURE 5.8: GLOBAL FEM MODEL OF THE VESSEL OF THE PRESENT STUDY [13]

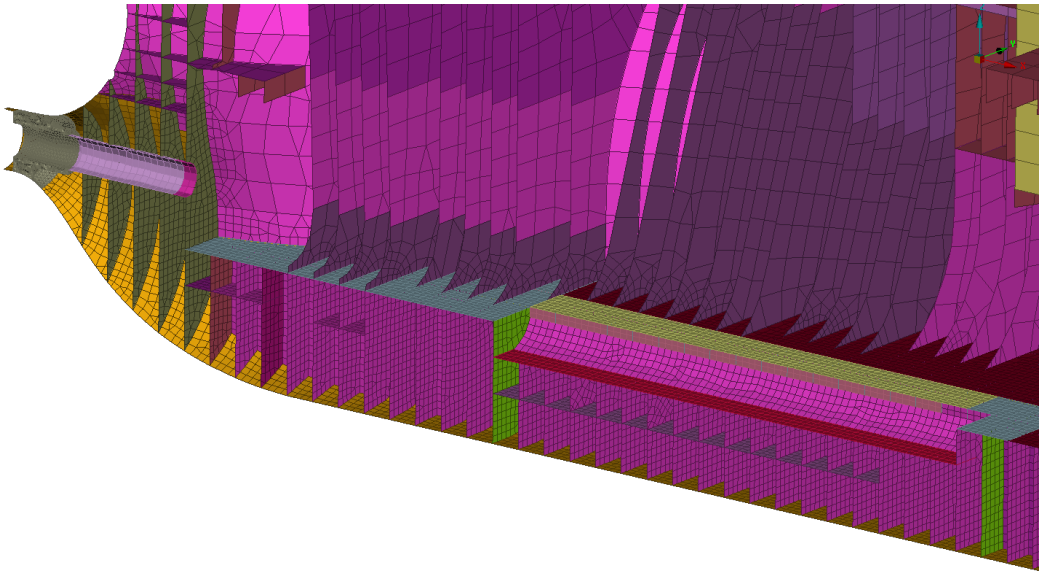

FIGURE 5.9: DETAIL OF THE GENERATED FEM MESH AT THE ENGINE ROOM REGION OF THE VESSEL [13]

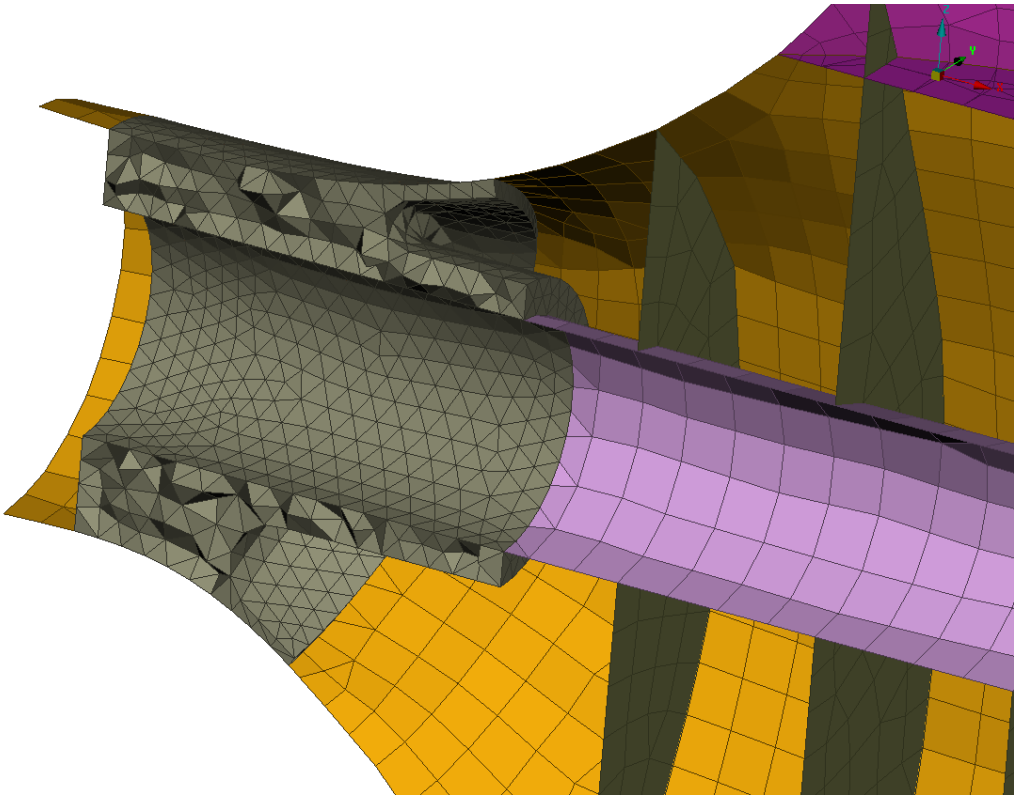

FIGURE 5.10: DETAIL OF THE GENERATED FE MESH AT THE STERN TUBE REGION OF THE VESSEL [13]

The mesh generation is an automated process performed by the ANSA Batch Meshing Tool. Meshing parameters and quality criteria are defined in two meshing scenarios (fine mesh for the engine room floor and coarse mesh for the rest of the structure, **Table 5-4**). Re-meshing algorithms act on areas with poor mesh quality until the predefined quality criteria are fulfilled. The final model comprises about 402.000 shell elements, 143.000 beams and 17.000 solid tetrahedrals (**Figures 5.8** to **5.10**).

Global Meshing Parameters (Scenario I)	
ELEMENT LENGTH	0.95 M
FILLING OPENINGS WITH DIAMETER	< 1 M
Engine room floor Meshing Parameters (Scenario II)	
ELEMENT LENGTH	0.2 M
FILLING OPENINGS WITH DIAMETER	< 0.5 M
Quality Criteria	
SKEWNESS (NASTRAN)	30°
ASPECT RATIO (NASTRAN)	3
ANGLE (QUADS)	45-135°
ANGLE (TRIAS)	30-120°
MINIMUM ELEMENT LENGTH	0.01 M
MAXIMUM ELEMENT LENGTH	1.5 M

TABLE 5-4: MESHING PARAMETERS AND QUALITY CRITERIA.

Stiffeners are represented by beam elements pasted on the shells. This method simplifies the model by avoiding the generation of very small shell elements. The properties of the beam elements are calculated in accordance with the cross section of each stiffener.

The shaft of the vessel comprises 39 beam elements of different properties and cross sections representing the diameter variations of the shaft along its length. The bearings are considered as rigid bodies and they are represented by RBE2 elements connecting the bearing foundation to the shaft centre line, **Figure 5.11**.

Machinery, auxiliary structures and small constructions that do not contribute to ship strength are not modelled in the present FEM model. Their mass is applied to the model as non-structural mass. This mass is appropriately distributed over the FEM model, so as to reach the prescribed lightship weight and the corresponding centre of gravity. The mass of the present structural model is 34,442 t, while the lightship weight is 43,938.7 t and its centre of gravity (L.C.G.) at 151.338 m. Thus, 9,496.7 t of lumped mass is appropriately distributed in holds, stern and bow by the automatic process of the ANSA Mass Balance Tool, **Figure 5.12**. The engine mass is represented by a lumped mass of 990 t distributed to the engine foundation positions by RBE3 elements.

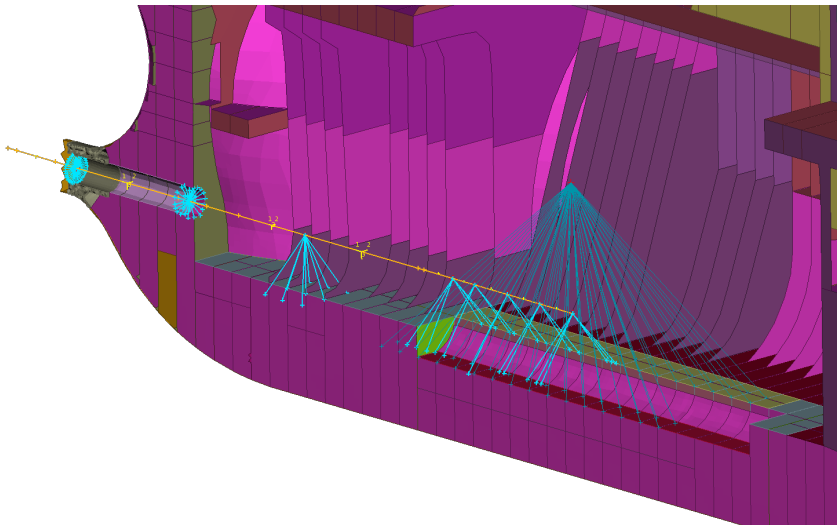

FIGURE 5.11: ENGINE AND BEARINGS REPRESENTATION IN THE PRESENT FEM MODEL [13]

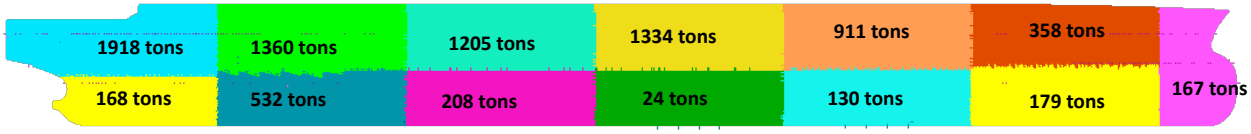

FIGURE 5.12: DISTRIBUTION OF NON-STRUCTURAL MASS IN THE PRESENT FEM MODEL [13]

Nine loading conditions of the vessel are considered in the present analysis as shown at **Figure 5.13**. The contents of the tanks are represented by lumped mass connected to each hold bottom with RBE3 elements. In order to set-up multiple FE models, one for each loading condition, a scripting process is used from the pre-processor which automatically applies the loads from a spreadsheet containing ship data. The ship is positioned on still water considering the vessel's total displacement and centre of gravity. Buoyancy is applied as pressure at the hull underneath the waterline using PLOAD4 entities, **Figure 5.14**. Finally, the vessel is trimmed in order to achieve static equilibrium between weight and buoyancy, which makes the model able to run without the need of displacement constraints (SPCs), which would lead to high local stresses. A NASTRAN keyword for inertia relief (INREL) is added for this solution.

LIGHTSHIP CONDITION

(L.C. 1)

DISPLACEMENT: 43939 TONES

DRAFT: 3.171 M

TRIM: 4.359 M

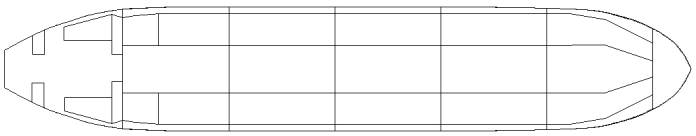

BALLAST ARR. CONDITION

(L.C. 4)

DISPLACEMENT: 145647 TONES

DRAFT: 9.69 M

TRIM: 2.12 M

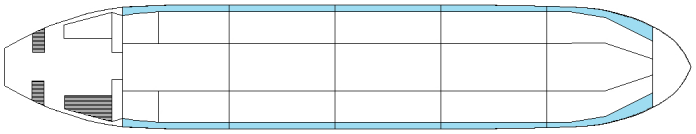

HOMO. DESIGN LOAD DEP. CONDITION

(S.G.=0.807) (L.C. 8)

DISPLACEMENT: 337362 TONES

DRAFT: 21.025 M

TRIM: 1.323 M

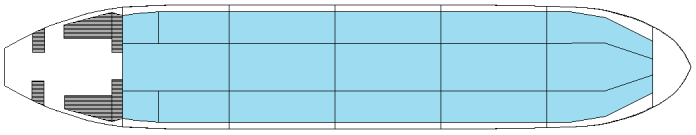

HOMO. SCANT. LOAD. DEP. CONDITION

(S.G.=0.833) (L.C. 11)

DISPLACEMENT: 364074 TONES

DRAFT: 22.525 M

TRIM: 0.114 M

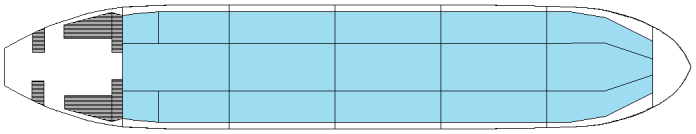

SEG. I LOAD DEP.

(23.8%, S.G.=0.883) (L.C. 14)

DISPLACEMENT: 169394 TONES

DRAFT: 11.158 M

TRIM: 3.446 M

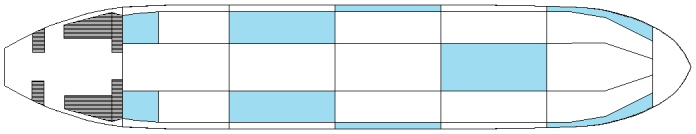

SEG. III LOAD INT.

(49.9%, S.G.=0.883) (L.C. 21)

DISPLACEMENT: 204046 TONES

DRAFT: 13.267 M

TRIM: 3.822 M

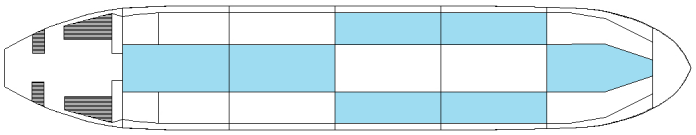

SEG. I+II LOAD DEP. CONDITION

(50.1%, S.G.=0.883) (L.C. 23)

DISPLACEMENT: 229276 TONES

DRAFT: 14.778 M

TRIM: 3.053 M

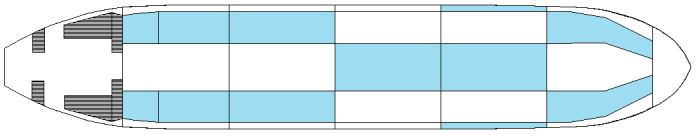

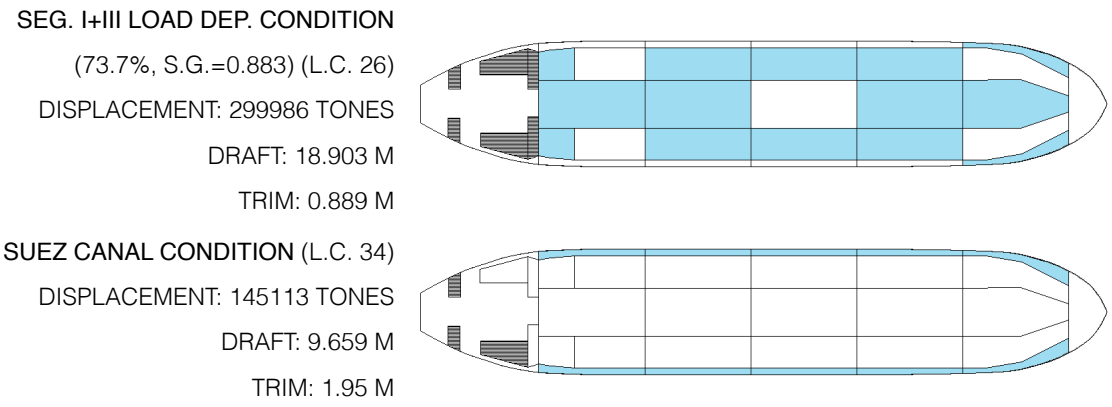

FIGURE 5.13: REPRESENTATIVE LOADING CONDITIONS OF THE VESSEL [13]

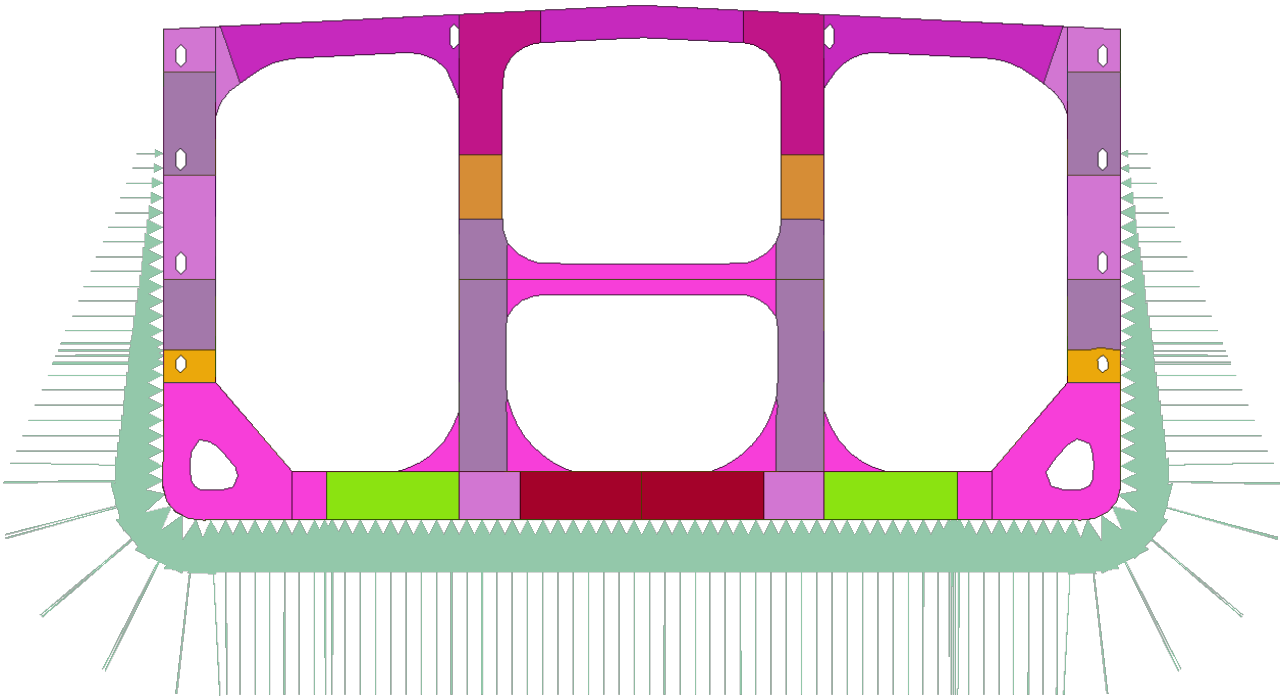

FIGURE 5.14: APPLICATION OF HYDROSTATIC PRESSURE DUE TO BUOYANCY IN THE FEM MODEL [13]

5.1.2. FEM analyses for the representative loading conditions

Hull deformations have been computed for the nine representative loading conditions. **Figures 5.15** and **5.16** show Von Misses stresses distributions at the ship hull and at the engine room region for the Ballast Arrival Loading Condition (L.C. 4). For loading conditions 4 and 34 the hull exhibits a hogging behaviour, which causes considerable displacements at the bearing positions. For loading conditions 8 and 11 the hull exhibits a sagging behaviour while for loading conditions 21 and 23 the vessel exhibits hogging at aft and sagging at fore.

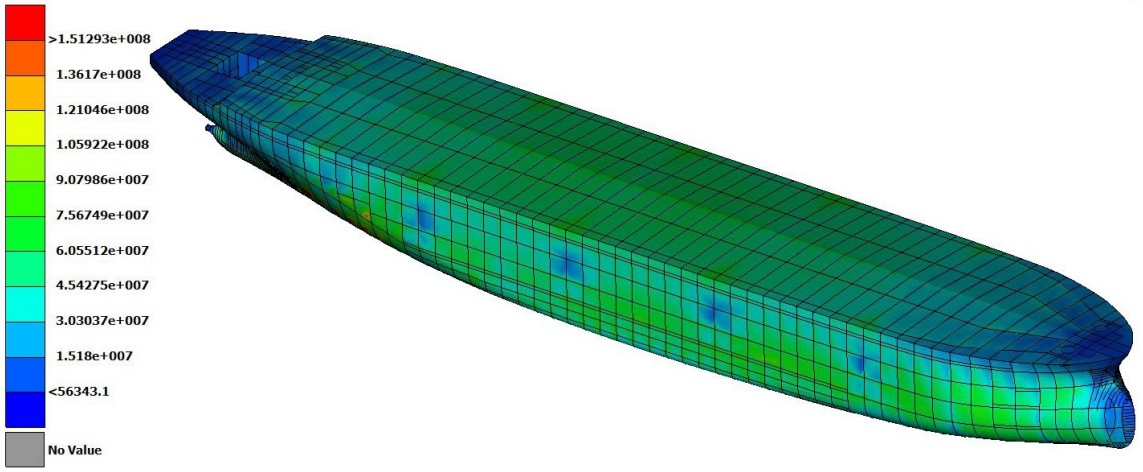

FIGURE 5.15: LOADING CONDITION 1 (BALLAST ARRIVAL CONDITION): DISTRIBUTION OF VON MISSES STRESSES ON HULL [13]

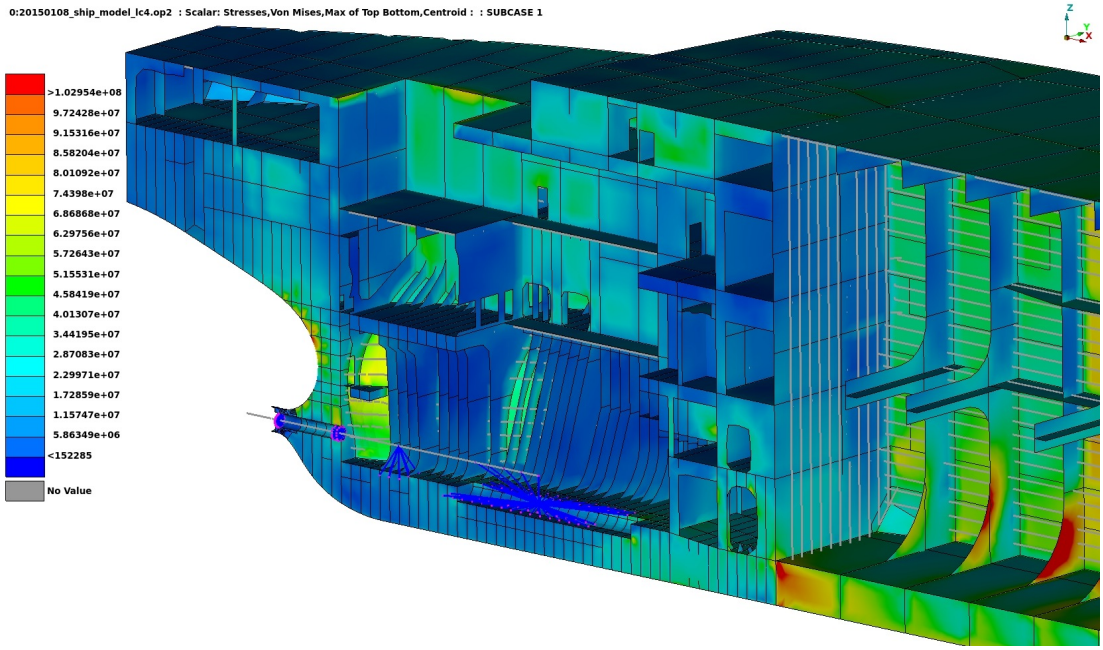

FIGURE 5.16: LOADING CONDITION 4 (BALLAST ARRIVAL CONDITION): DISTRIBUTION OF VON MISSES STRESSES AT ENGINE ROOM REGION [13]

5.2.Calculation of Static Shaft Alignment

5.2.1. Shafting System Particulars

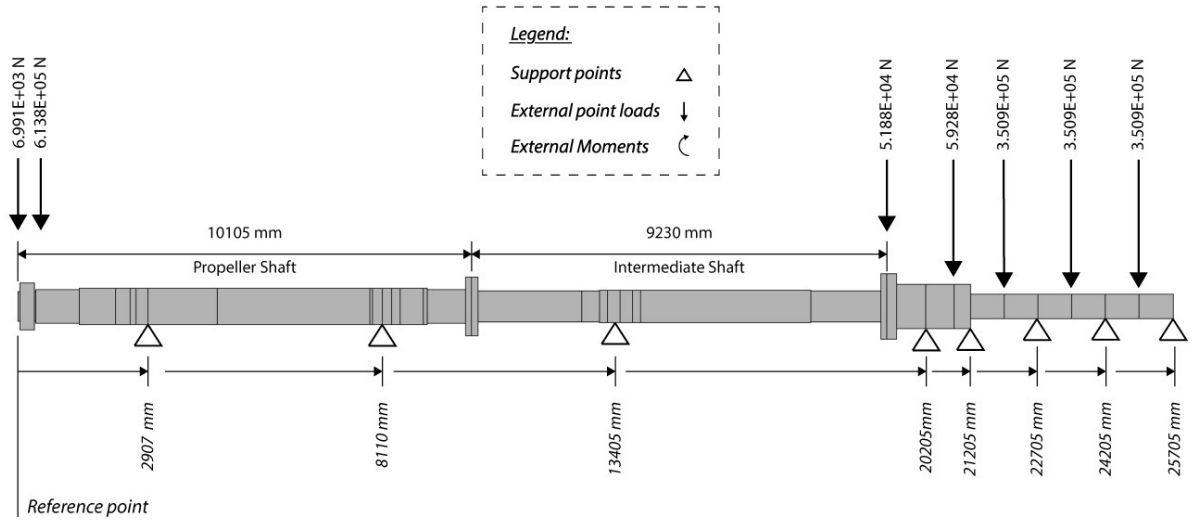

FIGURE 5.17: DETAILED MODEL OF THE SHAFTING SYSTEM OF THE PRESENT STUDY

A model of the shafting system studied in the present work is presented in **Figure 5.17**. The propeller shaft, the intermediate shaft and part of the crankshaft of the main engine are included in the calculations. The propeller shaft is supported by two stern tube bearings, the intermediate shaft by a line shaft bearing and the engine crankshaft by the crankshaft bearings (five of them are included in present calculations). Bearing details are presented hereinafter:

Stern tube bearings:

- Aft bearing: L/D = 2.23, foundation stiffness = $4x10^9$ N/m,
- Fore bearing: L/D = 0.55, foundation stiffness = $5x10^9$ N/m, slope boring = $3.59x10^{-4}$ rads,
- Both bearings have a radial clearance of 0.055 mm.

Other Bearings:

- Line shaft bearing: L/D = 1.13, foundation stiffness = 10^9 N/m, a radial clearance = 0.425 mm,
- M/E crankshaft bearings: Foundation stiffness = $6x10^9$ N/m, a radial clearance = 0.345 mm and L/D =0.3.

General Considerations:

- Density of the shaft material: 7850 kg/m^3, Young's modulus of elasticity: $2.06x10^{11}$ N/$m^{2,}$
- Lubricant dynamic viscosity: 0.1 Pa s

The shaft is discretised with 39 beam elements and a total of 40 nodes. The loads and geometry of each beam are presented in **Table 5-6**.

5.2.2. Hot M/E Condition parameters

For a running main engine, additional considerations have to be made, in order for the model to approximate real operational conditions as closely as possible. As described in a previous section the effects of thermal expansion are accounted for in this study. Each M/E bearing is elevated by 0.29 mm, as per the manufacturer's instructions when considering the hot M/E condition.

The ship of the present study is outfitted with a main engine capable of delivering 26,464 kW of power, at 73.4 RPM at N.C.R. which corresponds to a service speed of 15.7 knots. While some of the loading conditions, examined in the previous section, resemble the design draft (full load) condition, most of them amount to a displacement value of half or significantly less than half of the design displacement value. Under such conditions it is logical to assume that, in order to achieve the same service speed of 15.7 knots, the propeller rotational speed will be slower, given the decrease in total resistance.

	L.C. 1	L.C. 4	L.C. 8	L.C. 11	L.C. 14	L.C. 21	L.C. 23	L.C. 26	L.C. 34
N (RPM)	0	66.6	73.4	73.4	70	70	70	73.4	66.6

TABLE 5-5: ASSUMED VALUES OF PROPELLER ROTATIONAL SPEED FOR THE STUDIED LOADING CONDITIONS OF THE VESSEL

Through the use of available data, an estimation of the M/E rotational speed has been made for the loading conditions being studied here. Most of the present loading conditions can be grouped into three broad categories: Ballast, Half Load and Full Load. For each one of these categories an assumption was made that L.Cs. within each group have the same propeller rotational speed. Thus, hot main engine conditions have been established for three different sets of revolution speed as shown in **Figure 5.18**. **Table 5-5** outlines the final values of rotational speed assumed for each L.C.

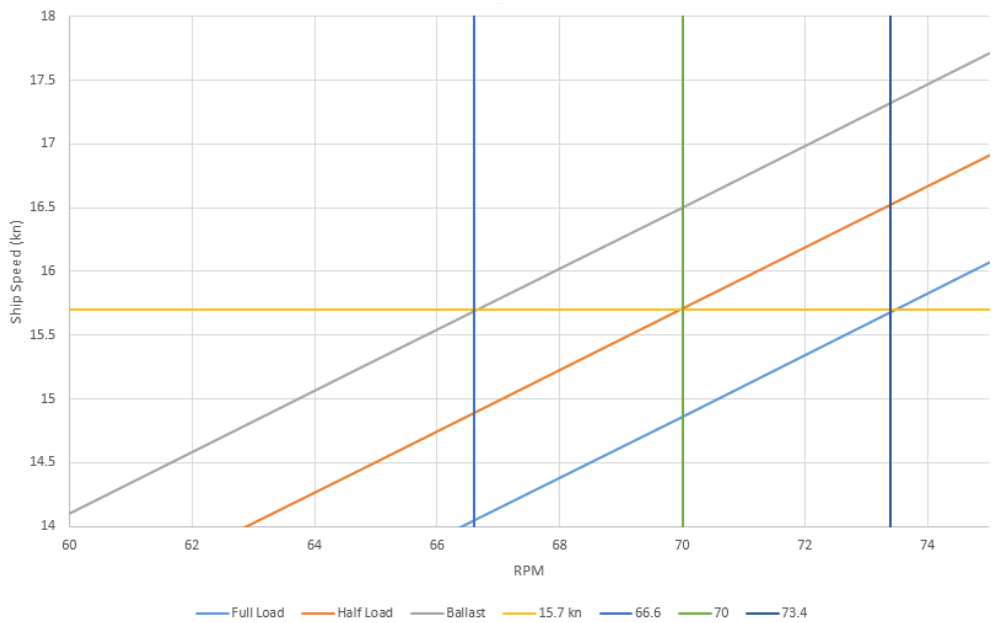

FIGURE 5.18: SHIP SPEED AS A FUNCTION OF PROPELLER (ENGINE) ROTATIONAL SPEED, FOR DIFFERENT LOADING CONDITIONS OF THE VESSEL

Element		Dist. to right end of element (m)	Length (m)	Diameter (m)		External Load (N)	Distributed Weight at dry dock (N/m)	Distributed Weight Imersed propeller (N/m)
No.	Type			Left	Right			
1		0.050	0.050	0.650	0.650		25553.79	22217.15
2	Load at right end	0.375	0.325	1.035	1.035	6.99E+06	64790.19	56330.32
3		0.405	0.030	0.650	0.650		25553.79	22217.15
4	Load at right end	1.372	0.967	0.726	0.775	6.14E+05	34078.79	29629.01
5		2.175	0.803	0.775	0.815		38234.41	33242.02
6		2.505	0.330	0.815	0.815		40173.88	34928.24
7		2.635	0.130	0.815	0.815		40173.88	40173.88
8	Bearing at right end	3.540	0.905	0.815	0.815		40173.88	40173.88
9		4.445	0.905	0.815	0.815		40173.88	40173.88
10		7.835	3.390	0.815	0.815		40173.88	40173.88
11		7.895	0.060	0.817	0.817		40371.29	40371.29
12	Bearing at right end	8.110	0.215	0.817	0.817		40371.29	40371.29
13		8.325	0.215	0.817	0.817		40371.29	40371.29
14		8.505	0.180	0.817	0.817		40371.29	40371.29
15		9.020	0.515	0.817	0.817		40371.29	40371.29
16		9.120	0.100	0.817	0.817		40371.29	40371.29
17		9.970	0.850	0.817	0.705		35089.81	35089.81
18		10.105	0.135	1.320	1.320		105384.42	105384.42
19		10.240	0.135	1.320	1.320		105384.42	105384.42
20		12.555	2.315	0.705	0.705		30061.23	30061.23
21		12.955	0.400	0.705	0.705		30061.23	30061.23
22		13.130	0.175	0.710	0.710		30489.14	30489.14
23	Bearing at right end	13.405	0.275	0.710	0.710		30489.14	30489.14
24		13.680	0.275	0.710	0.710		30489.14	30489.14
25		13.855	0.175	0.710	0.710		30489.14	30489.14
26		17.655	3.800	0.710	0.710		30489.14	30489.14
27		19.200	1.545	0.705	0.705		30061.23	30061.23
28		19.335	0.135	1.458	1.458		128571.17	128571.17
29	Load at right end	19.336	0.001	1.458	1.458	5.19E+04	128571.17	128571.17
30		19.555	0.219	1.458	1.458		128571.17	128571.17
31	Bearing at right end	20.205	0.650	0.980	0.980		58087.23	58087.23
32	Load at right end	20.840	0.635	0.980	0.980	5.93E+04	58087.23	58087.23
33	Bearing at right end	21.205	0.365	0.980	0.980		58087.23	58087.23
34	Load at right end	21.955	0.750	0.552	0.552	3.51E+05	18429.21	18429.21
35	Bearing at right end	22.705	0.750	0.552	0.552		18429.21	18429.21
36	Load at right end	23.455	0.750	0.552	0.552	3.51E+05	18429.21	18429.21
37	Bearing at right end	24.205	0.750	0.552	0.552		18429.21	18429.21
38	Load at right end	24.955	0.750	0.552	0.552	3.51E+05	18429.21	18429.21
39	Bearing at right end	25.705	0.750	0.552	0.552		18429.21	18429.21

TABLE 5-6: GEOMETRIC DATA OF THE PROPULSION SHAFT OF THE PRESENT STUDY

5.2.3. Initial static shaft alignment plan - Reference Condition

A reference line of the shafting system is defined as the one passing through the centres of the fore stern tube bearing and the M/E. Initially, no hull deformations are considered (this case resembles dry-docking conditions). The line shaft bearing and the engine crankshaft bearings are appropriately offset from the reference line, based on the shaft alignment plan of the vessel. In **Table 5-7**, the corresponding vertical offsets of each bearing are presented, accompanied by the properties of each bearing and by the calculations of reaction forces at each bearing support location, for the reference (dry-dock) condition. The following considerations have been made for the calculation presented in this section:

- The M/E is not running,
- The M/E is in cold condition and M/E bearings are offset by an additional -0.29 mm relative to other conditions where the M/E is running,
- Hull Deformations are zero,
- Applied tail shaft slope boring is equal to 0.5585 mrad,
- The propeller and parts of the propeller shaft are not immersed in water. Thus their weight is fully supported by the bearings alone.

Bearing No.	Bearing	Diametral Clearance (mm)	Bearing Foundation Stiffness (N/m)	L/D	Offsets (mm)	Reactions (N)	Mean Pressure (Pa)	Longitudinal Shifts (m)
1	Aft S/T	1.10	4.00E+09	2.23	-0.06	1.07E+06	7.12E+05	-
2	Fore S/T	1.10	5.00E+09	0.55	0.00	1.09E+05	2.95E+05	-
3	Intermediate	0.85	1.00E+09	1.13	-2.95	7.24E+04	1.27E+05	-
4	M/E 1	0.69	6.00E+09	0.3	-5.10	1.44E+05	4.99E+05	-
5	M/E 2	0.69	6.00E+09	0.3	-5.10	3.32E+05	1.15E+06	-
6	M/E 3	0.69	6.00E+09	0.3	-5.10	4.15E+05	1.44E+06	-
7	M/E 4	0.69	6.00E+09	0.3	-5.10	4.09E+05	1.42E+06	-
8	M/E 5	0.69	6.00E+09	0.3	-5.10	1.50E+05	5.22E+05	-

TABLE 5-7: INITIAL SHAFT ALIGNMENT PLAN - REFERENCE CONDITION

5.2.4. Hull Deformation Effects on Shaft Alignment

The hull deformations predicted by the FEM approach of section 5.1.2 are applied to the initial shafting plan corresponding to dry-dock conditions. The resulting vertical position of each bearing relative to the reference line, is presented in **Figure 5.19**, for every loading condition under consideration.

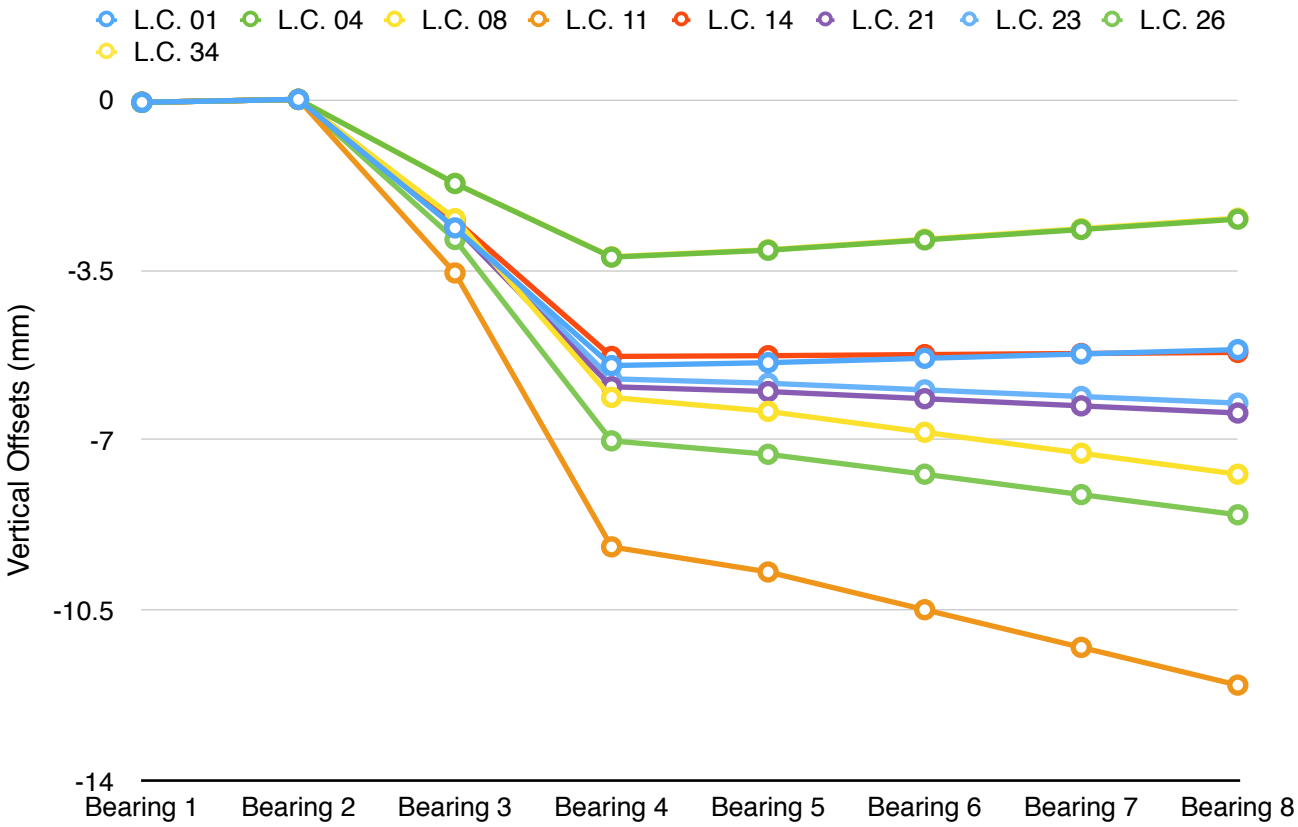

FIGURE 5.19: RELATIVE VERTICAL BEARING POSITIONS FOR DIFFERENT LOADING CONDITIONS OF THE VESSEL

In **Table 5-8** and **Figure 5.20**, the calculated bearing reaction forces are presented for the loading conditions studied in the present work. It is observed that, overall, although the vertical offsets of certain bearings are of the order of 11 mm, the differences in bearing reaction forces are not very pronounced. In particular, the reaction force of the aft stern tube bearing ranges from 980 kN to 1078 kN (maximum deviation of approximately 9.07%). Bearings 1 and 7 display the least amount of deviation from the reference condition.

Bearing 3 (Intermediate shaft bearing) exhibits the maximum deviation (162.99%) in reaction forces, ranging from -45.58 kN (LC11) to 75.8 kN (LC01). This bearing consistently appears to be either very lightly loaded, which almost defeats the purpose of installing a bearing at this longitudinal position, or worse negatively loaded. Thus, shafting plan design concerns should be raised as to whether the long held belief, that a simple study of a static shafting plan provides adequate information for the system's behaviour, can be upheld, or should be challenged. The above claim becomes even more valid if we consider the fact that a simple static analysis of shaft alignment disregarding foundation stiffness and bearing oil film concludes that the I/M shaft bearing is loaded at 118.9 kN for loading condition no.11.

Loading case 1				Loading case 4				Loading case 8			
Reactions (N)	Vertical Offsets (mm)	Dif. From Reference (%)	dL (mm)	Reactions (N)	Vertical Offsets (mm)	Dif. From Reference (%)	dL (mm)	Reactions (N)	Vertical Offsets (mm)	Dif. From Reference (%)	dL (mm)
1.048E+06	-0.06	2.35%	0.00	1.078E+06	-0.06	0.44%	-38.09	1.050E+06	-0.06	2.12%	-41.02
1.261E+05	0.00	15.97%	0.00	7.256E+04	0.00	33.25%	8.29	1.091E+05	0.00	0.36%	13.76
7.581E+04	-3.04	4.75%	0.00	6.436E+04	-2.13	11.07%	25.32	5.424E+04	-2.85	25.06%	37.87
9.561E+04	-5.17	33.49%	0.00	2.483E+05	-2.65	72.75%	-6.89	2.994E+05	-5.53	108.28%	15.59
3.551E+05	-5.11	6.99%	0.00	2.885E+05	-2.51	13.08%	-7.49	2.776E+05	-5.82	16.38%	15.38
4.330E+05	-5.02	4.22%	0.00	3.796E+05	-2.30	8.63%	-9.25	3.521E+05	-6.25	15.24%	20.20
4.086E+05	-4.93	0.10%	0.00	3.987E+05	-2.08	2.50%	-11.46	3.862E+05	-6.68	5.56%	18.61
1.496E+05	-4.84	0.54%	0.00	1.612E+05	-1.87	7.21%	-8.59	1.633E+05	-7.11	8.59%	6.49
Loading case 11				Loading case 14				Loading case 21			
Reactions (N)	Vertical Offsets (mm)	Dif. From Reference (%)	dL (mm)	Reactions (N)	Offsets (mm)	Dif. From Reference (%)	dL (mm)	Reactions (N)	Vertical Offsets (mm)	Dif. From Reference (%)	dL (mm)
9.801E+05	-0.06	8.67%	-48.91	1.047E+06	-0.06	2.43%	-42.29	1.041E+06	-0.06	2.98%	-43.16
2.596E+05	0.00	138.84%	46.65	1.235E+05	0.00	13.56%	16.87	1.320E+05	0.00	21.47%	18.66
-4.558E+04	-3.97	162.99%	-52.38	6.072E+04	-2.87	16.11%	30.00	5.402E+04	-3.02	25.36%	36.00
3.335E+05	-8.60	131.96%	32.46	1.903E+05	-4.69	32.40%	0.82	2.183E+05	-5.31	51.85%	5.40
2.893E+05	-9.12	12.85%	30.49	3.066E+05	-4.68	7.63%	1.14	2.981E+05	-5.41	10.19%	7.04
3.384E+05	-9.89	18.55%	38.36	4.070E+05	-4.65	2.03%	-0.62	3.923E+05	-5.56	5.57%	7.57
3.683E+05	-10.67	9.93%	35.97	3.977E+05	-4.63	2.75%	-2.14	3.986E+05	-5.71	2.54%	5.92
1.696E+05	-11.44	12.75%	15.11	1.587E+05	-4.61	5.54%	-3.60	1.574E+05	-5.85	4.66%	0.37
Loading case 23				Loading case 26				Loading case 34			
Reactions (N)	Vertical Offsets (mm)	Dif. From Reference (%)	dL (mm)	Reactions (N)	Offsets (mm)	Dif. From Reference (%)	dL (mm)	Vertical Offsets (mm)	Offsets (mm)	Dif. From Reference (%)	dL (mm)
1.046E+06	-0.06	2.52%	-42.65	1.017E+06	-0.06	5.22%	-44.98	1.078E+06	-0.06	0.44%	-38.08
1.209E+05	0.00	11.20%	16.65	1.860E+05	0.00	71.07%	28.26	7.250E+04	0.00	33.31%	8.27
6.204E+04	-2.92	14.27%	29.26	1.234E+03	-3.28	98.29%	61.8	6.461E+04	-2.13	10.73%	25.14
2.155E+05	-5.15	49.91%	5.07	3.001E+05	-6.43	108.75%	15.02	2.480E+05	-2.64	72.49%	-6.98
2.978E+05	-5.24	10.28%	6.64	2.798E+05	-6.70	15.69%	14.89	2.874E+05	-2.50	13.42%	-7.60
3.935E+05	-5.38	5.28%	7.04	3.608E+05	-7.11	13.15%	19.65	3.807E+05	-2.28	8.36%	-9.50
3.986E+05	-5.51	2.53%	5.40	3.840E+05	-7.53	6.09%	17.84	3.992E+05	-2.06	2.38%	-11.66
1.574E+05	-5.65	4.68%	0.12	1.633E+05	-7.94	8.57%	6.16	1.609E+05	-1.85	7.00%	-8.65

TABLE 5-8: LOADING CONDITIONS: BEARING PROPERTIES, VERTICAL OFFSETS AND REACTION FORCES

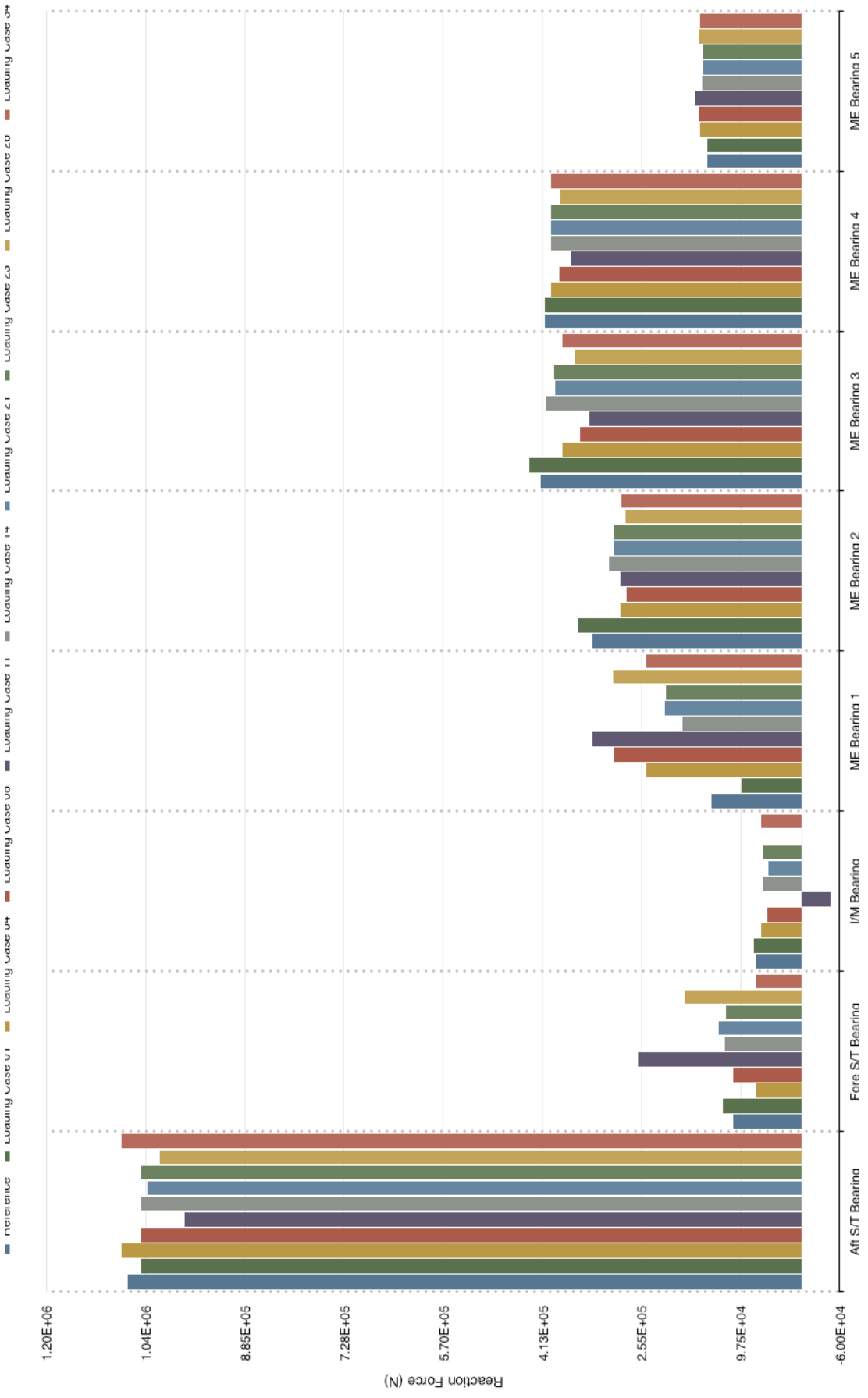

FIGURE 5.20: BEARING REACTIONS PER LOADING CONDITION

[Pa]	AFT S/T	FORE S/T	I/M	M/E NO.1	M/E NO.2	M/E NO.3	M/E NO.4	M/E NO.5
L.C. 01	6.95E+05	3.42E+05	1.33E+05	3.32E+05	1.23E+06	1.50E+06	1.42E+06	5.19E+05
L.C. 04	7.15E+05	1.97E+05	1.13E+05	8.62E+05	1.00E+06	1.32E+06	1.38E+06	5.60E+05
L.C. 08	6.97E+05	2.96E+05	9.50E+04	1.04E+06	9.63E+05	1.22E+06	1.34E+06	5.67E+05
L.C. 11	6.50E+05	7.05E+05	-7.98E+04	1.16E+06	1.00E+06	1.17E+06	1.28E+06	5.89E+05
L.C. 14	6.95E+05	3.35E+05	1.06E+05	6.61E+05	1.06E+06	1.41E+06	1.38E+06	5.51E+05
L.C. 21	6.91E+05	3.59E+05	9.46E+04	7.58E+05	1.03E+06	1.36E+06	1.38E+06	5.46E+05
L.C. 23	6.94E+05	3.28E+05	1.09E+05	7.48E+05	1.03E+06	1.37E+06	1.38E+06	5.46E+05
L.C. 26	6.75E+05	5.05E+05	2.16E+03	1.04E+06	9.71E+05	1.25E+06	1.33E+06	5.67E+05
L.C. 34	7.15E+05	1.97E+05	1.13E+05	8.61E+05	9.98E+05	1.32E+06	1.39E+06	5.58E+05

TABLE 5-9: LUBRICANT MEAN PRESSURE VALUES PER BEARING AND L.C.

Finally, the influence of trim on hull deformations becomes apparent, should L.C. 08 and L.C. 11 be examined side by side. Although these two conditions are very similar in terms of displacement, the trim difference drastically changes hull bending moments and deformations.

Loading condition No. 01 [Lightship]

The following assumptions have been made for the calculations presented in this section:

- The M/E is **not** running, which means the revolution rate is 0 RPM and no bearing lubrication takes place,
- The M/E is in cold condition,
- Hull Deformations are **not** zero,
- Applied tail shaft slope boring is equal to 0.5585 mrad,
- The propeller and parts of the propeller shaft are immersed in water. Thus their weight is partially supported by the bearings and the water.

Bearing	Reactions (N)	Mean Pressure (Pa)	Longitudinal Shifts (mm)	Total Offsets (m)	Initial Offsets (m)	Hull Deform. (m)	Support Elastic Deform. (m)	Film Thickness (m)
Aft S/T	1.048E+06	6.95E+05	-	-3.22E-04	-6.00E-05	0.00E+00	-2.62E-04	-
Fore S/T	1.261E+05	3.42E+05	-	-2.52E-05	0.00E+00	0.00E+00	-2.52E-05	-
I/M	7.581E+04	1.33E+05	-	-3.12E-03	-2.95E-03	-9.01E-05	-7.58E-05	-
M/E 1	9.561E+04	3.32E+05	-	-5.18E-03	-5.10E-03	-6.80E-05	-1.59E-05	-
M/E 2	3.551E+05	1.23E+06	-	-5.17E-03	-5.10E-03	-8.58E-06	-5.92E-05	-
M/E 3	4.330E+05	1.50E+06	-	-5.09E-03	-5.10E-03	8.08E-05	-7.22E-05	-
M/E 4	4.086E+05	1.42E+06	-	-5.00E-03	-5.10E-03	1.70E-04	-6.81E-05	-
M/E 5	1.496E+05	5.19E+05	-	-4.87E-03	-5.10E-03	2.59E-04	-2.49E-05	-

TABLE 5-10: L.C. 01 ANALYSIS BREAKDOWN

In **Table 5-9** and **Tables 5-10** through **5-17**, we can see a breakdown of the vertical offsets of each support point, as calculated by the program. In this case (L.C.01), the film thickness component is equal to zero, as this is a loading condition in which the M/E is not running and thus no hydrodynamic lubrication effects are present. This is also incorporated in the initial offsets column, where, M/E heat expansion offsets are equal to zero.

Another point of interest is the mean pressure within each bearing. Appendix **Figures A-1** to **A-3** depict the manufacturer's drawing for both stern tube bearings, as well as the I/M shaft bearing. Within these drawings, the maximum permissible mean pressure is prescribed:

- The limit is 0.8 MPa for the Aft Stern tube bearing and the value observed is 0.695 MPa,
- The limit is 1.2 MPa for the fore Stern tube bearing and the value observed is 0.342 MPa,
- The limit is 0.8 MPa for the I/M shaft bearing and the value observed is 0.133 MPa.

Finally the maximum permissible mean pressure for the crankshaft bearings is 3 MPa, and no values have been observed to exceed this limit. More details on maximum pressure can be found in segment 5.2.5 "*Effects on Bearing Lubrication Characteristics"*.

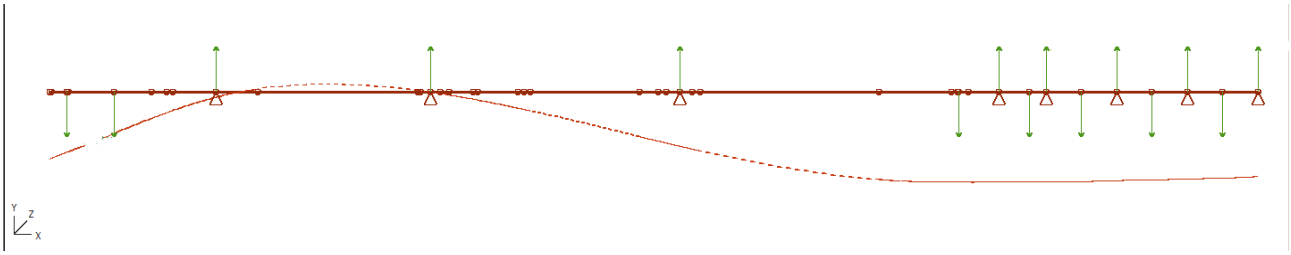

FIGURE 5.21: LOADING CONDITION NO. 01 SHAFT ALIGNMENT

Loading condition No. 04 [Ballast Arrival]

The following considerations have been made for the calculation presented in this section:

- The M/E is running at 66.6 RPM,
- The M/E is in hot condition and M/E bearings are offset by an additional 0.29 mm relative to other conditions where the M/E is not running,
- Hull Deformations are **not** zero,
- Applied tail shaft slope boring is equal to 0.5585 mrad,
- The propeller and parts of the propeller shaft are immersed in water. Thus, their weight is partially supported by the bearings and the water.

Bearing	Reactions (N)	Mean Pressure (Pa)	Longitudinal Shifts (mm)	Total Offsets (m)	Initial Offsets (m)	Hull Deform. (m)	Support Elastic Deform. (m)	Film Thickness (m)
Aft S/T	1.078E+06	7.15E+05	-38.09	-1.68E-04	-6.00E-05	0.00E+00	-2.69E-04	1.61E-04
Fore S/T	7.256E+04	1.97E+05	8.29	1.44E-04	0.00E+00	0.00E+00	-1.45E-05	1.59E-04
I/M	6.436E+04	1.13E+05	25.32	-2.07E-03	-2.95E-03	8.23E-04	-6.44E-05	1.23E-04
M/E 1	2.483E+05	8.62E+05	-6.89	-2.62E-03	-4.81E-03	2.16E-03	-4.14E-05	6.97E-05
M/E 2	2.885E+05	1.00E+06	-7.49	-2.49E-03	-4.81E-03	2.30E-03	-4.81E-05	6.55E-05
M/E 3	3.796E+05	1.32E+06	-9.25	-2.30E-03	-4.81E-03	2.51E-03	-6.33E-05	5.85E-05
M/E 4	3.987E+05	1.38E+06	-11.46	-2.09E-03	-4.81E-03	2.73E-03	-6.65E-05	5.84E-05
M/E 5	1.612E+05	5.60E+05	-8.59	-1.81E-03	-4.81E-03	2.94E-03	-2.69E-05	8.34E-05

TABLE 5-11: L.C. 04 ANALYSIS BREAKDOWN

On the rest of the tables, the condition of the M/E is incorporated in the initial offsets column where, M/E heat expansion offsets are equal to +0.29 mm.

Maximum permissible mean pressure:

- The limit is 0.8 MPa for the Aft Stern tube bearing and the value observed is 0.715 MPa,
- The limit is 1.2 MPa for the fore Stern tube bearing and the value observed is 0.197 MPa,
- The limit is 0.8 MPa for the I/M shaft bearing and the value observed is 0.113 MPa,
- No crankshaft bearing mean pressure value exceeds 3 MPa.

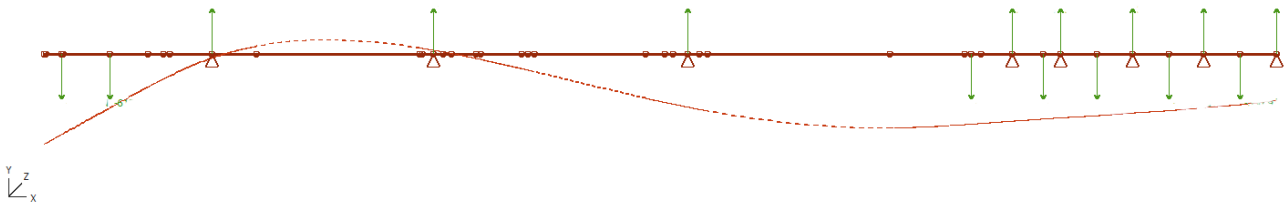

FIGURE 5.22: LOADING CONDITION NO. 04 SHAFT ALIGNMENT

Loading condition No. 08 [Homo. Design Load Dep.]

The following considerations have been made for the calculation presented in this section:

- The M/E is running at 73.4 RPM,
- The M/E is in hot condition and M/E bearings are offset by an additional 0.29 mm relative to other conditions where the M/E is not running,
- Hull Deformations are **not** zero,
- Applied tail shaft slope boring is equal to 0.5585 mrad,
- The propeller and parts of the propeller shaft are immersed in water. Thus their weight is partially supported by the bearings and the water.

Bearing	Reactions (N)	Mean Pressure (Pa)	Longitudinal Shifts (mm)	Total Offsets (m)	Initial Offsets (m)	Hull Deform. (m)	Support Elastic Deform. (m)	Film Thickness (m)
Aft S/T	1.050E+06	6.97E+05	-41.02	-1.56E-04	-6.00E-05	0.00E+00	-2.63E-04	1.67E-04
Fore S/T	1.091E+05	2.96E+05	13.76	1.24E-04	0.00E+00	0.00E+00	-2.18E-05	1.46E-04
I/M	5.424E+04	9.50E+04	37.87	-2.79E-03	-2.95E-03	1.01E-04	-5.42E-05	1.10E-04
M/E 1	2.994E+05	1.04E+06	15.59	-5.52E-03	-4.81E-03	-7.22E-04	-4.99E-05	5.79E-05
M/E 2	2.776E+05	9.63E+05	15.38	-5.80E-03	-4.81E-03	-1.01E-03	-4.63E-05	6.17E-05
M/E 3	3.521E+05	1.22E+06	20.20	-6.27E-03	-4.81E-03	-1.44E-03	-5.87E-05	4.19E-05
M/E 4	3.862E+05	1.34E+06	18.61	-6.70E-03	-4.81E-03	-1.87E-03	-6.44E-05	3.93E-05
M/E 5	1.633E+05	5.67E+05	6.49	-7.05E-03	-4.81E-03	-2.30E-03	-2.72E-05	8.46E-05

TABLE 5-12: L.C. 08 ANALYSIS BREAKDOWN

Maximum permissible mean pressure:

- The limit is 0.8 MPa for the Aft Stern tube bearing and the value observed is 0.697 MPa,
- The limit is 1.2 MPa for the fore Stern tube bearing and the value observed is 0.296 MPa,
- The limit is 0.8 MPa for the I/M shaft bearing and the value observed is 0.095 MPa,
- No crankshaft bearing mean pressure value exceeds 3 MPa.

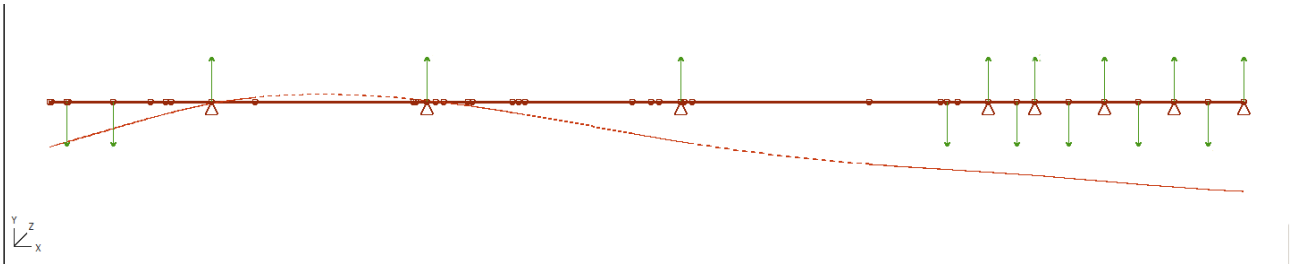

FIGURE 5.23: LOADING CONDITION NO. 08 SHAFT ALIGNMENT

Loading condition No. 11 [Homo. Scantling Load Dep.]

The following considerations have been made for the calculation presented in this section:

- The M/E is running at 73.4 RPM,
- The M/E is in hot condition and M/E bearings are offset by an additional 0.29 mm relative to other conditions where the M/E is not running,
- Hull Deformations are **not** zero,
- Applied tail shaft slope boring is equal to 0.5585 mrad,
- The propeller and parts of the propeller shaft are immersed in water. Thus their weight is partially supported by the bearings and the water.

Bearing	Reactions (N)	Mean Pressure (Pa)	Longitudinal Shifts (mm)	Total Offsets (m)	Initial Offsets (m)	Hull Deform. (m)	Support Elastic Deform. (m)	Film Thickness (m)
Aft S/T	9.801E+05	6.50E+05	-48.91	-1.30E-04	-6.00E-05	0.00E+00	-2.45E-04	1.75E-04
Fore S/T	2.596E+05	7.05E+05	46.65	-1.14E-05	0.00E+00	0.00E+00	-5.19E-05	4.05E-05
I/M	-4.558E+04	-7.98E+04	-52.38	-4.26E-03	-2.95E-03	-1.02E-03	4.56E-05	-3.39E-04
M/E 1	3.335E+05	1.16E+06	32.46	-8.63E-03	-4.81E-03	-3.79E-03	-5.56E-05	2.42E-05
M/E 2	2.893E+05	1.00E+06	30.49	-9.13E-03	-4.81E-03	-4.31E-03	-4.82E-05	3.98E-05
M/E 3	3.384E+05	1.17E+06	38.36	-9.94E-03	-4.81E-03	-5.08E-03	-5.64E-05	1.12E-05
M/E 4	3.683E+05	1.28E+06	35.97	-1.07E-02	-4.81E-03	-5.86E-03	-6.14E-05	6.09E-06
M/E 5	1.696E+05	5.89E+05	15.11	-1.14E-02	-4.81E-03	-6.63E-03	-2.83E-05	8.33E-05

TABLE 5-13: L.C. 11 ANALYSIS BREAKDOWN

Maximum permissible mean pressure:

- The limit is 0.8 MPa for the Aft Stern tube bearing and the value observed is 0.650 MPa,
- The limit is 1.2 MPa for the fore Stern tube bearing and the value observed is 0.705 MPa,
- The limit is 0.8 MPa for the I/M shaft bearing and the value observed is 0.079 MPa,
- No crankshaft bearing mean pressure value exceeds 3 MPa.

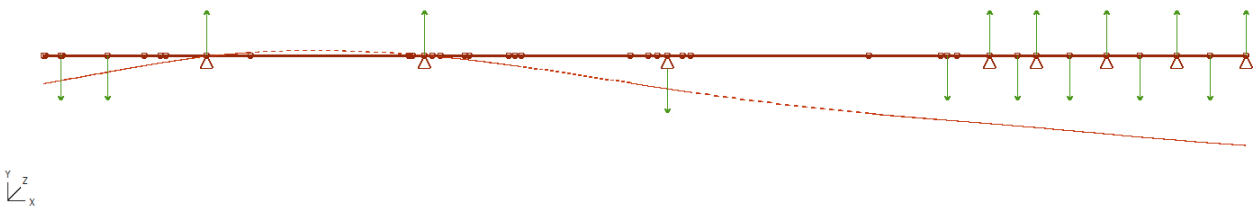

FIGURE 5.24: LOADING CONDITION NO. 11 SHAFT ALIGNMENT

Loading condition No. 14 [Segregated I Load Dep.]

The following considerations have been made for the calculation presented in this section:

- The M/E is running at 70.0 RPM,
- The M/E is in hot condition and M/E bearings are offset by an additional 0.29 mm relative to other conditions where the M/E is not running,
- Hull Deformations are **not** zero,
- Applied tail shaft slope boring is equal to 0.5585 mrad,
- The propeller and parts of the propeller shaft are immersed in water. Thus their weight is partially supported by the bearings and the water.

Bearing	Reactions (N)	Mean Pressure (Pa)	Longitudinal Shifts (mm)	Total Offsets (m)	Initial Offsets (m)	Hull Deform. (m)	Support Elastic Deform. (m)	Film Thickness (m)
Aft S/T	1.047E+06	6.95E+05	-42.29	-1.56E-04	-6.00E-05	0.00E+00	-2.62E-04	1.65E-04
Fore S/T	1.235E+05	3.35E+05	16.87	1.13E-04	0.00E+00	0.00E+00	-2.47E-05	1.37E-04
I/M	6.072E+04	1.06E+05	30.00	-2.80E-03	-2.95E-03	7.87E-05	-6.07E-05	1.28E-04
M/E 1	1.903E+05	6.61E+05	0.82	-4.64E-03	-4.81E-03	1.20E-04	-3.17E-05	7.76E-05
M/E 2	3.066E+05	1.06E+06	1.14	-4.66E-03	-4.81E-03	1.35E-04	-5.11E-05	6.35E-05
M/E 3	4.070E+05	1.41E+06	-0.62	-4.66E-03	-4.81E-03	1.57E-04	-6.78E-05	5.61E-05
M/E 4	3.977E+05	1.38E+06	-2.14	-4.64E-03	-4.81E-03	1.80E-04	-6.63E-05	5.68E-05
M/E 5	1.587E+05	5.51E+05	-3.60	-4.55E-03	-4.81E-03	2.02E-04	-2.65E-05	8.30E-05

TABLE 5-14: L.C. 14 ANALYSIS BREAKDOWN

Maximum permissible mean pressure:

- The limit is 0.8 MPa for the Aft Stern tube bearing and the value observed is 0.695 MPa,
- The limit is 1.2 MPa for the fore Stern tube bearing and the value observed is 0.334 MPa,
- The limit is 0.8 MPa for the I/M shaft bearing and the value observed is 0.106 MPa,
- No crankshaft bearing mean pressure value exceeds 3 MPa.

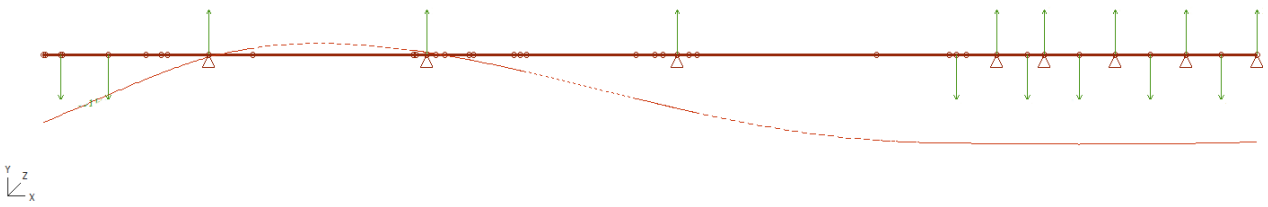

FIGURE 5.25: LOADING CONDITION NO. 14 SHAFT ALIGNMENT

Loading condition No. 21 [Segregated III Load Int.]

The following considerations have been made for the calculation presented in this section:

- The M/E is running at 70.0 RPM,
- The M/E is in hot condition and M/E bearings are offset by an additional 0.29 mm relative to other conditions where the M/E is not running,
- Hull Deformations are not zero,
- Applied tail shaft slope boring is equal to 0.5585 mrad,
- The propeller and parts of the propeller shaft are immersed in water. Thus their weight is partially supported by the bearings and the water.

Bearing	Reactions (N)	Mean Pressure (Pa)	Longitudinal Shifts (mm)	Total Offsets (m)	Initial Offsets (m)	Hull Deform. (m)	Support Elastic Deform. (m)	Film Thickness (m)
Aft S/T	1.041E+06	6.91E+05	-43.16	-1.54E-04	-6.00E-05	0.00E+00	-2.60E-04	1.66E-04
Fore S/T	1.320E+05	3.59E+05	18.66	1.05E-04	0.00E+00	0.00E+00	-2.64E-05	1.31E-04
I/M	5.402E+04	9.46E+04	36.00	-2.96E-03	-2.95E-03	-6.56E-05	-5.40E-05	1.09E-04
M/E 1	2.183E+05	7.58E+05	5.40	-5.28E-03	-4.81E-03	-5.04E-04	-3.64E-05	7.39E-05
M/E 2	2.981E+05	1.03E+06	7.04	-5.40E-03	-4.81E-03	-6.02E-04	-4.97E-05	6.38E-05
M/E 3	3.923E+05	1.36E+06	7.57	-5.57E-03	-4.81E-03	-7.49E-04	-6.54E-05	5.50E-05
M/E 4	3.986E+05	1.38E+06	5.92	-5.72E-03	-4.81E-03	-8.96E-04	-6.64E-05	5.73E-05
M/E 5	1.574E+05	5.46E+05	0.37	-5.80E-03	-4.81E-03	-1.04E-03	-2.62E-05	8.27E-05

TABLE 5-15: L.C. 21 ANALYSIS BREAKDOWN

Maximum permissible mean pressure:

- The limit is 0.8 MPa for the Aft Stern tube bearing and the value observed is 0.691 MPa,
- The limit is 1.2 MPa for the fore Stern tube bearing and the value observed is 0.359 MPa,
- The limit is 0.8 MPa for the I/M shaft bearing and the value observed is 0.094 MPa,
- No crankshaft bearing mean pressure value exceeds 3 MPa.

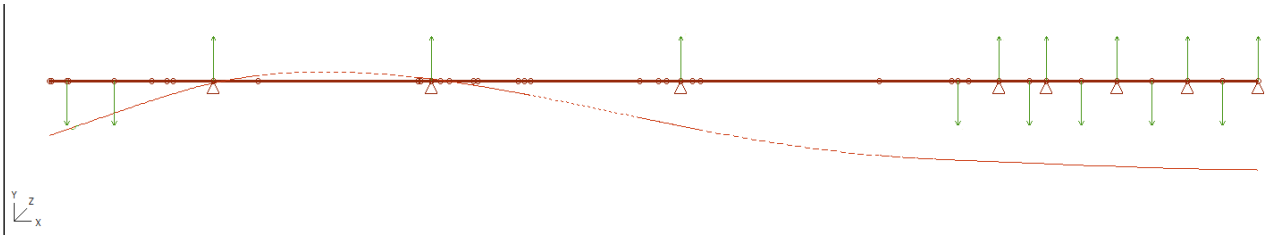

FIGURE 5.26: LOADING CONDITION NO. 21 SHAFT ALIGNMENT

Loading condition No. 23 [Segregated I+II Load Dep.]

The following considerations have been made for the calculation presented in this section:

- The M/E is running at 70.0 RPM,
- The M/E is in hot condition and M/E bearings are offset by an additional 0.29 mm relative to other conditions where the M/E is not running,
- Hull Deformations are **not** zero,
- Applied tail shaft slope boring is equal to 0.5585 mrad,
- The propeller and parts of the propeller shaft are immersed in water. Thus their weight is partially supported by the bearings and the water.

Bearing	Reactions (N)	Mean Pressure (Pa)	Longitudinal Shifts (mm)	Total Offsets (m)	Initial Offsets (m)	Hull Deform. (m)	Support Elastic Deform. (m)	Film Thickness (m)
Aft S/T	1.046E+06	6.94E+05	-42.65	-1.56E-04	-6.00E-05	0.00E+00	-2.62E-04	1.65E-04
Fore S/T	1.209E+05	3.28E+05	16.65	1.15E-04	0.00E+00	0.00E+00	-2.42E-05	1.39E-04
I/M	6.204E+04	1.09E+05	29.26	-2.85E-03	-2.95E-03	2.81E-05	-6.20E-05	1.32E-04
M/E 1	2.155E+05	7.48E+05	5.07	-5.11E-03	-4.81E-03	-3.41E-04	-3.59E-05	7.48E-05
M/E 2	2.978E+05	1.03E+06	6.64	-5.23E-03	-4.81E-03	-4.32E-04	-4.96E-05	6.38E-05
M/E 3	3.935E+05	1.37E+06	7.04	-5.39E-03	-4.81E-03	-5.68E-04	-6.56E-05	5.54E-05
M/E 4	3.986E+05	1.38E+06	5.40	-5.52E-03	-4.81E-03	-7.04E-04	-6.64E-05	5.72E-05
M/E 5	1.574E+05	5.46E+05	0.12	-5.59E-03	-4.81E-03	-8.40E-04	-2.62E-05	8.27E-05

TABLE 5-16: L.C. 23 ANALYSIS BREAKDOWN

Maximum permissible mean pressure:

- The limit is 0.8 MPa for the Aft Stern tube bearing and the value observed is 0.694 MPa,
- The limit is 1.2 MPa for the fore Stern tube bearing and the value observed is 0.328 MPa,
- The limit is 0.8 MPa for the I/M shaft bearing and the value observed is 0.109 MPa,
- No crankshaft bearing mean pressure value exceeds 3 MPa.

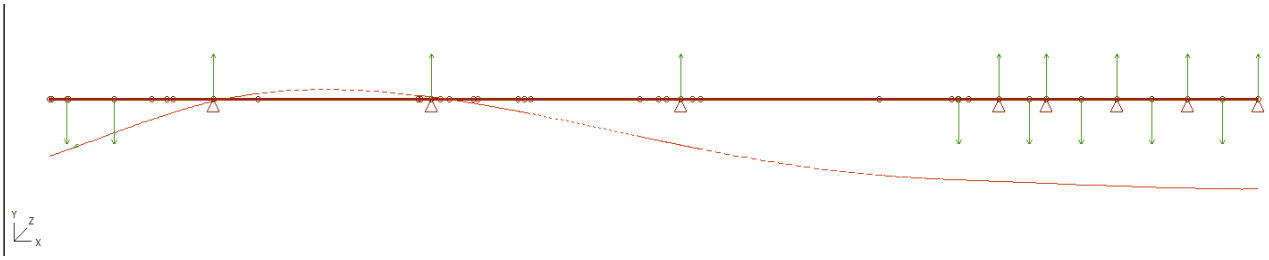

FIGURE 5.27: LOADING CONDITION NO. 23 SHAFT ALIGNMENT

Loading condition No. 26 [Segregated I+III Load Dep.]

The following considerations have been made for the calculation presented in this section:

- The M/E is running at 73.4 RPM,
- The M/E is in hot condition and M/E bearings are offset by an additional 0.29 mm relative to other conditions where the M/E is not running,
- Hull Deformations are **not** zero,
- Applied tail shaft slope boring is equal to 0.5585 mrad,
- The propeller and parts of the propeller shaft are immersed in water. Thus their weight is partially supported by the bearings and the water.

Bearing	Reactions (N)	Mean Pressure (Pa)	Longitudinal Shifts (mm)	Total Offsets (m)	Initial Offsets (m)	Hull Deform. (m)	Support Elastic Deform. (m)	Film Thickness (m)
Aft S/T	1.017E+06	6.75E+05	-44.98	-1.45E-04	-6.00E-05	0.00E+00	-2.54E-04	1.69E-04
Fore S/T	1.860E+05	5.05E+05	28.26	6.42E-05	0.00E+00	0.00E+00	-3.72E-05	1.01E-04
I/M	1.234E+03	2.16E+03	61.8	-3.57E-03	-2.95E-03	-3.29E-04	-1.23E-06	-2.88E-04
M/E 1	3.001E+05	1.04E+06	15.02	-6.42E-03	-4.81E-03	-1.62E-03	-5.00E-05	5.87E-05
M/E 2	2.798E+05	9.71E+05	14.89	-6.69E-03	-4.81E-03	-1.89E-03	-4.66E-05	6.19E-05
M/E 3	3.608E+05	1.25E+06	19.65	-7.13E-03	-4.81E-03	-2.30E-03	-6.01E-05	4.17E-05
M/E 4	3.840E+05	1.33E+06	17.84	-7.55E-03	-4.81E-03	-2.72E-03	-6.40E-05	4.11E-05
M/E 5	1.633E+05	5.67E+05	6.16	-7.89E-03	-4.81E-03	-3.13E-03	-2.72E-05	8.39E-05

TABLE 5-17: L.C. 26 ANALYSIS BREAKDOWN

Maximum permissible mean pressure:

- The limit is 0.8 MPa for the Aft Stern tube bearing and the value observed is 0.675 MPa,
- The limit is 1.2 MPa for the fore Stern tube bearing and the value observed is 0.505 MPa,
- The limit is 0.8 MPa for the I/M shaft bearing and the value observed is 0.002 MPa,
- No crankshaft bearing mean pressure value exceeds 3 MPa.

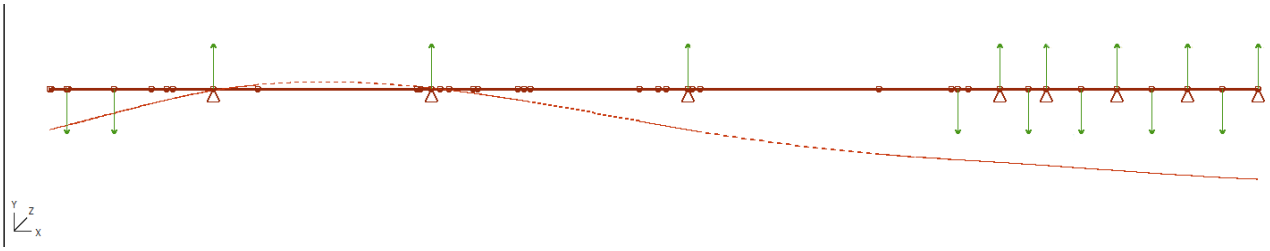

FIGURE 5.28: LOADING CONDITION NO. 26 SHAFT ALIGNMENT

Loading condition No. 34 [Suez Canal Condition]

The following considerations have been made for the calculation presented in this section:

- The M/E is running at 66.6 RPM,
- The M/E is in hot condition and M/E bearings are offset by an additional 0.29 mm relative to other conditions where the M/E is not running,
- Hull Deformations are not zero,
- Applied tail shaft slope boring is equal to 0.5585 mrad,
- The propeller and parts of the propeller shaft are immersed in water. Thus their weight is partially supported by the bearings and the water.

Bearing	Reactions (N)	Mean Pressure (Pa)	Longitudinal Shifts (mm)	Total Offsets (m)	Initial Offsets (m)	Hull Deform. (m)	Support Elastic Deform. (m)	Film Thickness (m)
Aft S/T	1.078E+06	7.15E+05	-38.08	-1.68E-04	-6.00E-05	0.00E+00	-2.69E-04	1.61E-04
Fore S/T	7.250E+04	1.97E+05	8.27	1.44E-04	0.00E+00	0.00E+00	-1.45E-05	1.59E-04
I/M	6.461E+04	1.13E+05	25.14	-2.07E-03	-2.95E-03	8.24E-04	-6.46E-05	1.23E-04
M/E 1	2.480E+05	8.61E+05	-6.98	-2.61E-03	-4.81E-03	2.17E-03	-4.13E-05	6.98E-05
M/E 2	2.874E+05	9.98E+05	-7.60	-2.48E-03	-4.81E-03	2.31E-03	-4.79E-05	6.56E-05
M/E 3	3.807E+05	1.32E+06	-9.50	-2.29E-03	-4.81E-03	2.53E-03	-6.35E-05	5.84E-05
M/E 4	3.992E+05	1.39E+06	-11.66	-2.07E-03	-4.81E-03	2.75E-03	-6.65E-05	5.84E-05
M/E 5	1.609E+05	5.58E+05	-8.65	-1.79E-03	-4.81E-03	2.96E-03	-2.68E-05	8.35E-05

TABLE 5-18: L.C. 34 ANALYSIS BREAKDOWN

Maximum permissible mean pressure:

- The limit is 0.8 MPa for the Aft Stern tube bearing and the value observed is 0.715 MPa,
- The limit is 1.2 MPa for the fore Stern tube bearing and the value observed is 0.197 MPa,
- The limit is 0.8 MPa for the I/M shaft bearing and the value observed is 0.113 MPa,
- No crankshaft bearing mean pressure value exceeds 3 MPa.

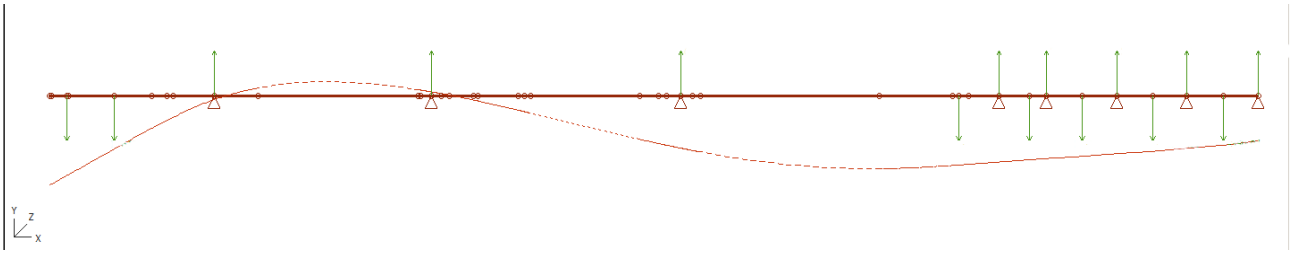

FIGURE 5.29: LOADING CONDITION NO. 34 SHAFT ALIGNMENT

5.2.5. Effects on Bearing Lubrication Characteristics

Having solved the coupled problem, presented in previous sections, for pressure, shear stress and other important quantities, we can estimate how good or problematic bearing operation will be under different vessel loading conditions.

In most loading conditions, the lubricant domain solutions of the eight bearings modelled in the present work, do not raise any alarm concerning wear and malfunction, although acute misalignment in some loading conditions might be encountered.

Misalignment issues

In **Figure 5.30**, pressure, shear stress and a 3D representation of oil film thickness are plotted for the fore S/T bearing, under L.C. no. 11. Even in this short bearing, the effects of misalignment are important. Such extreme misalignment values may lead to accelerated bushing surface wear and shortening of bearing life span. For this loading case even the four aft-most crankshaft bearings are heavily misaligned (**Figure 5.31**), which is generally unacceptable and leads to bad M/E operation.

Another measure of how great bearing misalignment can become, is the longitudinal shift of support points. For the cases presented in **Figures 5.30 and 5.31**, the fore S/T bearing support point has shifted by 46.65 mm, while the fourth M/E bearing support point has shifted by 35.97 mm. By contrast, the average values of longitudinal shift, across all L.Cs., for these two bearings are 17.49 mm and 6.50 mm respectively.

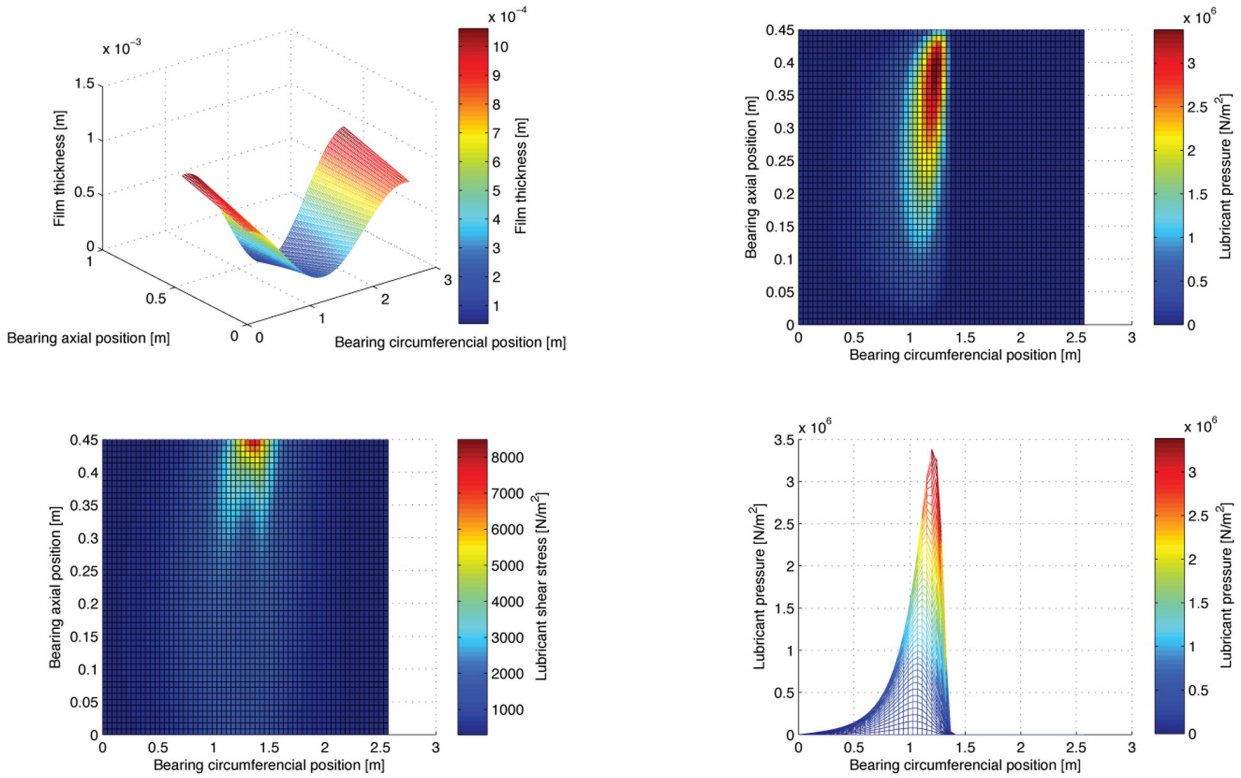

FIGURE 5.30: L.C. 11; FORE S/T BEARING FILM THICKNESS, PRESSURE AND SHEAR STRESS DISTRIBUTIONS

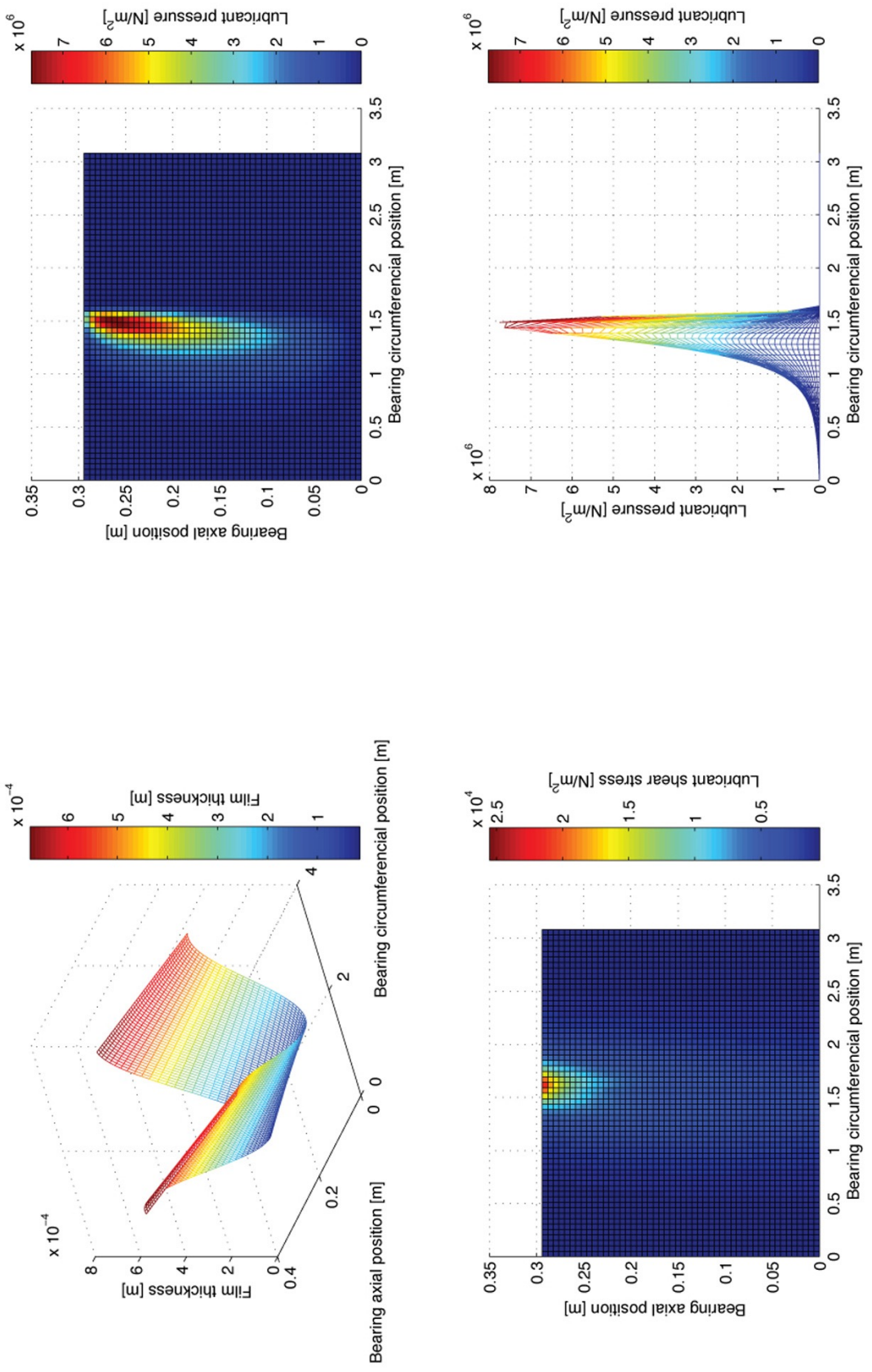

FIGURE 5.31: L.C. 11, CRANKSHAFT BEARING NO. 4; FILM THICKNESS, PRESSURE AND SHEAR STRESS DISTRIBUTIONS

Lightly Loaded Bearings

All loading conditions examined within the scope of this work exhibit a common characteristic: the I/M shaft bearing is very lightly loaded. This is true for even the reference condition. However, bearing load decreases even further as a set of various hull deformations is added to the initial offsets. Arguably, the source of this problem is the choice of reference condition vertical offsets. Despite the many problems and shortcomings that this reference condition has, it can exhibit such issues and help investigate the way they propagate, or change, into all the other loading conditions.

The effects of a very small reaction force on a bearing that was designed to support much greater loadings, can be evaluated by studying **Figures 5.32** and **5.33**. For L.C. 21, the I/M shaft bearing reaction force is equal to 54 kN, while the force of the same bearing in L.C. 26 is even smaller at 1.23 kN. In the latter case, the shaft is practically floating inside the bushing.

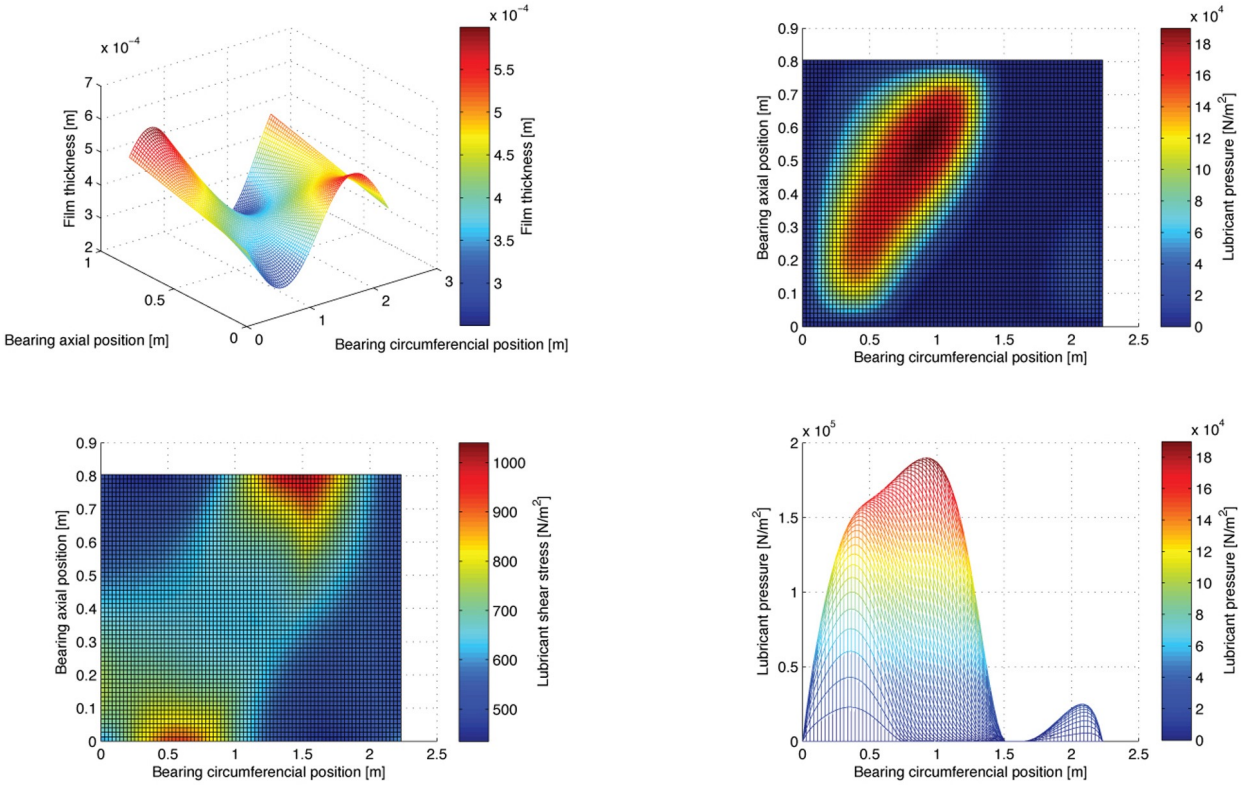

FIGURE 5.32: L.C. 21, I/M SHAFT BEARING; FILM THICKNESS, PRESSURE AND SHEAR STRESS DISTRIBUTIONS

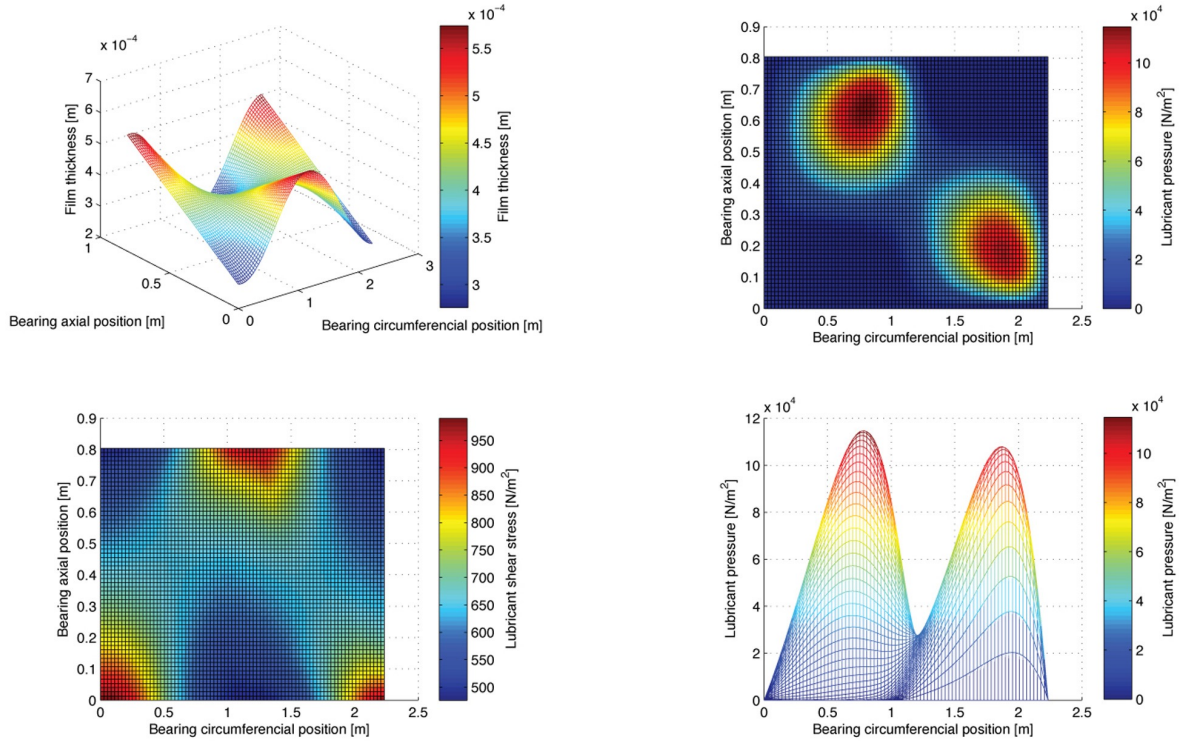

FIGURE 5.33: L.C. 26, I/M SHAFT BEARING; FILM THICKNESS, PRESSURE AND SHEAR STRESS DISTRIBUTIONS

Maximum Pressure Values

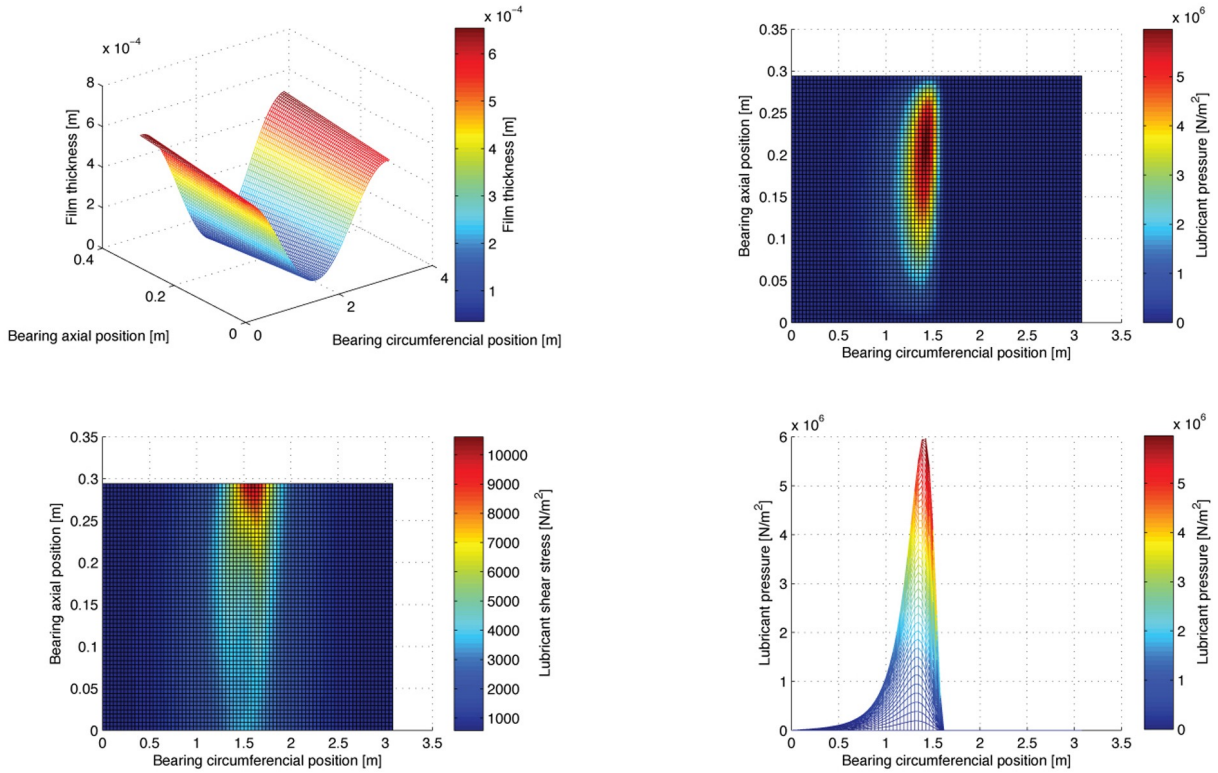

FIGURE 5.34: L.C. 08; 4TH CRANKSHAFT BEARING, FILM THICKNESS, PRESSURE AND SHEAR STRESS DISTRIBUTIONS

With regards to shaft alignment calculations, the approach followed in the present study allows the designer of any such system to evaluate the maxima of a number of parameters. One key aspect in the process of estimating the life span of a journal bearing, is the maximum pressure value developed during its operation. **Figure 5.34** illustrates, in the bottom right section, the local pressure values of a crankshaft bearing for L.C. 08. Local pressure, according to this diagram, peaks at, roughly, 6 MPa. This Figure is almost twice the maximum allowed mean pressure prescribed in the manufacturer's manual (3 MPa). In this respect, all maximum pressure values can and should be checked against the values provided by the bearing manufacturer to ensure trouble free operation of the shafting system.

5.3. Comparison of Shaft Alignment Calculation Methods

5.3.1. Elastic .vs. Non-Elastic Support

As explained in detail in section 4.3.3, shafting system support points can be modelled in many different ways. Should the choice be made to incorporate bearing hydrodynamic lubrication simulations into the calculation process, the only modelling option left is whether the bearings' foundations will be able to deform elastically or not. Using the reference condition described in **section 5.2.3**, a comparison between these two solution methods can can be made. The results can be found in **Table 5-19**. For the exact same operating conditions and vertical offsets, the deference between the two are substantial.

The most obvious point is that, for the non-elastic support modelling, this shafting arrangement is not even an acceptable solution, as the first M/E bearing is severely negatively loaded. Apart form that, most bearings situated close to the first M/E bearing are also influenced by this extreme difference and their reactions display the largest amount of deviation from the ones calculated through the elastic support model.

Although it could be argued that the reference condition presented, in this work, is not the optimal choice, it has the capacity to expose this situation of extreme contrast. This contrast also leads to another conclusion about whether this approximation of elastic bearing foundations is necessary. The stark difference between the two options, even if it concerns a small number of cases, fully justifies the use of this type of modelling.

	Aft S/T	Fore S/T	I/M	M/E 1	M/E 2	M/E 3	M/E 4	M/E 5
Elastic Support	1.06E+06	1.19E+05	7.15E+04	1.61E+05	3.15E+05	4.20E+05	3.98E+05	1.58E+05
NON Elastic Support	1.09E+06	3.96E+04	1.91E+05	-4.39E+05	9.58E+05	2.96E+05	4.17E+05	1.48E+05
Diff. %	2.83%	66.67%	166.59%	372.29%	204.36%	29.43%	4.66%	6.09%

TABLE 5-19: COMPARISON OF SUPPORT MODELLING METHODS

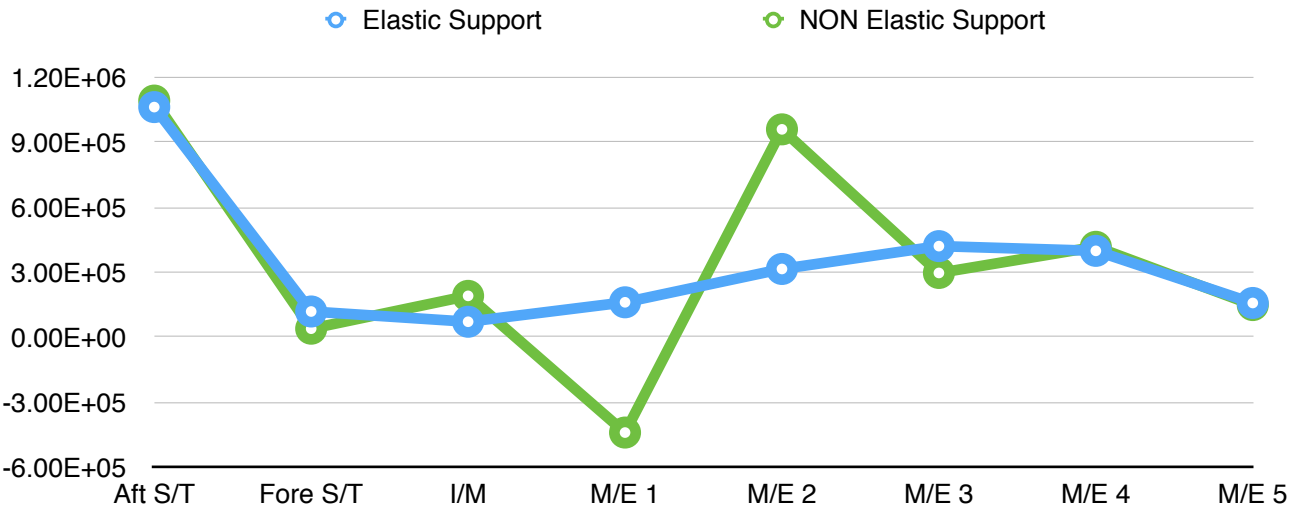

FIGURE 5.35: ELASTIC VERSUS NON-ELASTIC SUPPORT COMPARISON

5.3.2. Bearing Estimates .vs. Full Solution Process

The solution algorithm described in previous sections indicates that, for any given bearing reaction force, most of the hydrodynamic lubrication parameters can be found using only a pair of estimates for eccentricity and attitude angle values. In the full solution process, the program will make use of the estimates to narrow down the range of values it needs to look through and try, in order to achieve an equilibrium of internal and external forces. In this type of solution, the estimates are used directly without any other process, or, optionally, they can be used to calculate all lubricant domain variables.

This type of solution has significant advantages regarding the amount of time it requires, compared to the full solution process. A reduction factor with a minimum value of three times is achieved in most cases.

	Aft S/T	Fore S/T	I/M	M/E 1	M/E 2	M/E 3	M/E 4	M/E 5
Estimates	1.06E+06	1.18E+05	7.33E+04	1.58E+05	3.15E+05	4.21E+05	3.98E+05	1.58E+05
Full Solution	1.06E+06	1.19E+05	7.15E+04	1.61E+05	3.15E+05	4.20E+05	3.98E+05	1.58E+05
Diff. %	0.00%	1.06%	2.34%	1.73%	0.27%	0.28%	0.01%	0.11%

TABLE 5-20: REFERENCE CONDITION; EFFECT OF BEARING SOLUTION TYPE ON REACTION FORCES

As for differences in the results obtained from each method, **Table 5-20**, summarises the reaction forces obtained in both cases, using the reference condition described in **section 5.2.3**. The estimates in this case were taken in 0.5% increments on the eccentricity values. The maximum difference value of 2.39% indicates that this method is good enough for most calculations.

Additionally, the precision of this method can be augmented by using a smaller increment value for the production of these estimates and thus, obtaining a more dense table of data. This way the difference between the estimated e and φ values and the actual ones will be smaller and the need to search for a closer match could be completely eliminated.

5.4. Power Loss Estimation

The full solution of the hydrodynamic lubrication problem for each bearing allows for power loss estimates to be drawn. Friction forces develop in the lubricant domain and are calculated though equation EQ.3-6. From that point the normalised friction coefficient is calculated as the ratio of total friction force to the total hydrodynamic load. Finally friction torque and friction power loss can be estimated using the above results. In this section, a series of diagrams is provided, depicting the levels of normalised friction coefficients, friction forces, friction torque and friction power losses, for each bearing under every loading condition considered in this work.

Validation for the calculations presented in this section is provided by comparison of this work's results with examples of friction power loss calculations, existing in recent literature [15]. **Figure 5.36** illustrates how closely, the calculation model employed in this study, matches the results provided in a test case by Roldo et. al [15].

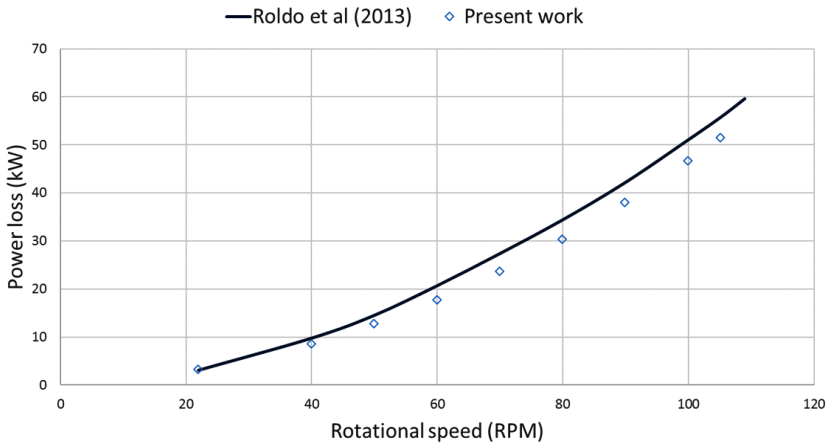

FIGURE 5.36: VALIDATION OF FRICTION POWER LOSS CALCULATION; THE CASE OF ROLDO ET. ALL

Loading condition No. 04

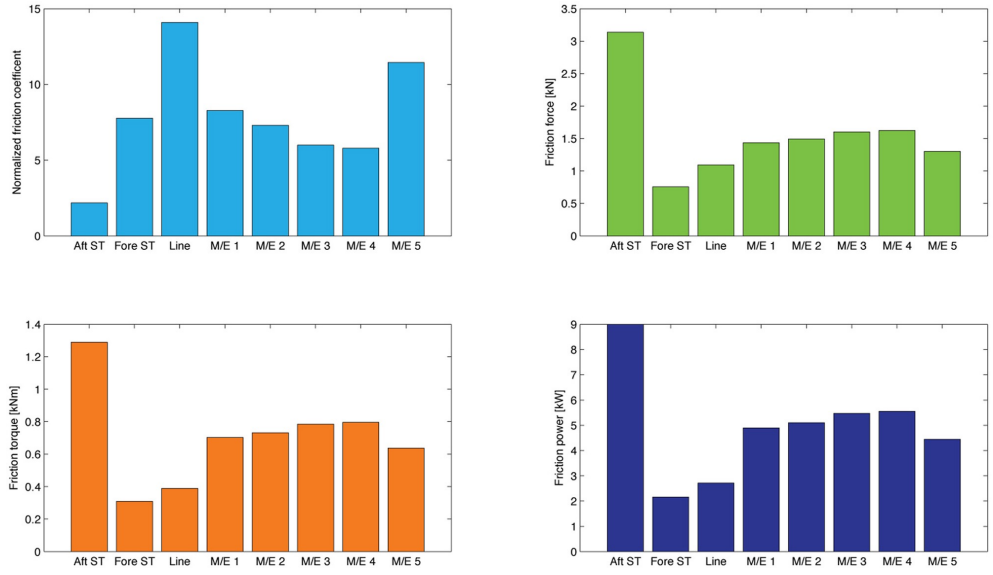

FIGURE 5.37: L.C. 04 FRICTION COEFFICIENT, FRICTION FORCE, FRICTION TORQUE AND FRICTION POWER LOSS FOR EACH BEARING

Loading condition No. 08

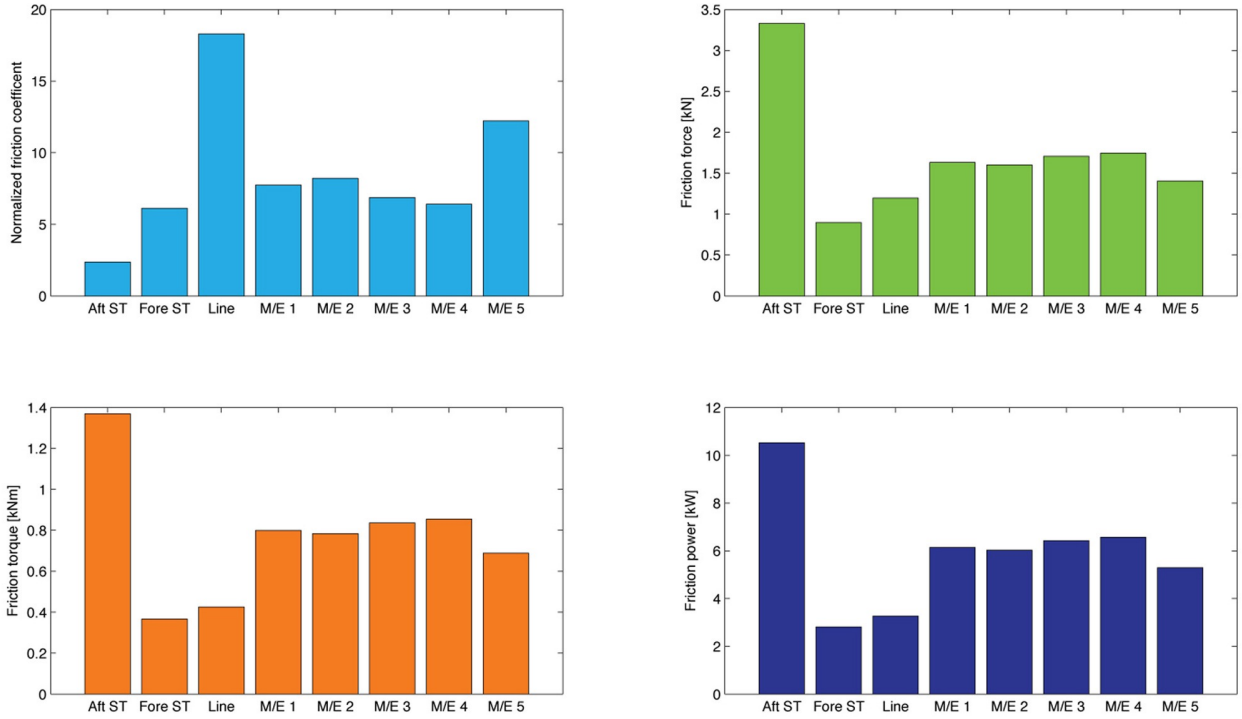

FIGURE 5.38: L.C. 08 FRICTION COEFFICIENT, FRICTION FORCE, FRICTION TORQUE AND FRICTION POWER LOSS FOR EACH BEARING

Loading condition No. 11

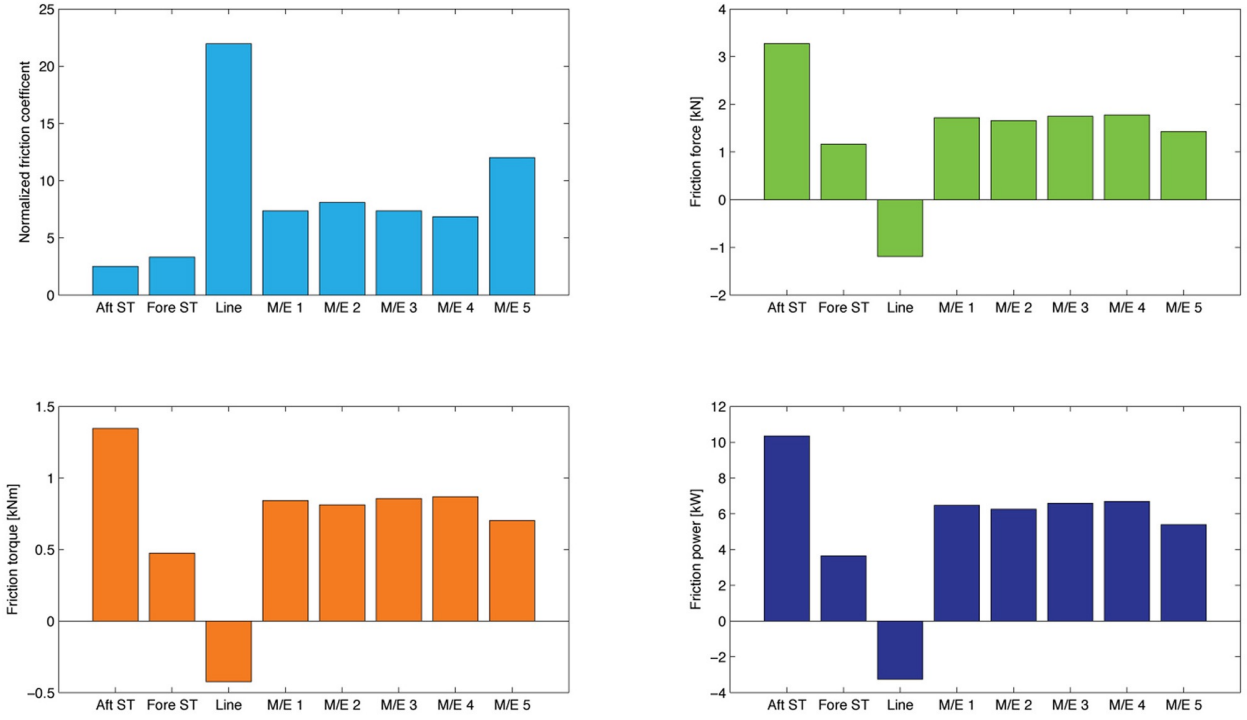

FIGURE 5.39: L.C. 11 FRICTION COEFFICIENT, FRICTION FORCE, FRICTION TORQUE AND FRICTION POWER LOSS FOR EACH BEARING

Loading condition No. 14

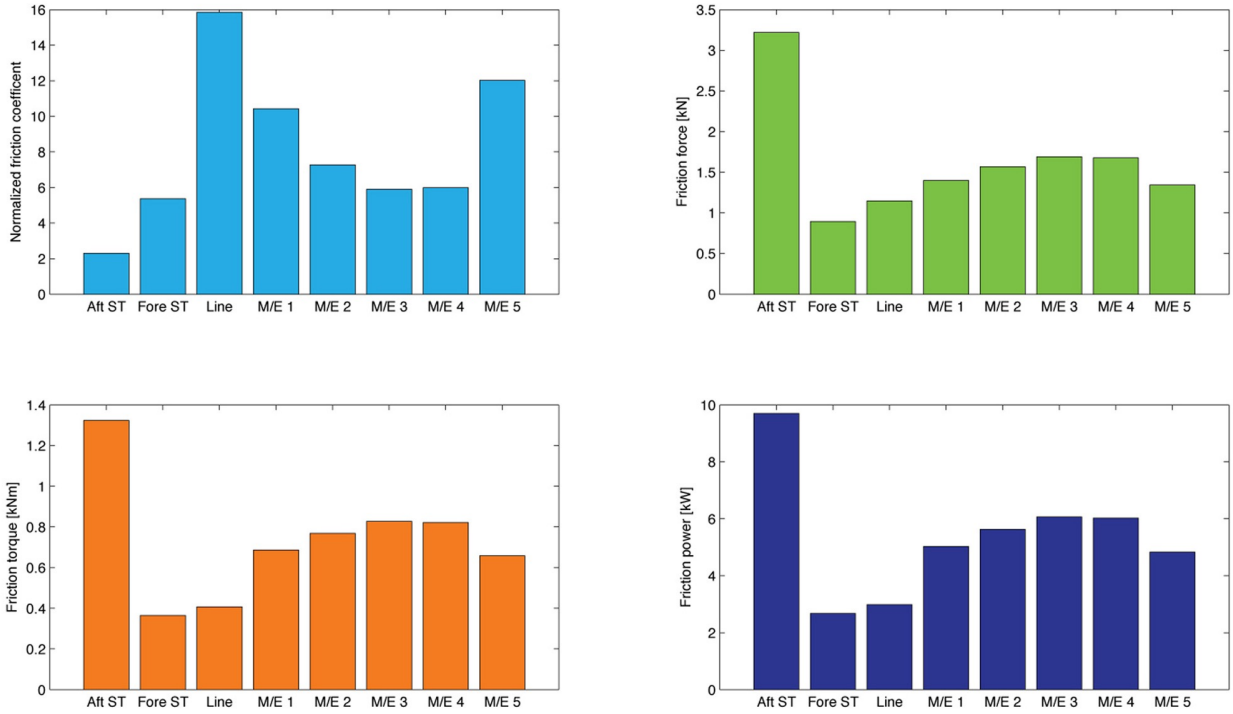

FIGURE 5.40: L.C. 14 FRICTION COEFFICIENT, FRICTION FORCE, FRICTION TORQUE AND FRICTION POWER LOSS FOR EACH BEARING

Loading condition No. 21

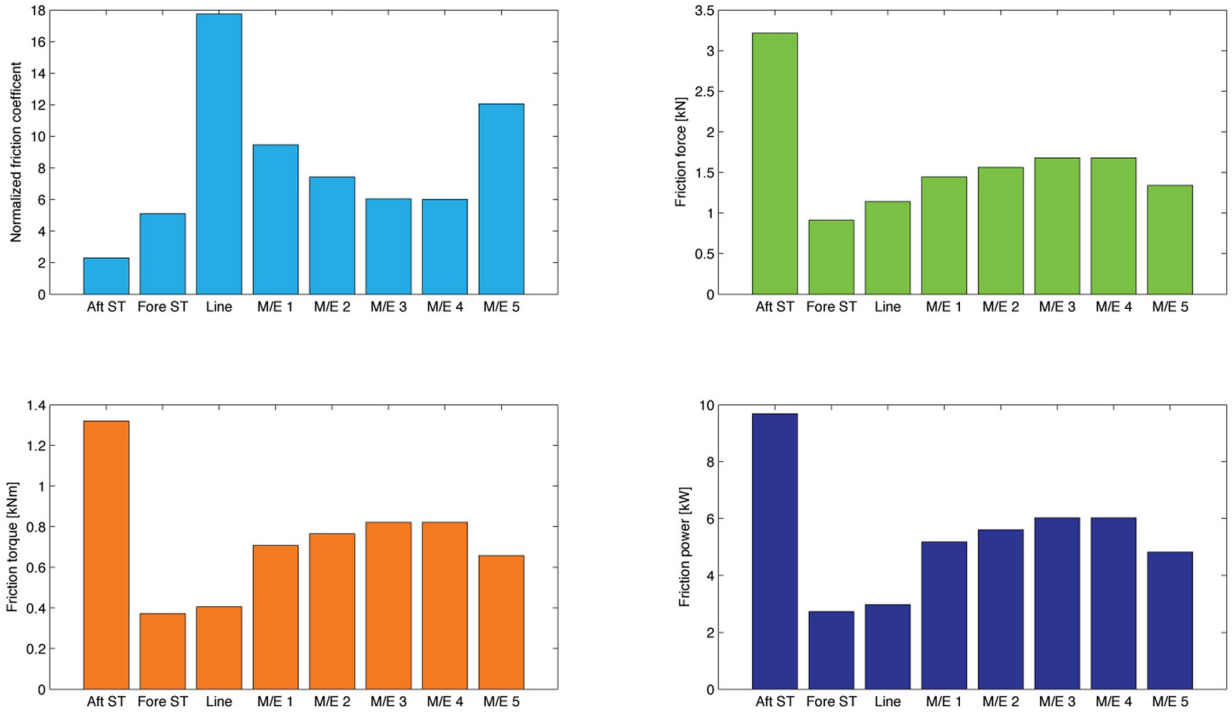

FIGURE 5.41: L.C. 21 FRICTION COEFFICIENT, FRICTION FORCE, FRICTION TORQUE AND FRICTION POWER LOSS FOR EACH BEARING

Loading condition No. 23

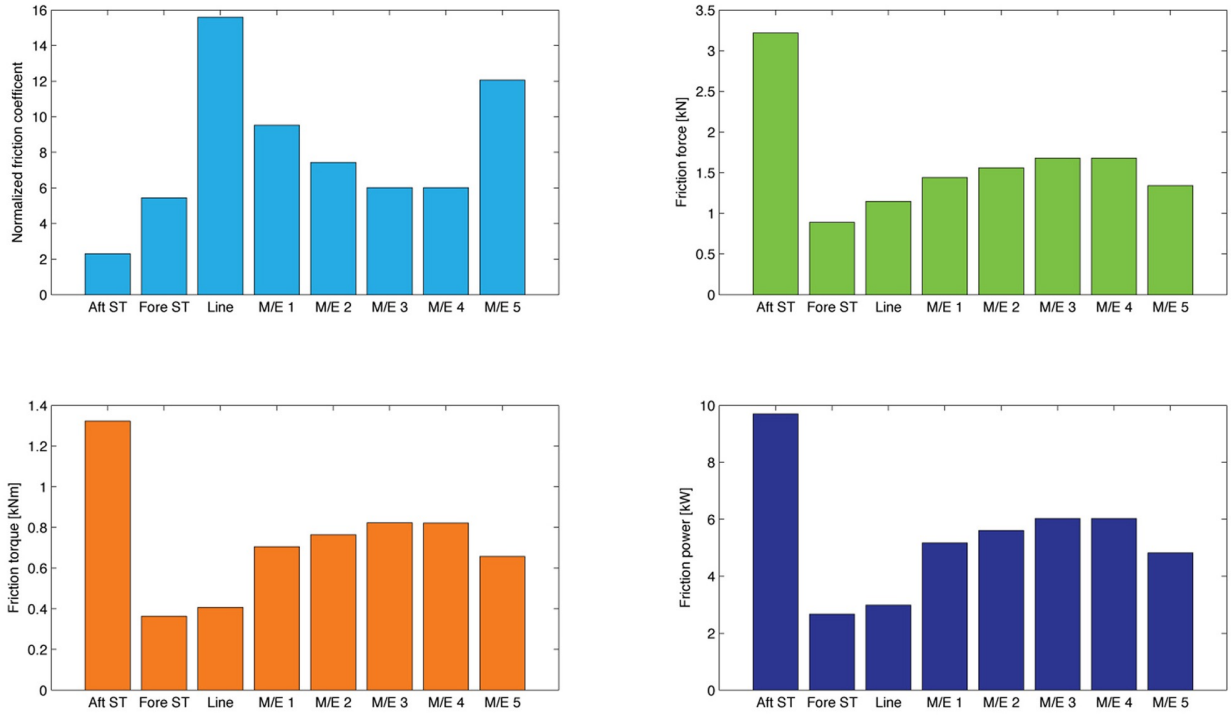

FIGURE 5.42: L.C. 23 FRICTION COEFFICIENT, FRICTION FORCE, FRICTION TORQUE AND FRICTION POWER LOSS FOR EACH BEARING

Loading condition No. 26

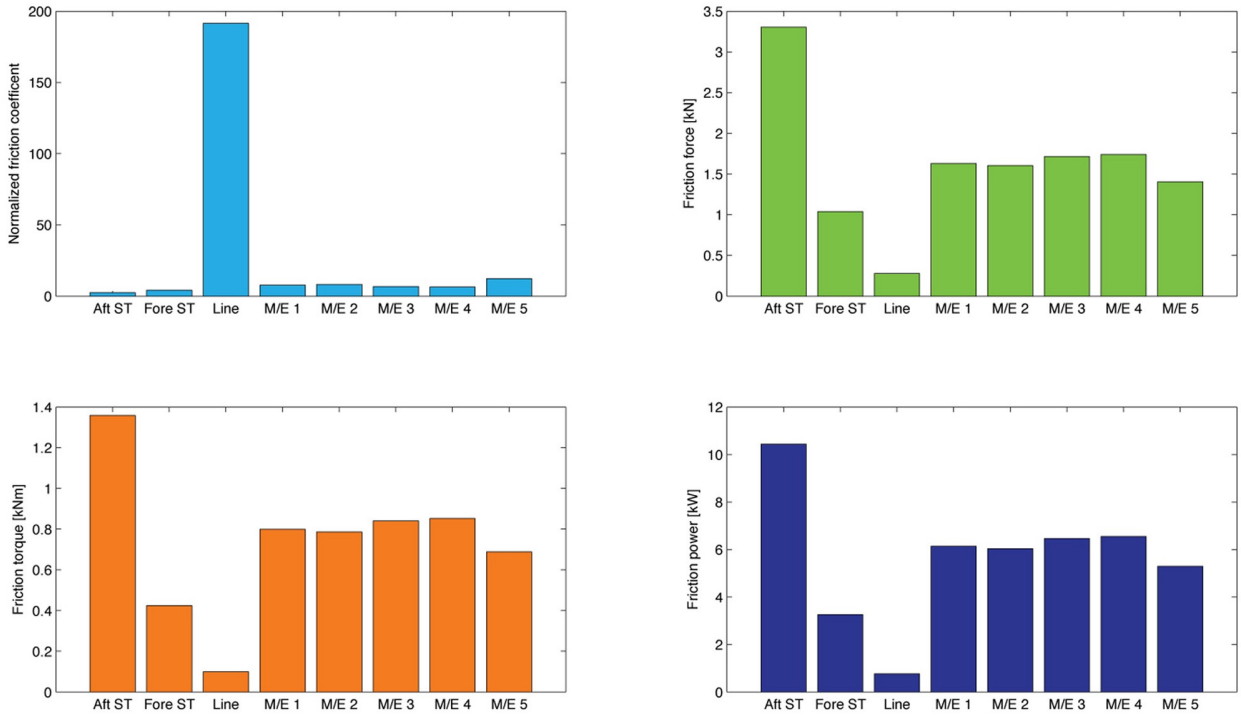

FIGURE 5.43: L.C. 26 FRICTION COEFFICIENT, FRICTION FORCE, FRICTION TORQUE AND FRICTION POWER LOSS FOR EACH BEARING

Loading condition No. 34

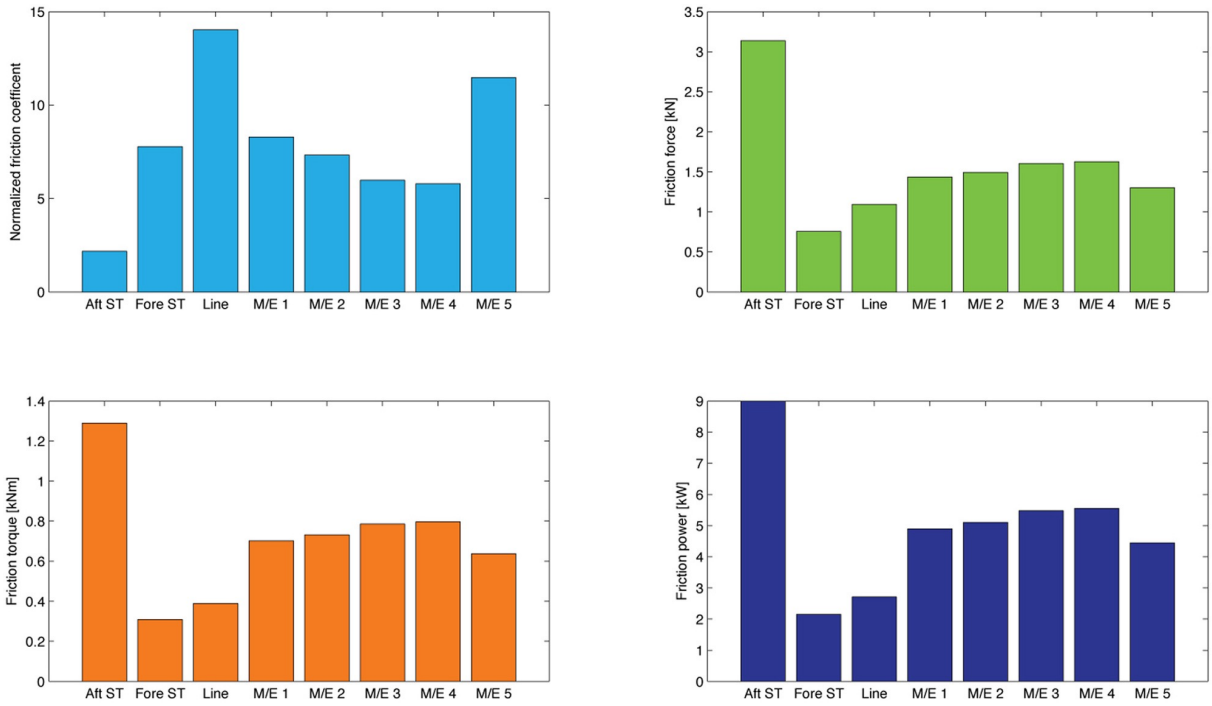

FIGURE 5.44: L.C. 34 FRICTION COEFFICIENT, FRICTION FORCE, FRICTION TORQUE AND FRICTION POWER LOSS FOR EACH BEARING

Concluding Remarks

The figure most widely believed to accurately represent shafting power losses is 0.5 ~ 1% of the M/E's BHP at M.C.R. This is an estimate very commonly found in literature. It is important to note, here, that "shafting power losses" includes only the intermediate shaft and propeller shaft bearings. With these two considerations in mind, it is quite evident that the results presented, in this section, openly contradict that long-held belief. **Table 5-21** summarises the results displayed above and the percentage of M.C.R. (29,404 kW) the three aft-mosts bearings consume. The maximum of 0.052% for L.Cs. 23, 21 and 14 is an order of magnitude smaller than the expected value of 0.5%.

	Aft S/T	Fore S/T	I/M	M/E 1	M/E 2	M/E 3	M/E 4	M/E 5	% OF BHP
L.C. 04	8.994	2.169	2.710	4.918	5.107	5.482	5.559	4.454	0.0470%
L.C. 08	10.480	3.095	0.907	6.431	5.955	6.325	6.565	5.308	0.0490%
L.C. 11	10.351	3.614	-3.252	6.432	6.258	6.609	6.682	5.392	0.0360%
L.C. 14	9.700	2.688	2.982	5.049	5.636	6.071	6.033	4.831	0.0520%
L.C. 21	9.689	2.720	2.978	5.191	5.609	6.035	6.040	4.821	0.0520%
L.C. 23	9.698	2.673	2.985	5.182	5.615	6.034	6.035	4.824	0.0520%
L.C. 26	10.438	3.264	0.487	6.149	6.040	6.470	6.559	5.296	0.0480%
L.C. 34	8.994	2.168	2.710	4.916	5.102	5.487	5.561	4.452	0.0470%

TABLE 5-21: POWER LOSS PER LOADING CONDITION AND BEARING IN KW

5.5. Parametric Analysis: Viscosity

Added value for the method used in this work for shaft alignment calculations comes from its ability to allow the designer to explore the influence that each and every parameter has on any given shafting system. In this section, an analysis of the effects that lubricant viscosity may have, on a pre-conceived shafting plan, are explored, using loading condition no. 8 described in **section 5.2.4**. The two main output variables examined,here, are friction power loss and reaction forces.

kW	μ = 0.08	μ = 0.1	μ = 0.12	μ = 0.15	μ = 0.2	μ = 0.25	μ = 0.3
Aft S/T	9.07	10.48	11.99	14.32	18.33	22.45	26.62
Fore S/T	2.37	3.10	3.54	4.19	5.23	6.27	7.00
I/M	2.64	0.91	0.39	0.15	0.11	0.00	9.69
M/E 1	5.20	6.43	7.37	8.72	10.87	12.94	14.56
M/E 2	5.14	5.96	6.80	8.05	10.05	11.99	14.01
M/E 3	5.48	6.33	7.24	8.57	10.68	12.71	14.85
M/E 4	5.59	6.57	7.51	8.89	11.07	13.18	15.23
M/E 5	4.46	5.31	6.12	7.30	9.21	11.07	12.90

TABLE 5-22: POWER LOSS IN KW FOR VARIOUS VALUES OF VISCOSITY

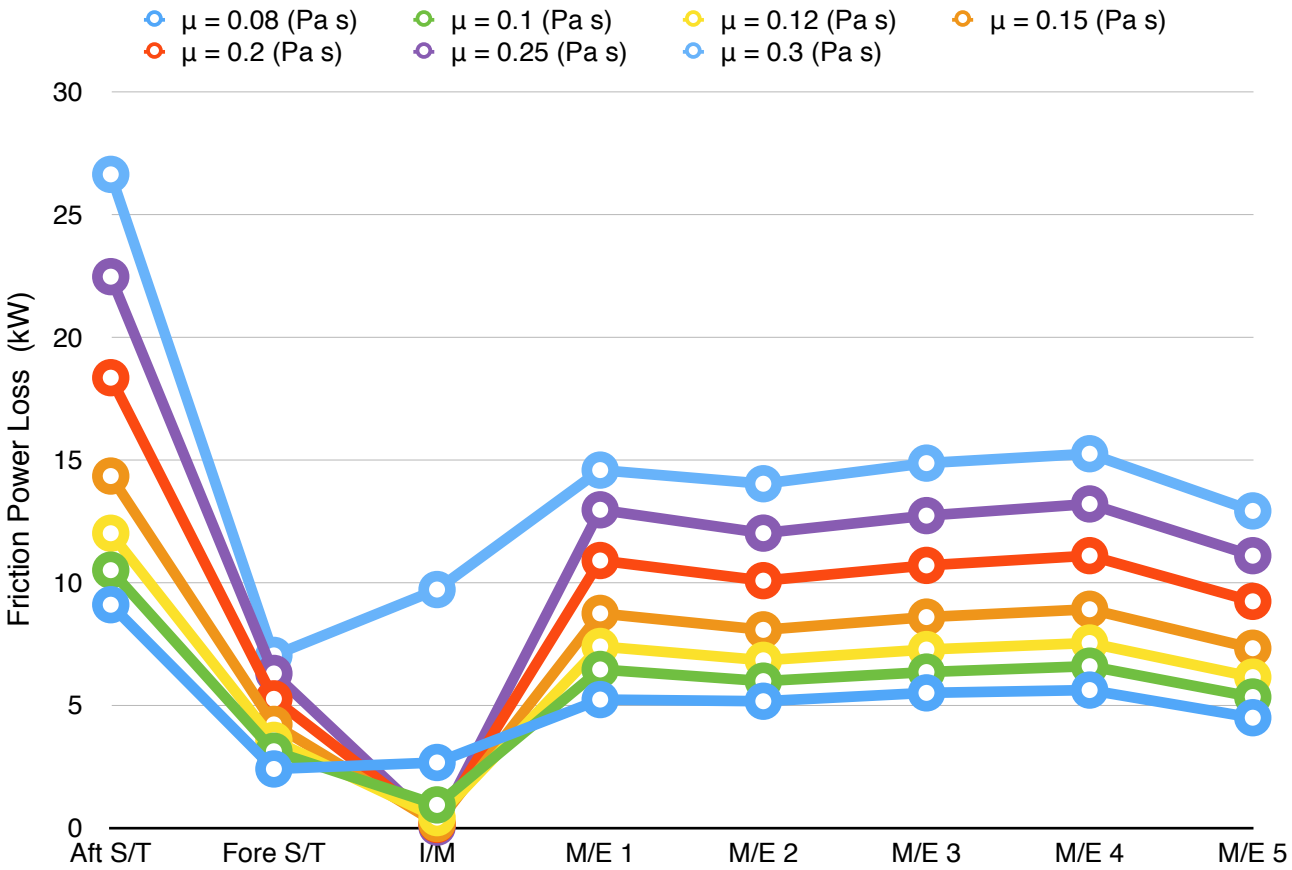

FIGURE 5.45: FRICTION POWER CONSUMPTION PER BEARING FOR VARIOUS LUBRICANT VISCOSITY VALUES

N	μ = 0.08	μ = 0.1	μ = 0.12	μ = 0.15	μ = 0.2	μ = 0.25	μ = 0.3
Aft S/T	1.05E+06	1.05E+06	1.03E+06	1.03E+06	1.03E+06	1.03E+06	1.04E+06
Fore S/T	1.07E+05	1.09E+05	1.56E+05	1.57E+05	1.56E+05	1.57E+05	1.23E+05
I/M	5.79E+04	5.42E+04	6.33E+02	2.44E+02	1.92E+02	3.41E+01	4.00E+04
M/E 1	2.96E+05	2.99E+05	3.60E+05	3.62E+05	3.64E+05	3.68E+05	3.21E+05
M/E 2	2.81E+05	2.78E+05	2.61E+05	2.57E+05	2.52E+05	2.46E+05	2.60E+05
M/E 3	3.52E+05	3.52E+05	3.31E+05	3.32E+05	3.32E+05	3.33E+05	3.49E+05
M/E 4	3.84E+05	3.86E+05	3.85E+05	3.88E+05	3.91E+05	3.94E+05	3.98E+05
M/E 5	1.64E+05	1.63E+05	1.64E+05	1.63E+05	1.62E+05	1.61E+05	1.58E+05

TABLE 5-23: REACTION FORCES IN N FOR VARIOUS VALUES OF VISCOSITY

Figure 5.43 and the data on **Table 5-22** suggest that the maximum friction power loss amounts to 0.147% of the M/E's break horse power (BHP) at M.C.R. (29,404 kW), for μ=0.3 Pa s. This figure is still, roughly, five times smaller than the lowest estimate of 0.5% for friction power loss found in literature. Additionally, as viscosity values get bigger, an increase in friction power consumption can be observed, as expected, in most cases. The intermediate shaft bearing stands as an outlier. This bearing does not follow the observed trend of increasing power consumption, and its behaviour changes randomly across the board.

The I/M bearing's behaviour cannot be explained by analysing the power consumption data only. An examination of **Table 5-22** in conjunction with the data provided on **Table 5-23** reveals that the change in power loss can be attributed to a corresponding change in the bearing reaction force. This in turn can be justified if the static solution of this multi-supported beam, that represents the shafting system, is considered. All other things being constant, a slight upward offset of any given bearing will usually result in an increase, or decrease, of its reaction force. Similarly, this difference in load will have to be subtracted from the rest of the support points. Most of the time, the bearings that are closer, lengthwise, to the one that was vertically offset, have to absorb this change.

In this particular example, the I/M bearing is influenced by the changing offsets of its surrounding bearings that rose higher as the film thickness value in these bearings increased along with viscosity values. The load difference between maximum and minimum load, for the I/M bearing, is close to 98.6%, where as for the fore S/T bearing and the first M/E bearing, the figures are 56.58% and 52.95 % respectively.

6. Conclusions and suggestions for future work

6.1.Conclusions

In the present work, an extensive study of shaft alignment in a typical VLCC vessel has been conducted. The propulsion shaft of the ship has been modelled as a statically indeterminate, multi-supported beam and solved using matrix analysis. To account for hull deformations, a detailed finite element model of the hull structure of the ship has been generated, characterised by a very fine mesh at the engine room region of the ship. For normal ship operation, the bearing lubricant film and the stiffness of the bearing foundation have been taken into account.

First, considering the non-deformed (even-keel) hull of the vessel, a reference shaft alignment plan has been assumed, and a pseudo-dynamic equilibrium of the shaft has been calculated, yielding the reaction forces at the shaft bearings. Next, nine representative loading conditions of the vessel, corresponding to full-load, partial load and ballast conditions have been simulated. The corresponding hull deflections have been computed, the offset of the bearings due to hull deflections have been determined, and the bearing reaction forces have been calculated.

The results demonstrate that, in general, the differences in bearing reaction forces at different loading conditions are not very pronounced. At the aft stern tube bearing, reaction force exhibits a maximum deviation of approximately 7.8%. Bearing 4 (aft engine bearing) exhibits the most pronounced deviations in reaction forces and tends to be lightly loaded following a rule of thumb used by shipbuilding yards. The results of the present study mostly support, for this specific case and vessel, the conclusions drawn by other researchers in the recent literature, that an appropriate even-keel shaft alignment plan exhibits reasonably good performance at other loading conditions of the vessel. However, the possibility of having one of the system bearings negatively loaded still exists and it is advised that anyone tasked with the design of such a system should consider all or most of the parameters described in this study.

The detailed calculation of bearing lubrication characteristics allows us to gain deeper insight into how bearings perform under real-life conditions. Additionally, estimates can be made for various operational parameters of the system such as wear, and friction, which carries some importance with regard to performance-oriented design. The results presented in the present work have been extended to the detailed calculation of friction power losses along the shafting system and aid in the discovery of a balance between designs that favour minimal bearing wear and designs that optimise for minimal power losses. The figures presented in this study have not yet been verified through an experimental process, but so far appear to deviate from most estimates made up to date. For the assumed design and operational parameters, maximum power shafting losses were found to be approximately ten times smaller than the common used estimate of 0.5% of the main engine BHP at M.C.R.

Finally, a parametric study of system power losses and reaction forces, has been made, with viscosity as the independent variable. The shafting system behaves as expected with total friction power consumption increasing when more viscous lubricants are employed, followed by an increase of lubricant film thickness, which may lead to decreased values of bearing wear rates.

6.2. Suggestions for Future Work

The modelling concept, for ship shafting systems, proposed in the present work, opens up the path to many additional improvements on the shaft alignment calculation process. The software developed in the scope of this study can be further improved to accommodate more functionalities that will make an even better approximation of the actual system possible.

6.2.1. Bearing Clearance Modelled as Gap

For this study, bearing clearance is considered as a parameter only when the shaft is rotating and the bearing is in “running” condition. The actual assembly and alignment of the shafting system takes place with a cold M/E and non-rotating shaft. In this respect, a functionality that emulates bearing clearance as a gap with contact conditions would be very helpful to the implementation and validation of any given shaft alignment plan. The suggested algorithms for this type of modelling have, already, been included in FE modelling software, but can also be integrated to the existing matrix analysis code.

6.2.2. Output of SAG and GAP Values - Temporary Support Inclusion - Inverse Problem Solution

In conjunction with the “clearance as gap” modelling suggested above, the calculations required for the implementation of a shaft alignment plan can be further simplified if the desired SAG and GAP values of each decoupled shaft could be output for every possible solution of the coupled shaft alignment problem. This functionality could be further enhanced by a provision for the inclusion of temporary support points during the coupling process.

Finally, some researchers have suggested that it would also be helpful to know, at any given moment, what the SAG and GAP values would be if the shafts of a system were decoupled for a number of reasons, such as inspection, or overhauling.

6.2.3. Optimisation of Shafting Plan

As described in the introduction, an optimisation process can be carried out for a number of shafting plan parameters:

- Minimum Bearing misalignment values,
- Better mean pressure values distribution amongst system bearings,
- Power loss minimisation,
- Minimisation of maximum lubricant pressure, and,
- Minimisation of shaft bending moments.

6.2.4. Shaft Bending Calculation within the Stern Tube Bearing - Required (Multi) Slope Boring Prediction

Some researchers have suggested that shaft bending inside a bearing, with a large Length-over-Diameter ratio, is large enough to justify the application of more than one boring angles. This mainly affects tailshaft bearings, that are heavily misaligned under the influence of propeller weight. To properly calculate the desired multi-slope boring values, a detailed calculation of the shaft bending within such bearings must be carried out, first.

A functionality that would carry out such calculations and help predict the required slope boring values for trouble free operation, under most loading conditions, would be a valuable addition to the research of shaft alignment issues.

7. Literature - References

[1] RAPTIS L., Software development for the solution of hydrodynamic lubrication problems in main bearings of marine Diesel engines, Diploma Thesis, National Technical University of Athens, School of Naval Architecture & Marine Engineering, Athens (March 2014)

[2] AMERICAN BUREAU OF SHIPPING –ABS, Guidance Notes on Propulsion Shafting Alignment, (2004)

[3] BUREAU VERITAS, Elastic Shaft Alignment (ESA), 2013.

[4] DAHLER G. et. al., A study on Flexible Hulls, Flexible Engines, Crank Shaft Deflections and Engine Bearing Loads for VLCC propulsion machinery, CIMAC Congress, Paper 48, Kyoto, 2004.

[5] DEVANNEY, J., KENNEDY, M., The down ratchet and the deterioration of tanker newbuilding standards, Center for Tankship Excellence, 2003.

[6] HUGHES, F.O., PAIK J.K. (2010), Ship structural analysis and design, SNAME.

[7] MURAWSKI L., Shaft Line Alignment Analysis Taking Ship Construction Flexibility and Deformations into Consideration, Marine Structures 18, pp. 62–84 2005.

[8] NIPPON KAIJI KYOKAI –NKK, Guidelines on Shafting Alignment 2006.

[9] SVERKO D., Design concerns in propulsion shafting alignment, ABS Technical Papers,2003.

[10] SVERKO D., A Solution to Robust Shaft Alignment Design, ABS Technical Papers, 2006.

[11] VOLCY G.C., Experience With Marine Engineering Systems Over The Last Thirty Years, BV Technical Paper, December 1983

[12] DET NORSKE VERITAS, Rotating Machinery, Power Transmission, January 2013.

[13] KORBETIS G.,VLACHOS O., CHARITOPOULOS A., PAPADOPOULOS C. I., Effects Of Hull Deformation On The Static Shaft Alignment Characteristics Of VLCCs: A Case Study Compit 2014, Redworth, U.K. MAY 2014.

[14] FRAGOPOULOS C. A., Ship Energy Systems, Volume C: Propulsion Shaft Alignment, Athens 2005 (in Greek).

[15] ROLDO L., KOMAR I., VULIĆ N., Design and Materials Selection for Environmentally Friendly Ship Propulsion System, Journal of Mechanical Engineering 59(2013), 25-31.

APPENDIX A

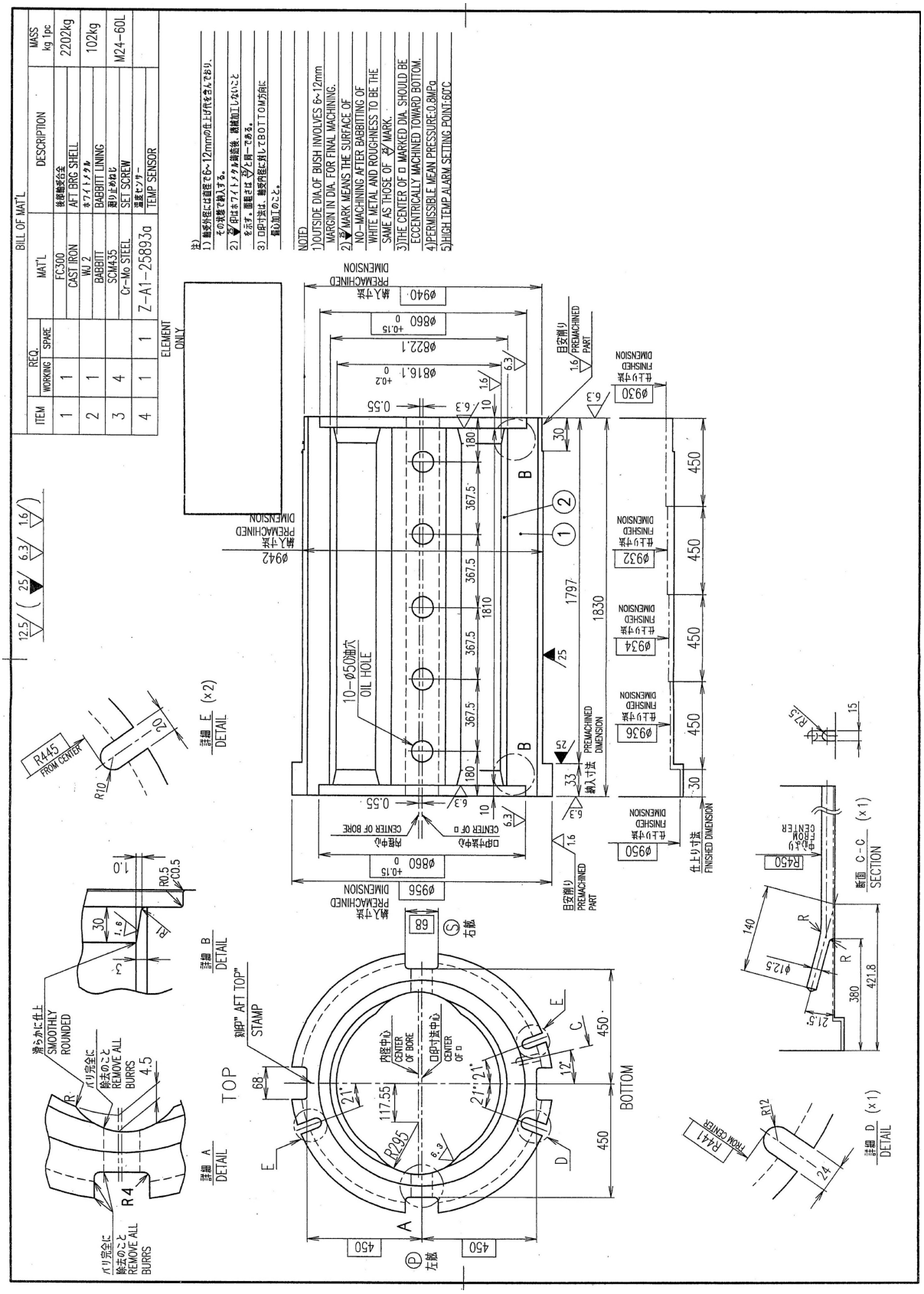

FIGURE A-1: AFT STERN TUBE BEARING DRAWING

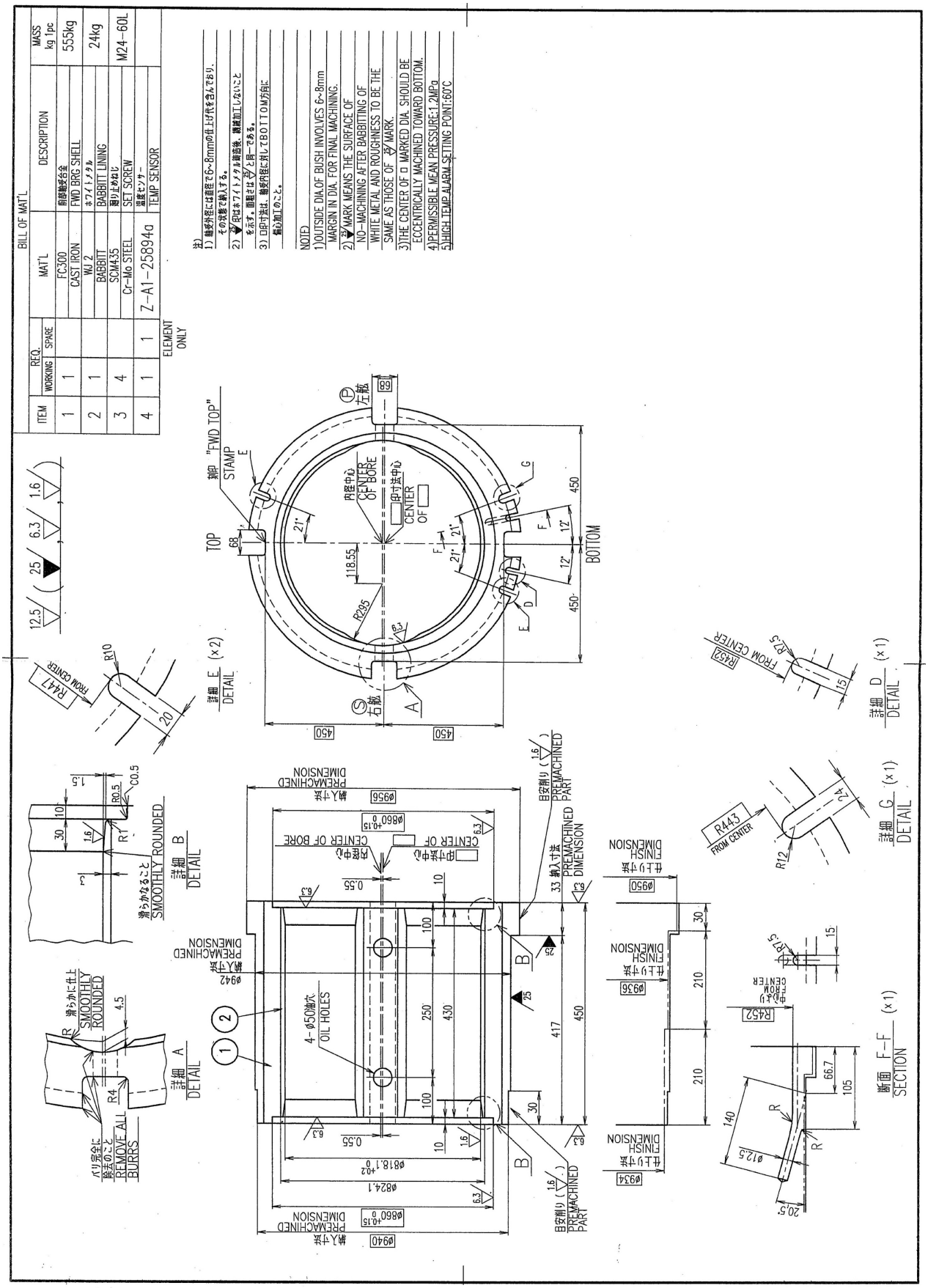

FIGURE A-2: FORE STERN TUBE BEARING DRAWING

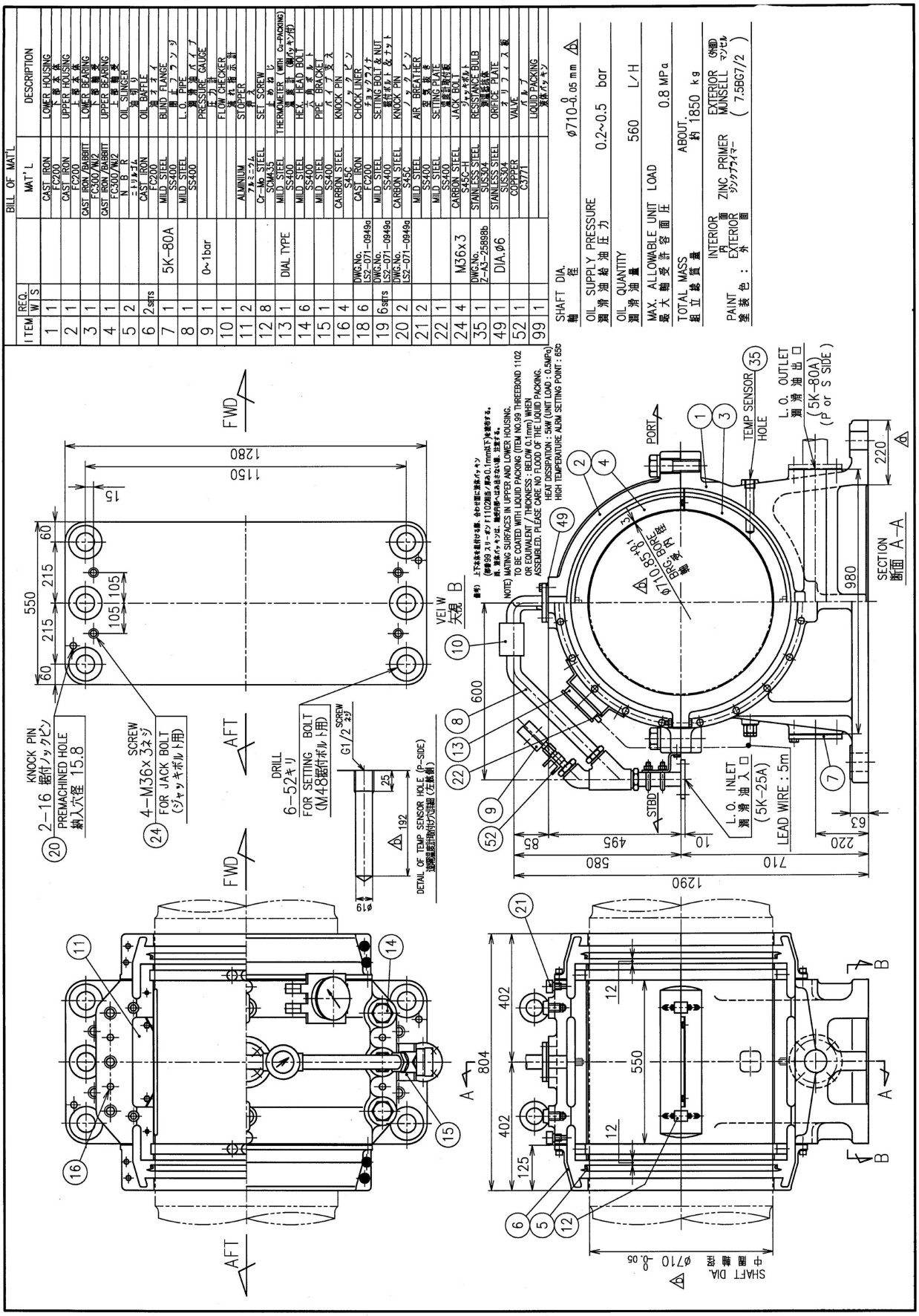

FIGURE A-3: INTERMEDIATE SHAFT BEARING DRAWING

APPENDIX B

Loading Condition No.04

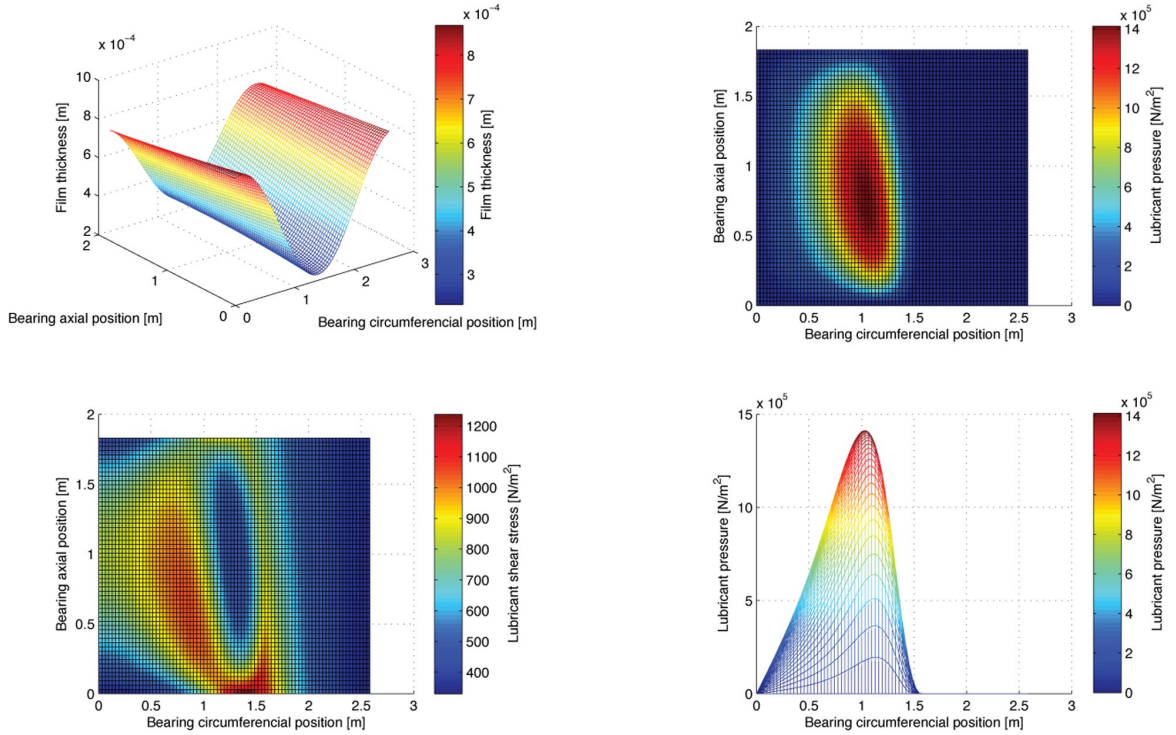

FIGURE B.1: L.C. 04, AFT S/T BEARING, FILM THICKNESS, PRESSURE AND SHEAR STRESS DISTRIBUTIONS

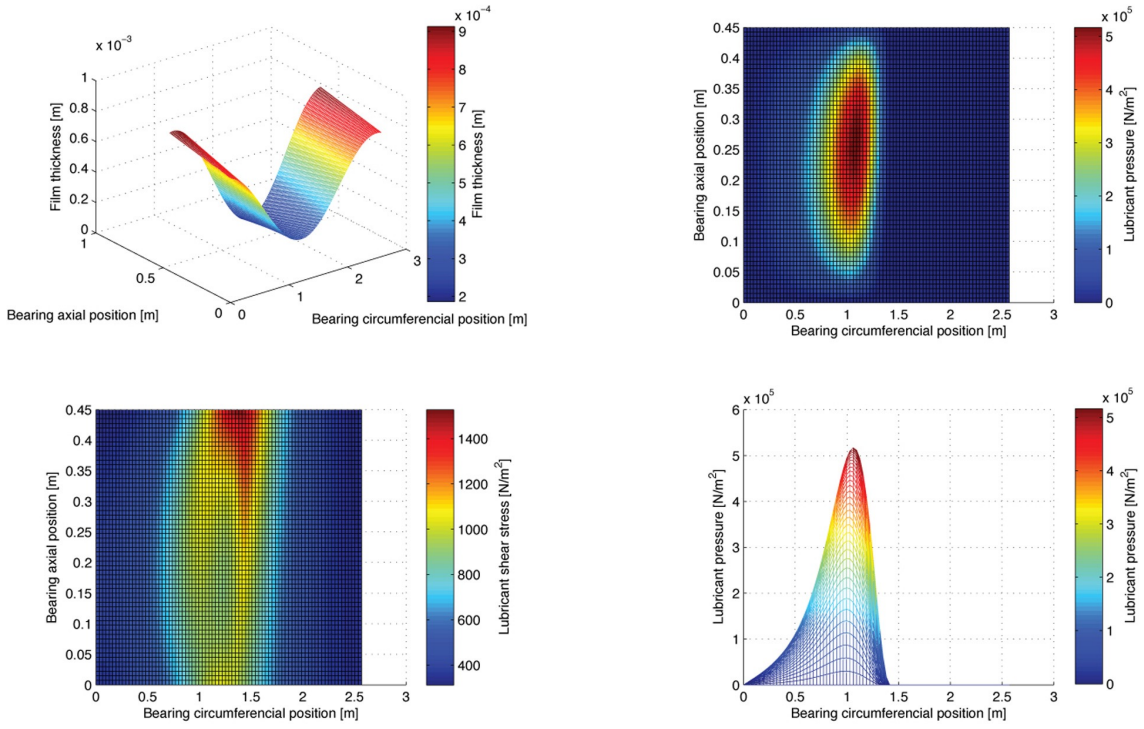

FIGURE B.2: L.C. 04, FORE S/T BEARING, FILM THICKNESS, PRESSURE AND SHEAR STRESS DISTRIBUTIONS

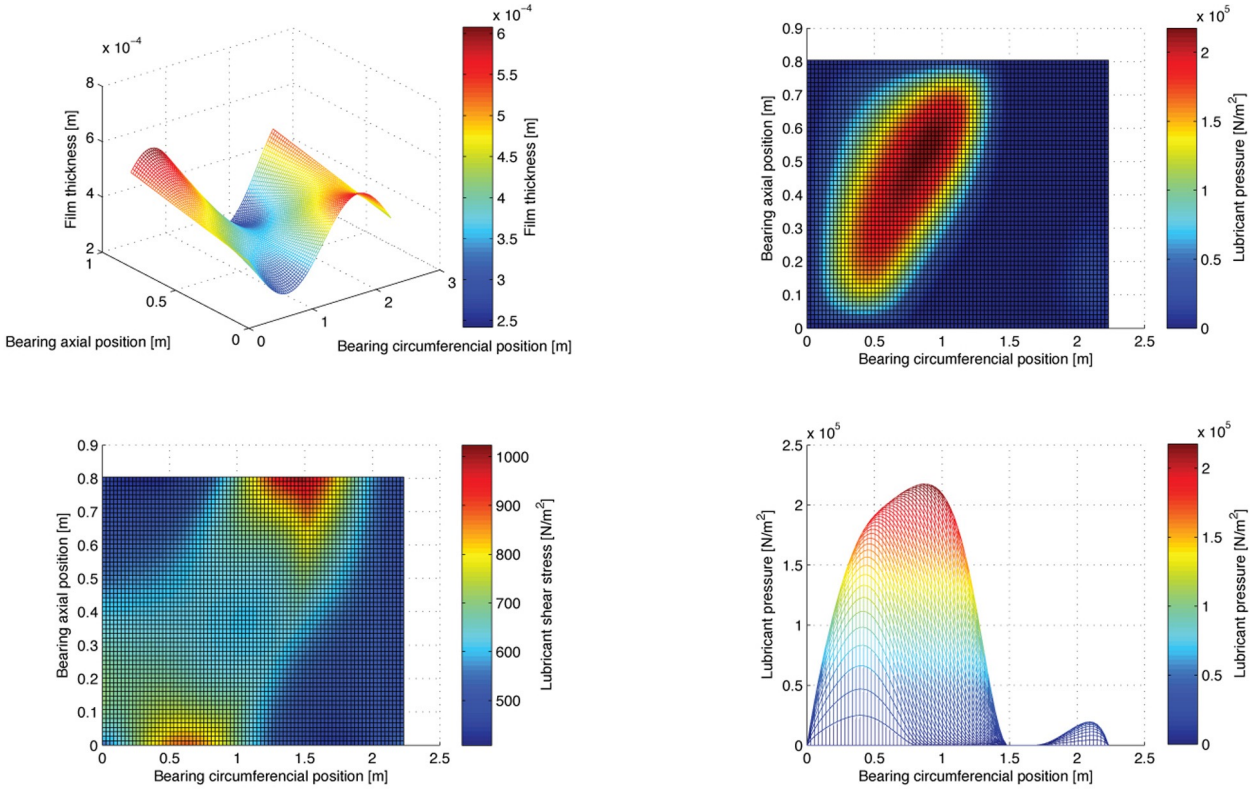

FIGURE B.3: L.C. 04, I/M BEARING, FILM THICKNESS, PRESSURE AND SHEAR STRESS DISTRIBUTIONS

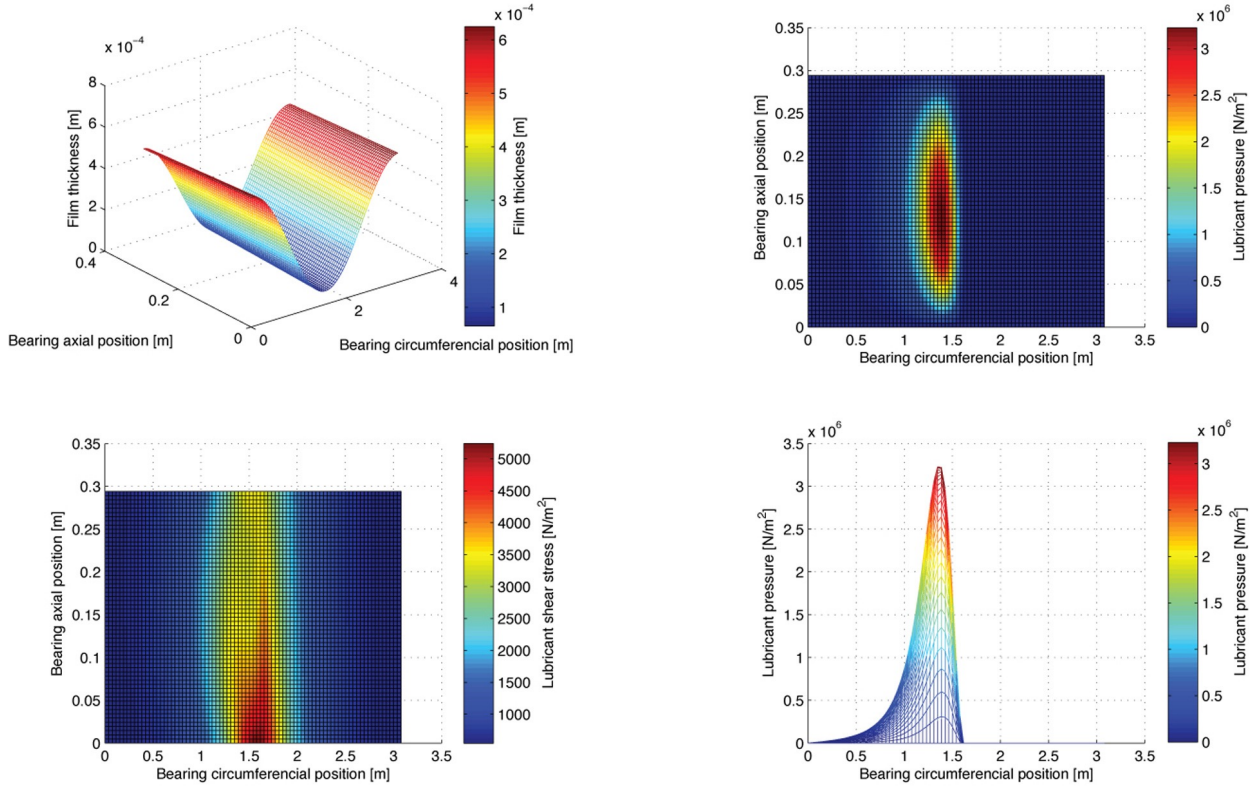

FIGURE B.4: L.C. 04, 1ST M/E BEARING, FILM THICKNESS, PRESSURE AND SHEAR STRESS DISTRIBUTIONS

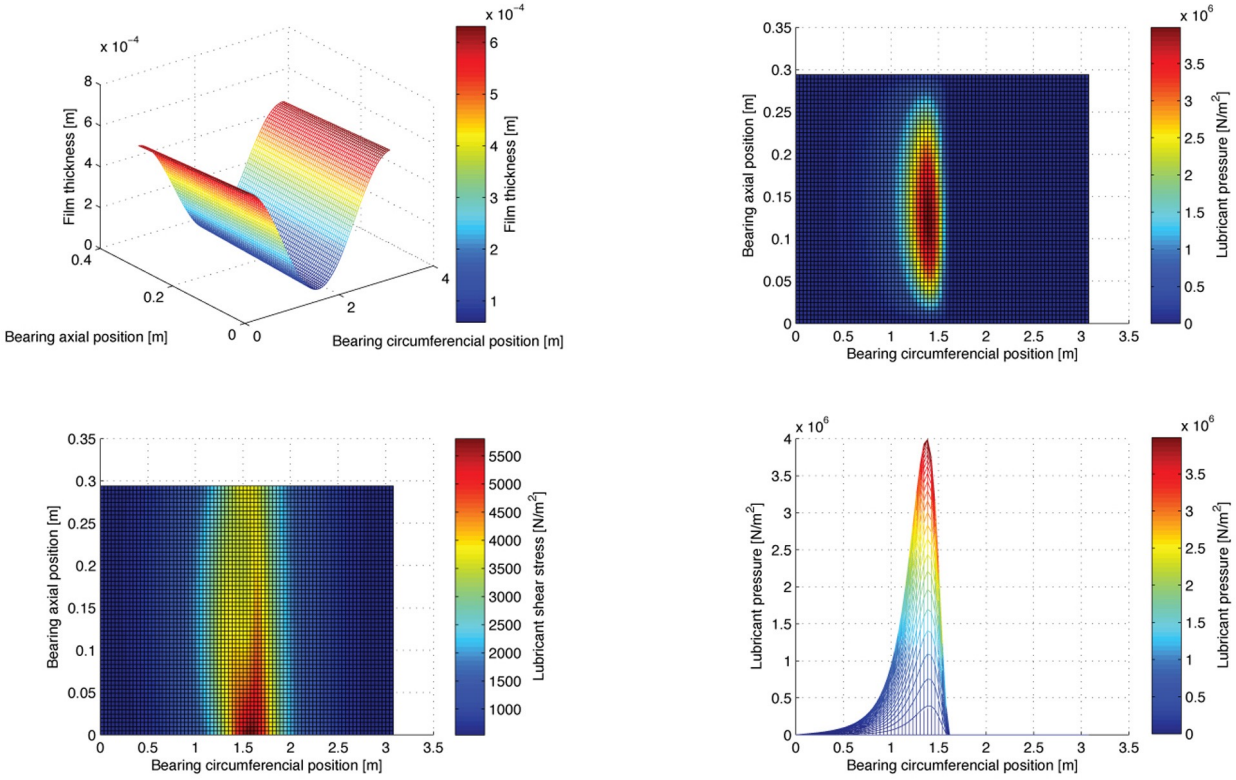

FIGURE B.5: L.C. 04, 2ND M/E BEARING, FILM THICKNESS, PRESSURE AND SHEAR STRESS DISTRIBUTIONS

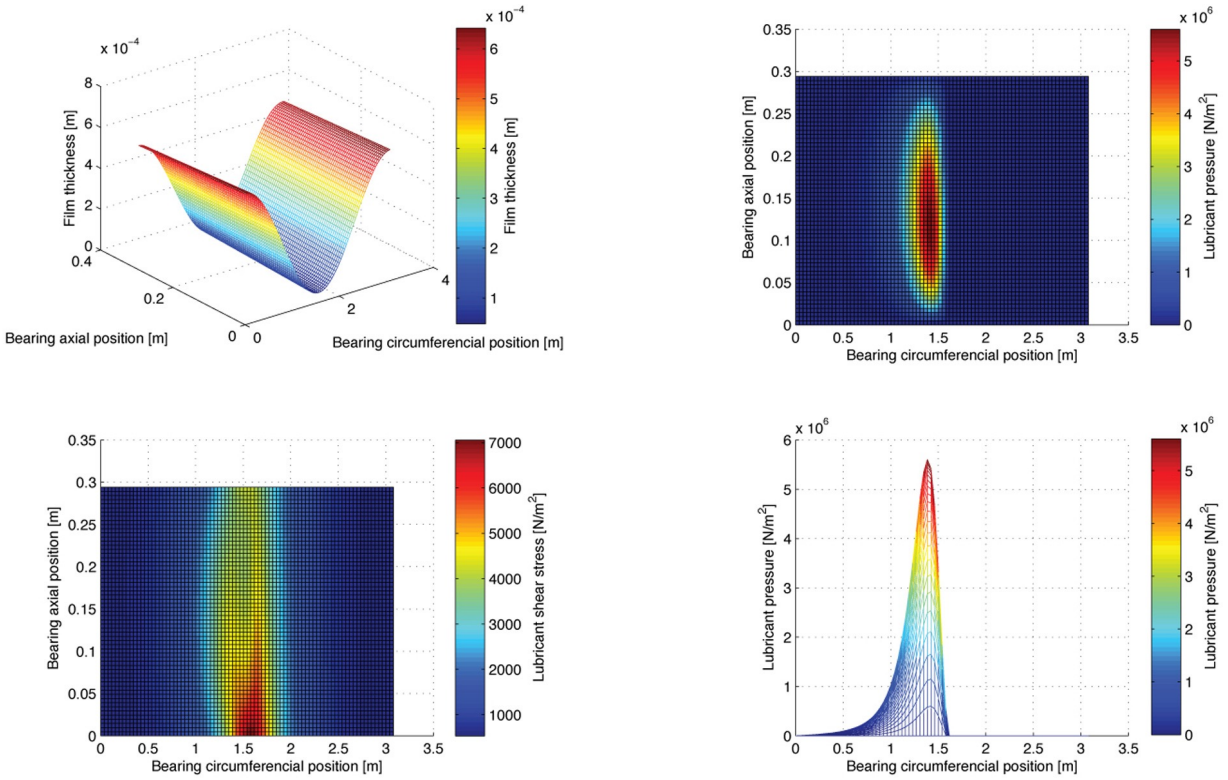

FIGURE B.6: L.C. 04, 3RD M/E BEARING, FILM THICKNESS, PRESSURE AND SHEAR STRESS DISTRIBUTIONS

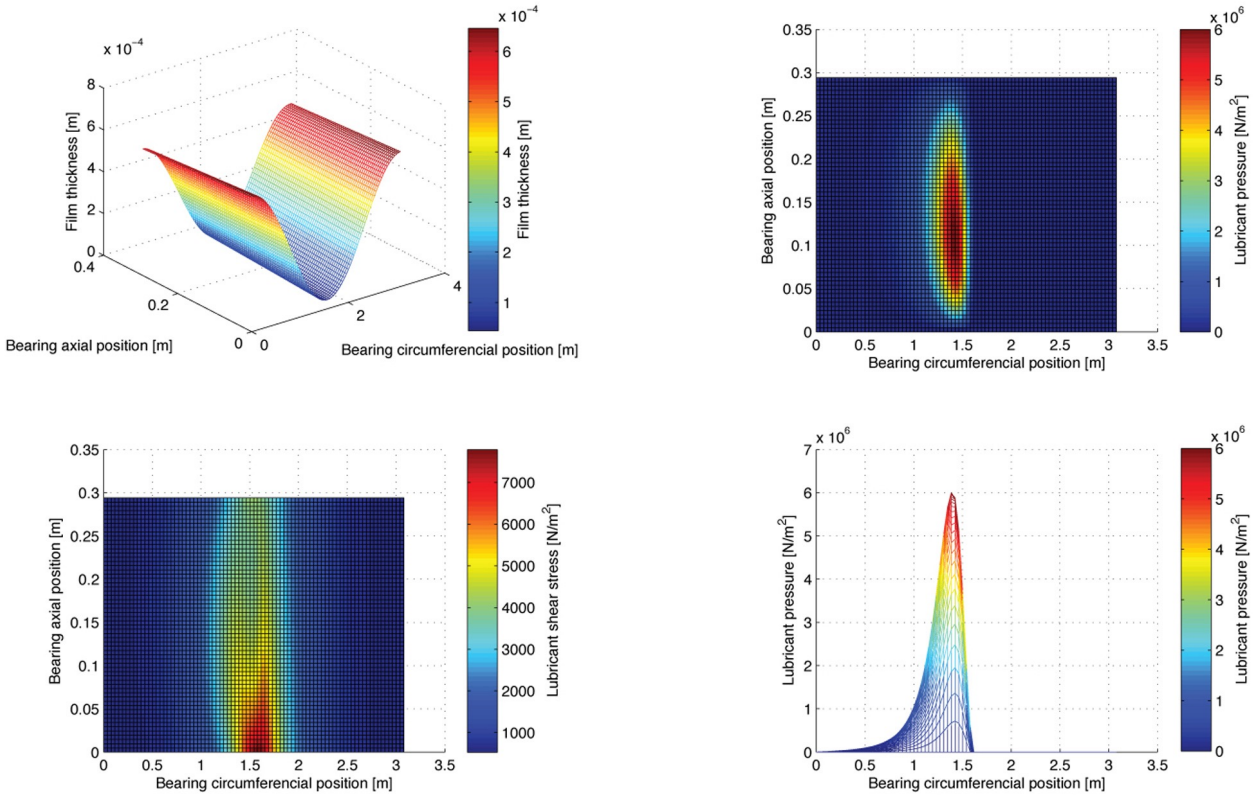

FIGURE B.7: L.C. 04, 4TH M/E BEARING, FILM THICKNESS, PRESSURE AND SHEAR STRESS DISTRIBUTIONS

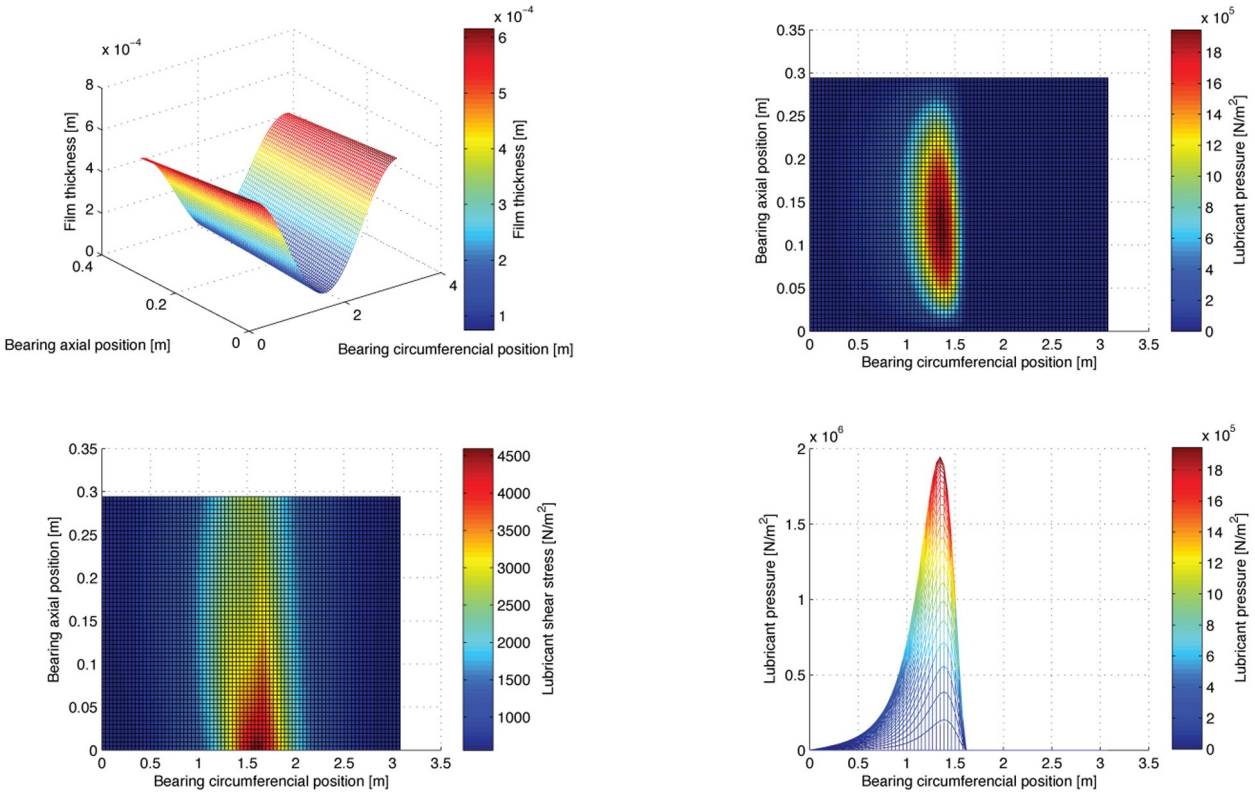

FIGURE B.8: L.C. 04, 5TH M/E BEARING, FILM THICKNESS, PRESSURE AND SHEAR STRESS DISTRIBUTIONS

Loading Condition No.11

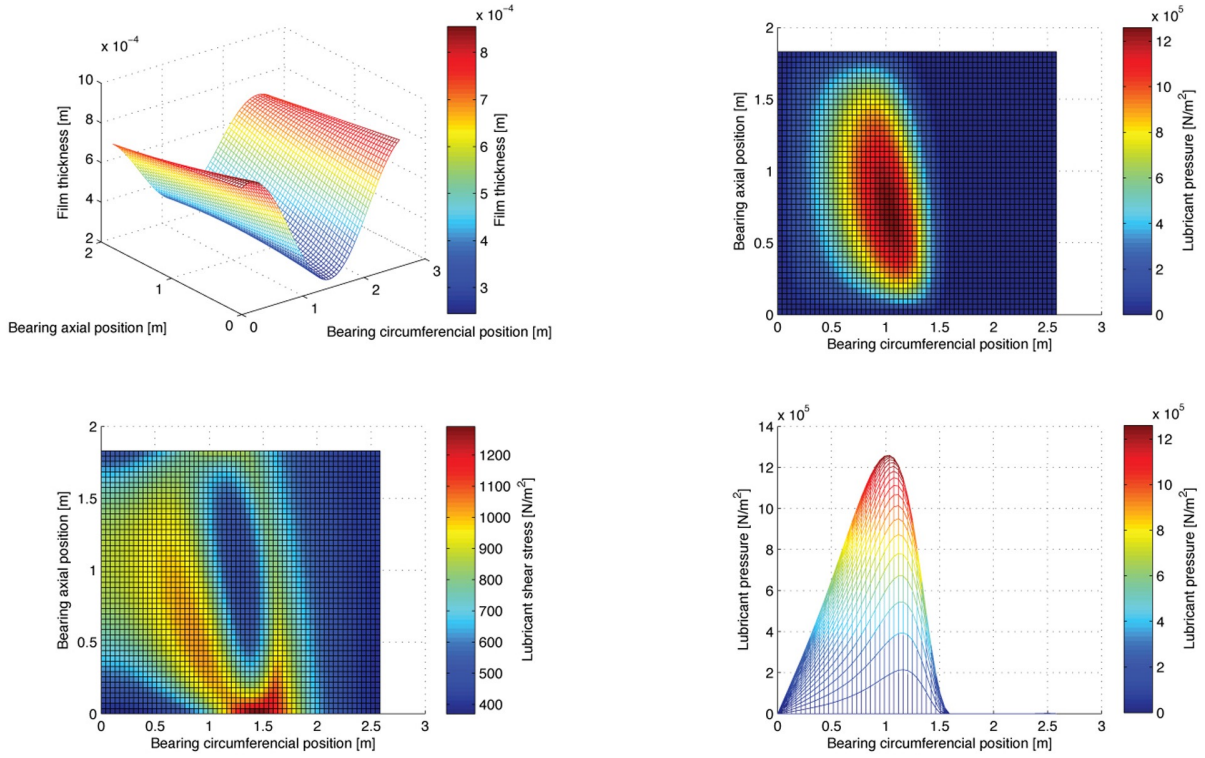

FIGURE B.9: L.C. 11, AFT S/T BEARING, FILM THICKNESS, PRESSURE AND SHEAR STRESS DISTRIBUTIONS

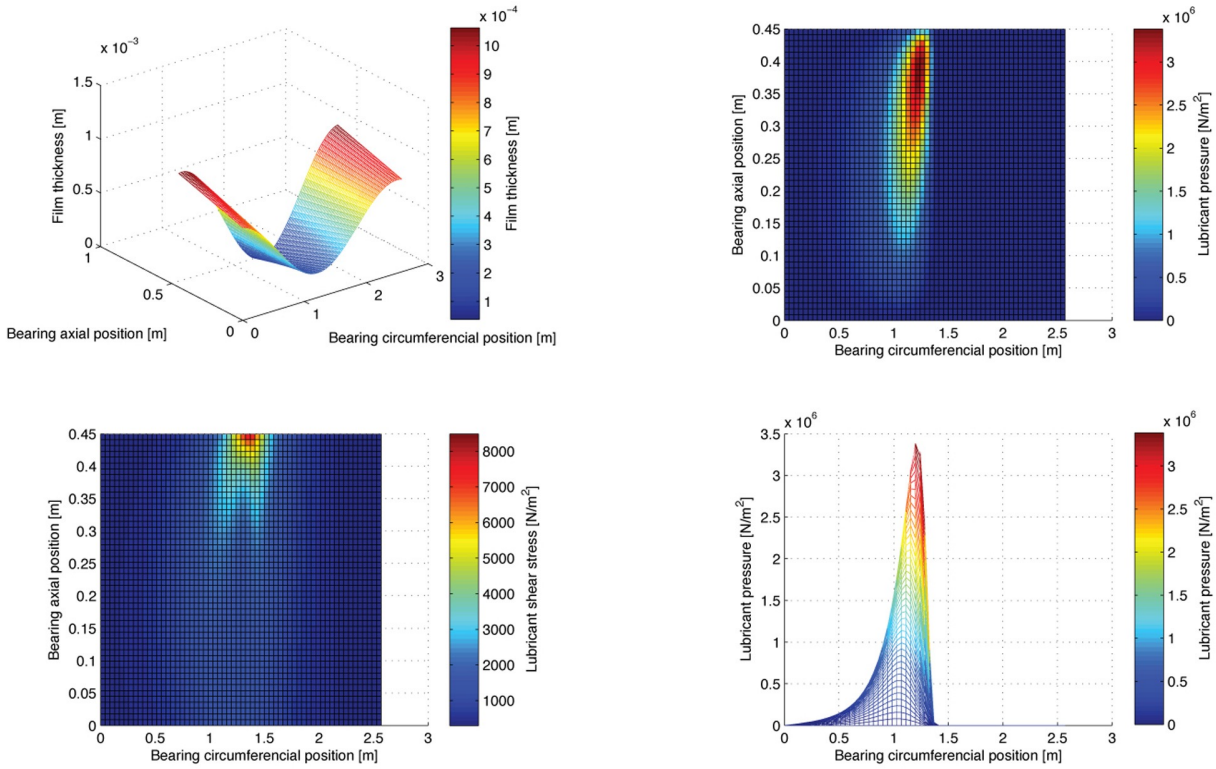

FIGURE B.10: L.C. 11, FORE S/T BEARING, FILM THICKNESS, PRESSURE AND SHEAR STRESS DISTRIBUTIONS

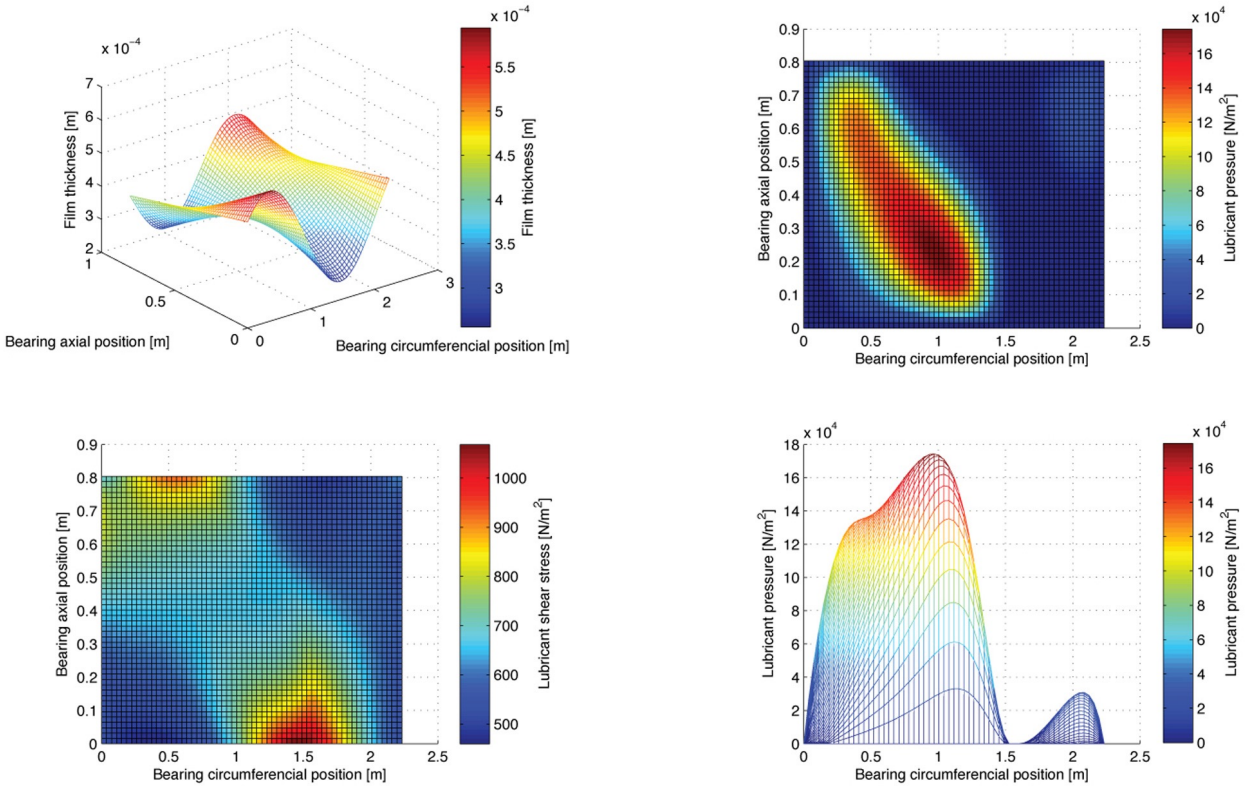

FIGURE B.11: L.C. 11, I/M BEARING, FILM THICKNESS, PRESSURE AND SHEAR STRESS DISTRIBUTIONS

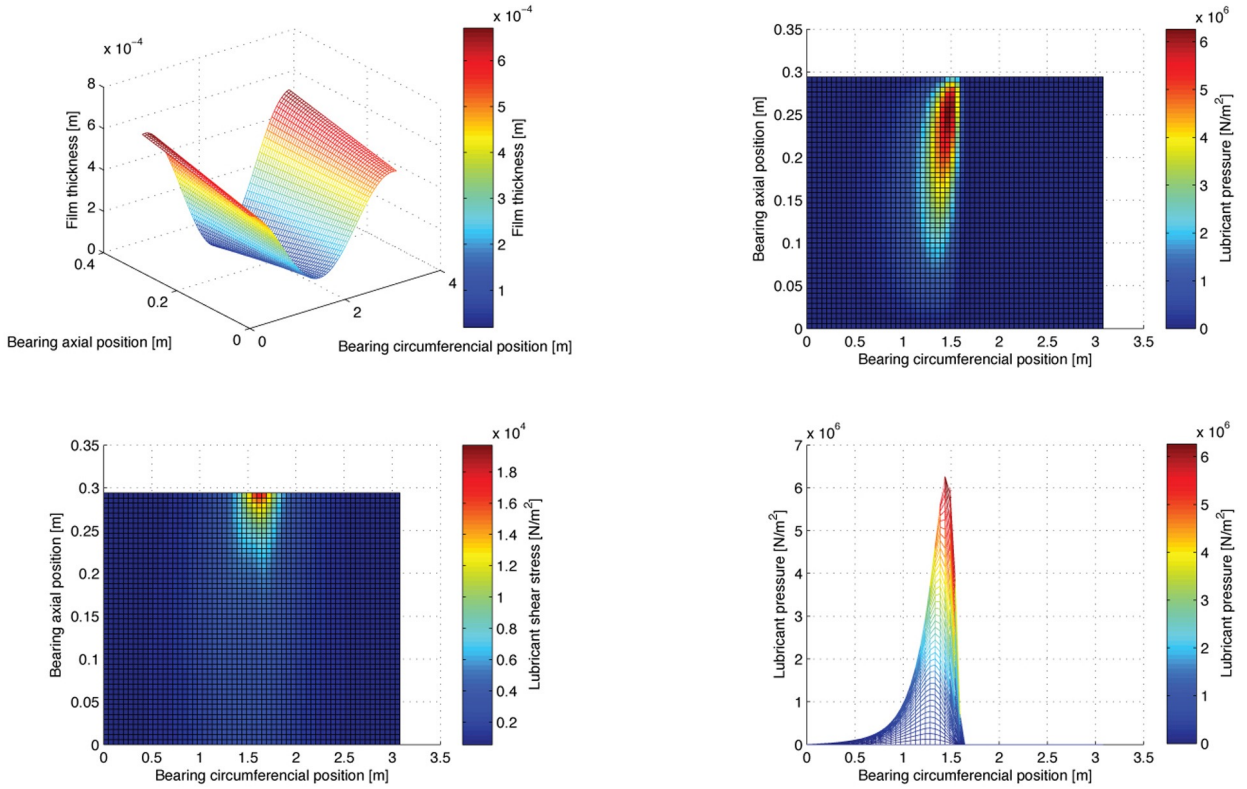

FIGURE B.12: L.C. 11, 1ST M/E BEARING, FILM THICKNESS, PRESSURE AND SHEAR STRESS DISTRIBUTIONS

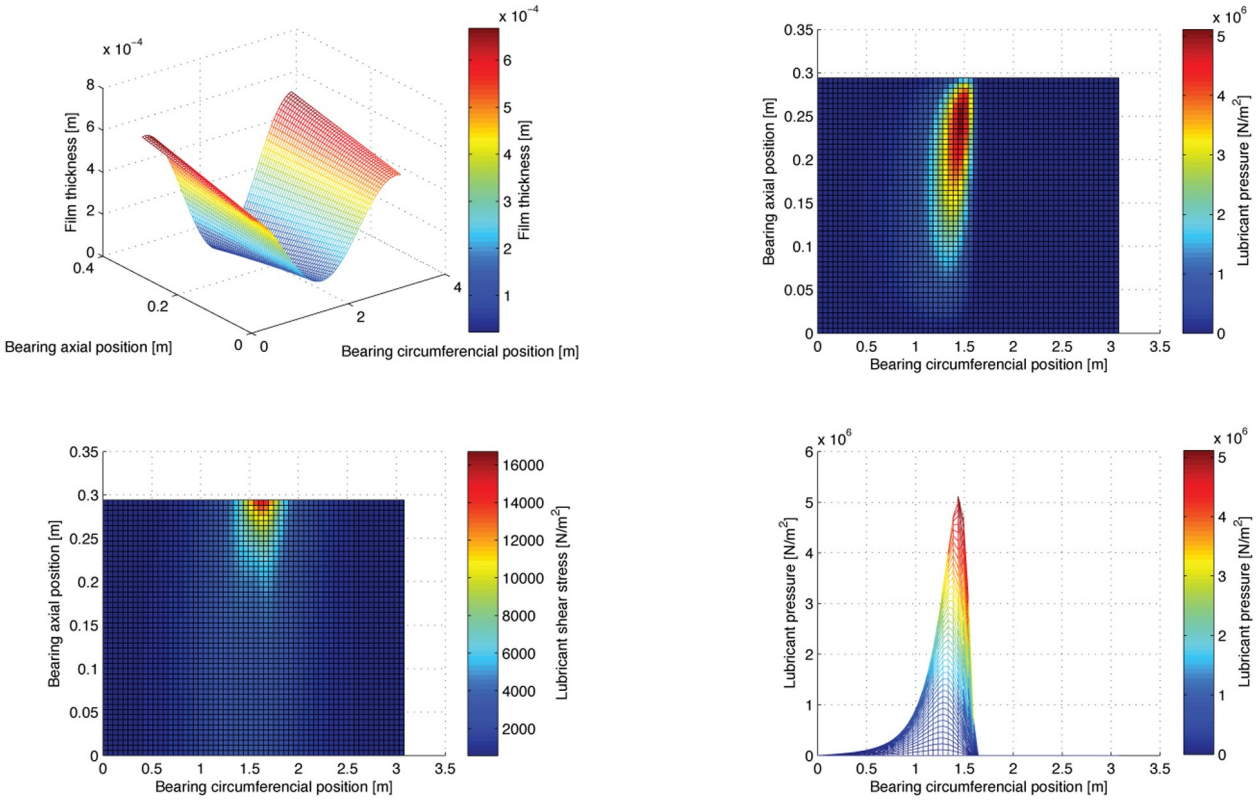

FIGURE B.13: L.C. 11, 2ND M/E BEARING, FILM THICKNESS, PRESSURE AND SHEAR STRESS DISTRIBUTIONS

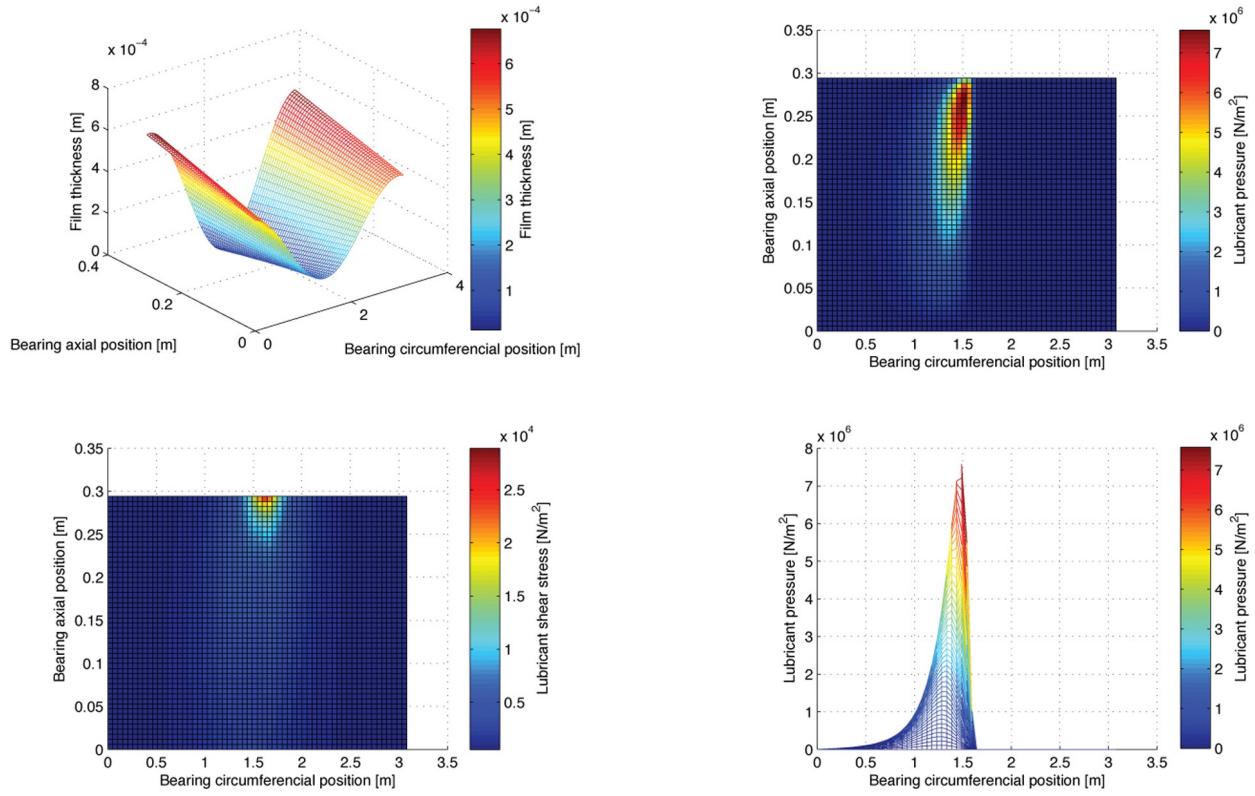

FIGURE B.14: L.C. 11, 3RD M/E BEARING, FILM THICKNESS, PRESSURE AND SHEAR STRESS DISTRIBUTIONS

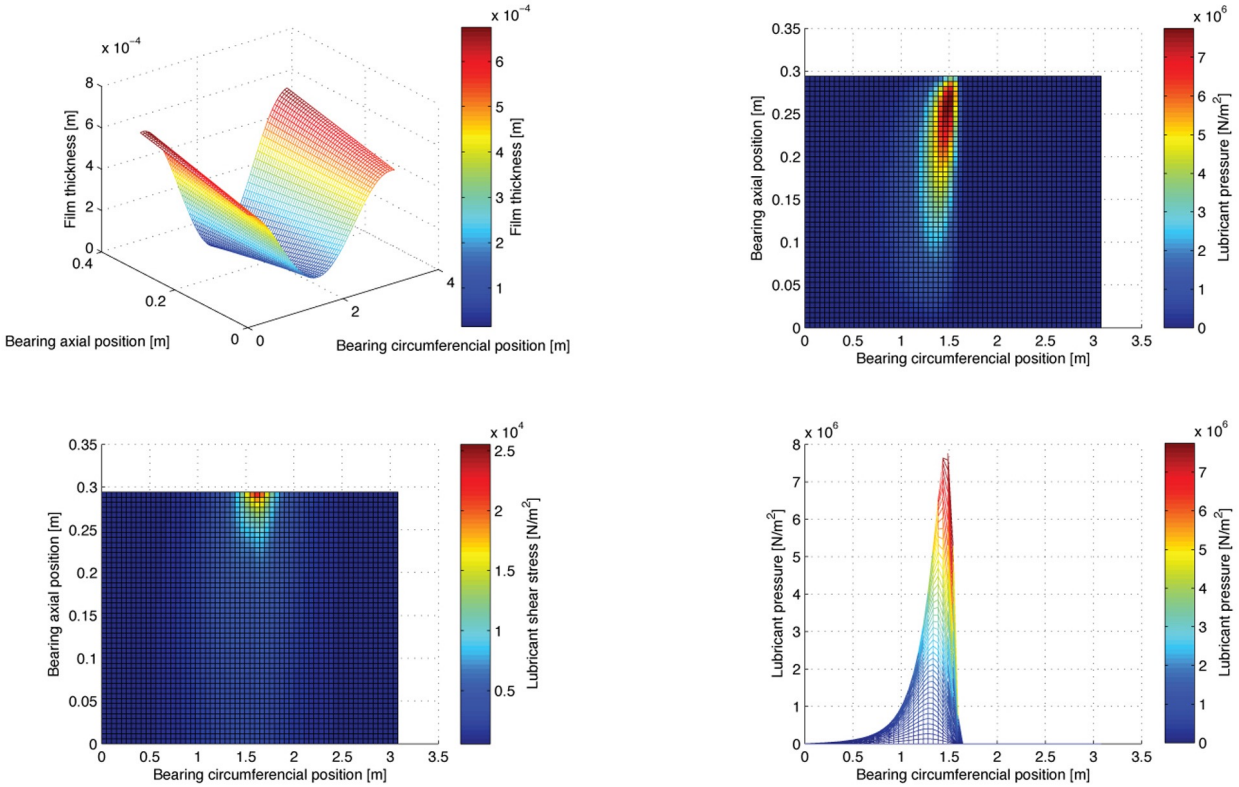

FIGURE B.15: L.C. 11, 4TH M/E BEARING, FILM THICKNESS, PRESSURE AND SHEAR STRESS DISTRIBUTIONS

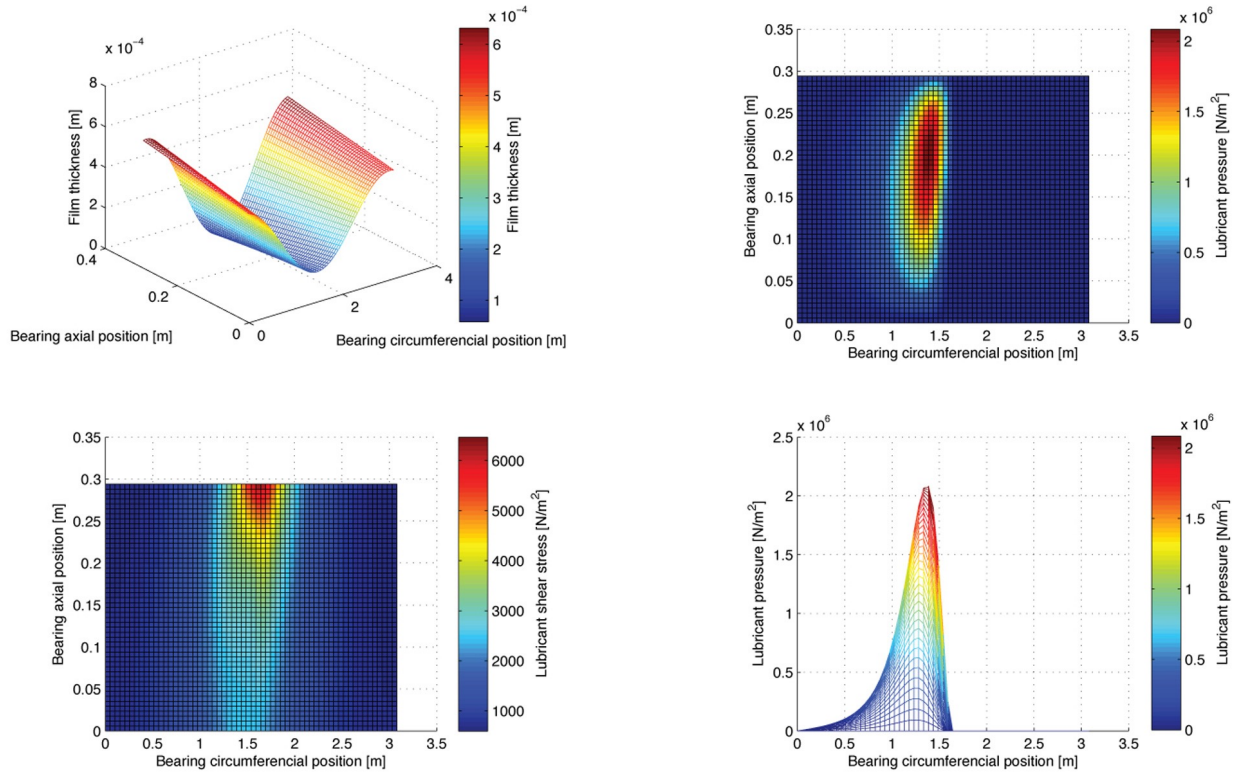

FIGURE B.16: L.C. 11, 5TH M/E BEARING, FILM THICKNESS, PRESSURE AND SHEAR STRESS DISTRIBUTIONS

Loading Condition No.21

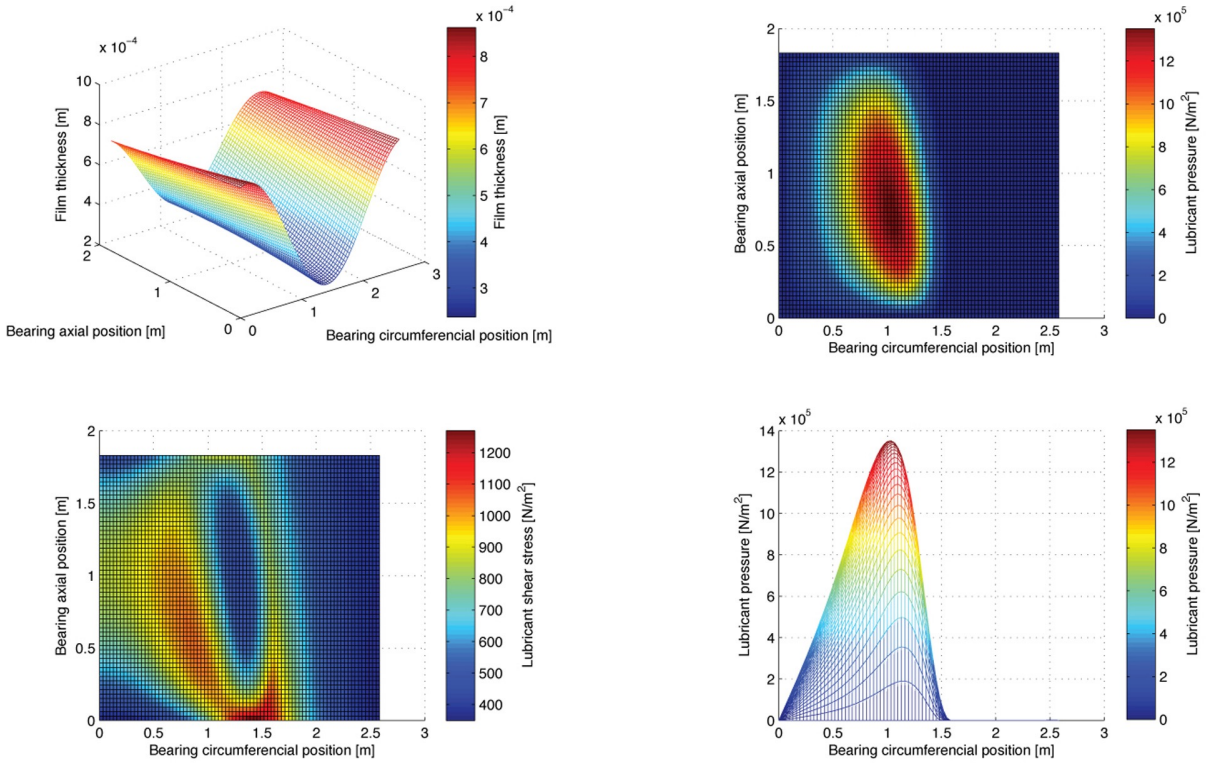

FIGURE B.17: L.C. 21, AFT S/T BEARING, FILM THICKNESS, PRESSURE AND SHEAR STRESS DISTRIBUTIONS

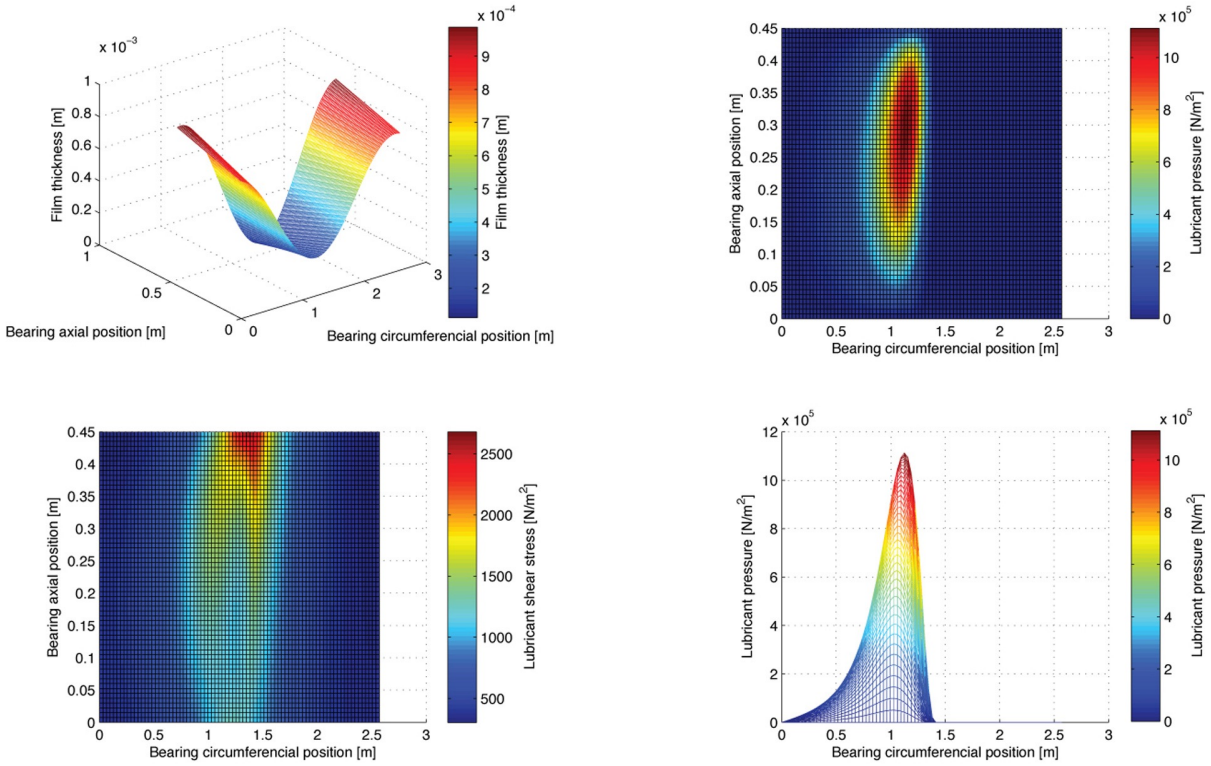

FIGURE B.18: L.C. 21, FORE S/T BEARING, FILM THICKNESS, PRESSURE AND SHEAR STRESS DISTRIBUTIONS

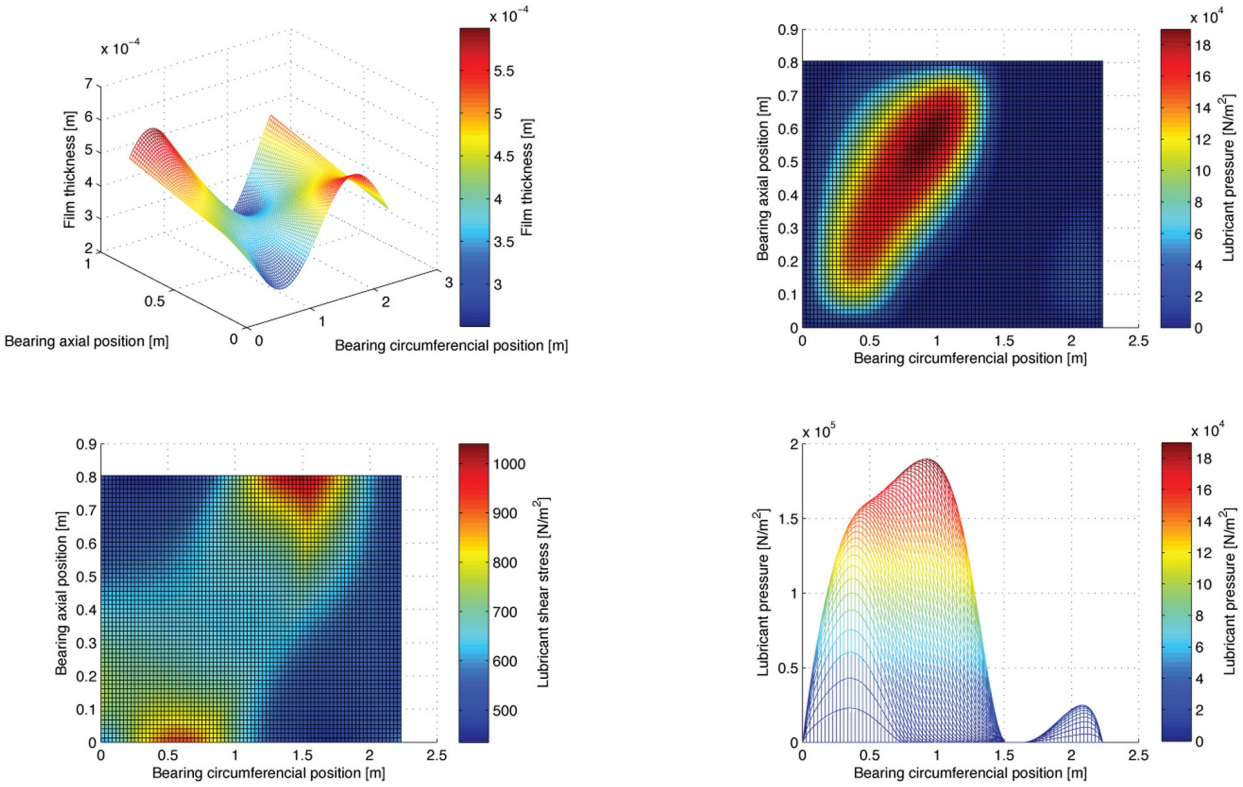

FIGURE B.19: L.C. 21, I/M BEARING, FILM THICKNESS, PRESSURE AND SHEAR STRESS DISTRIBUTIONS

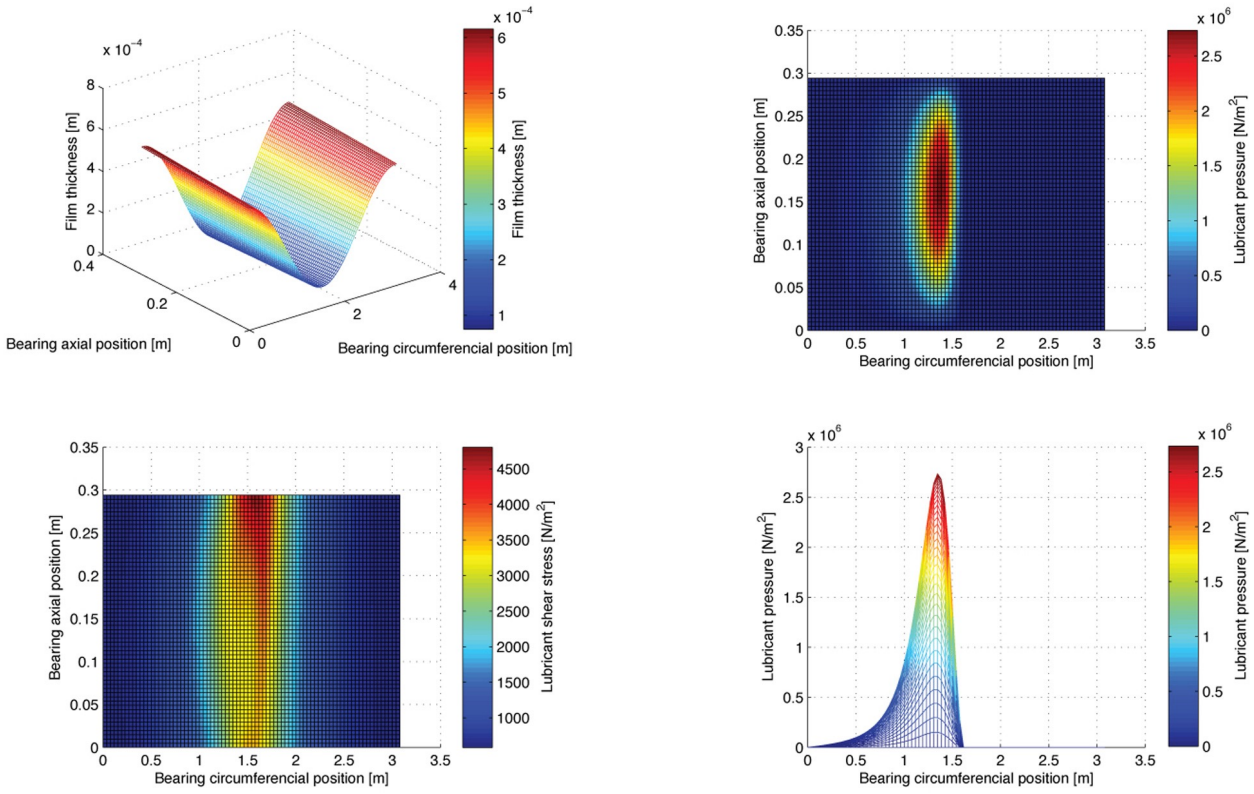

FIGURE B.20: L.C. 21, 1ST M/E BEARING, FILM THICKNESS, PRESSURE AND SHEAR STRESS DISTRIBUTIONS

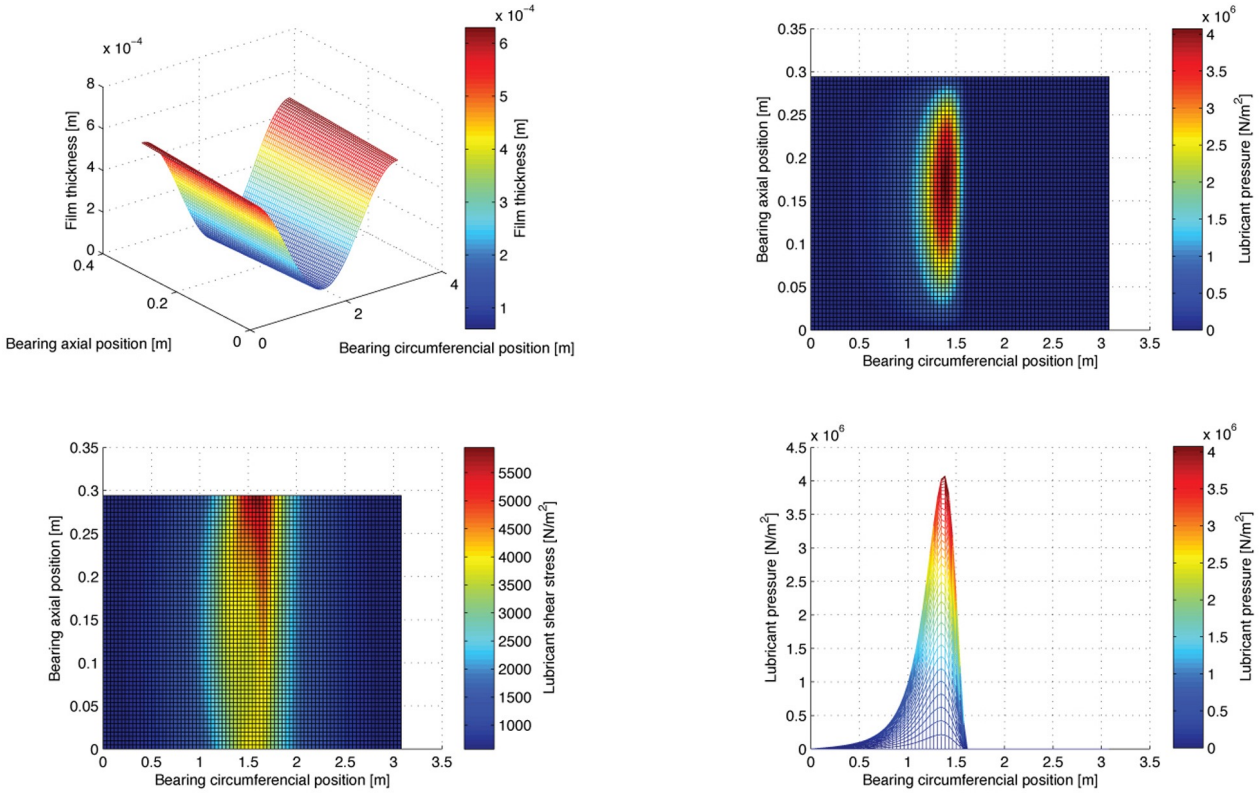

FIGURE B.21: L.C. 21, 2ND M/E BEARING, FILM THICKNESS, PRESSURE AND SHEAR STRESS DISTRIBUTIONS

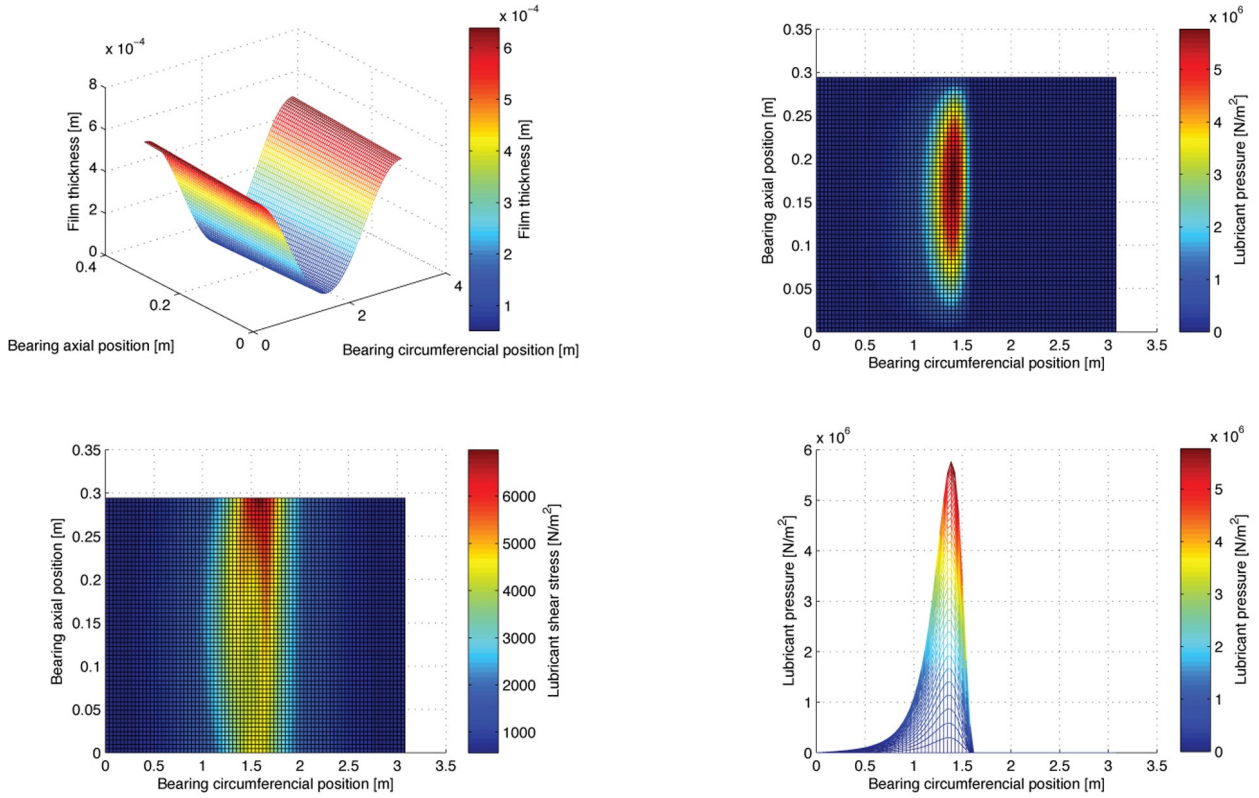

FIGURE B.22: L.C. 21, 3RD M/E BEARING, FILM THICKNESS, PRESSURE AND SHEAR STRESS DISTRIBUTIONS

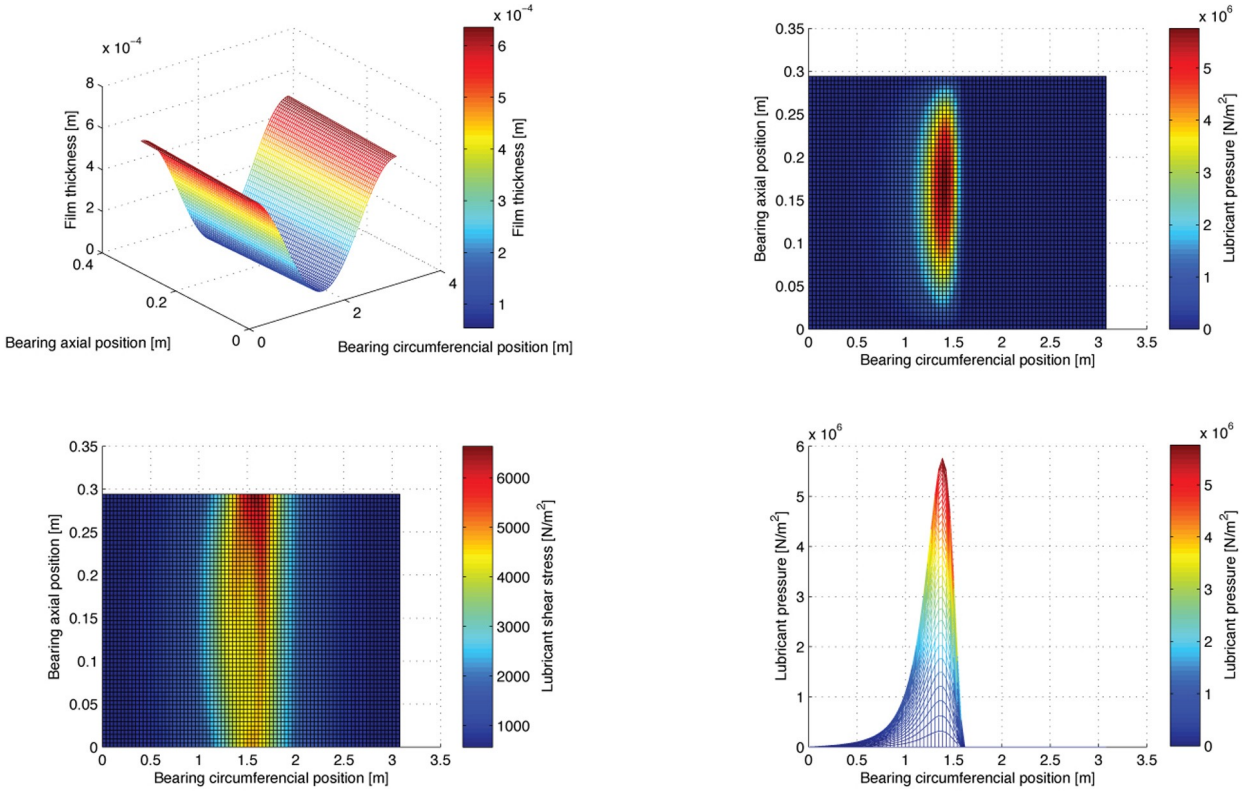

FIGURE B.23: L.C. 21, 4TH M/E BEARING, FILM THICKNESS, PRESSURE AND SHEAR STRESS DISTRIBUTIONS

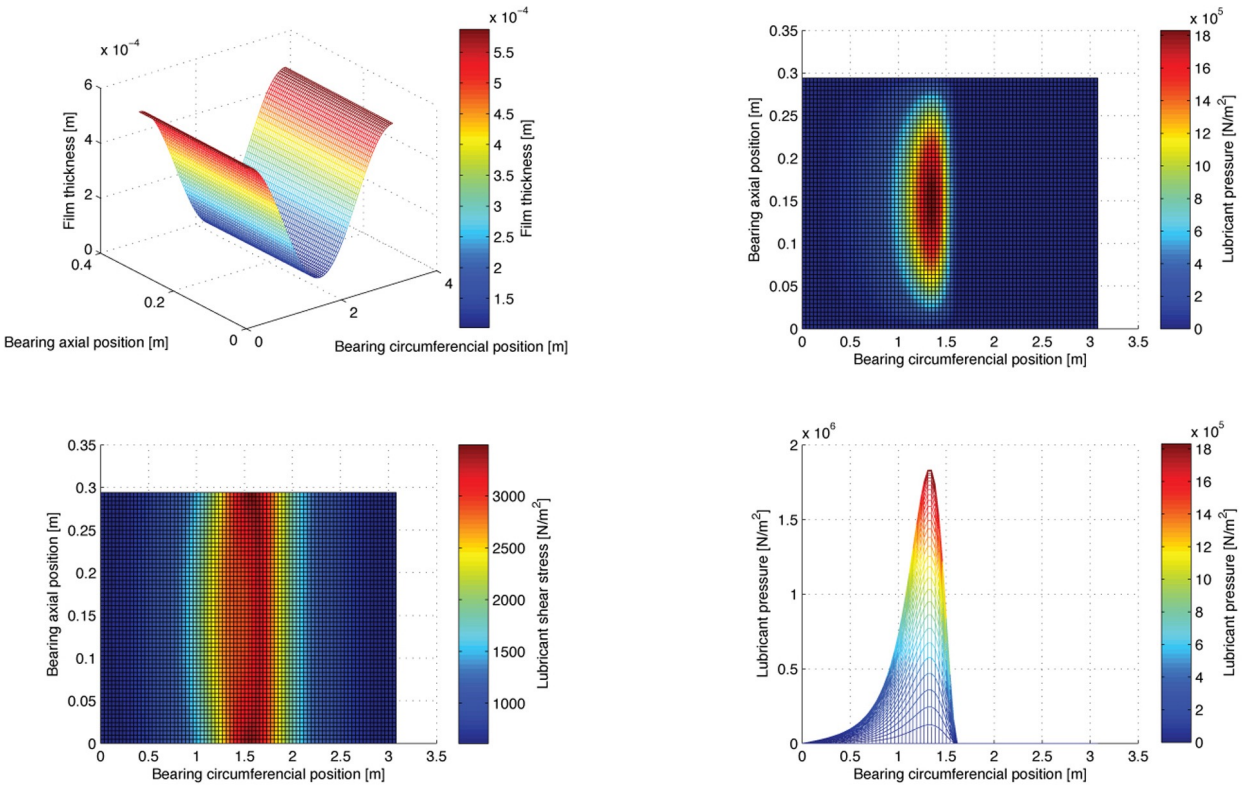

FIGURE B.24: L.C. 21, 5TH M/E BEARING, FILM THICKNESS, PRESSURE AND SHEAR STRESS DISTRIBUTIONS